

Dissertation zu Erlangung des Doktorgrades
der Fakultät für Chemie und Pharmazie
der Ludwig-Maximilians-Universität München



Anticancer effects of the V-ATPase inhibitor Archazolid B

Romina Madeleine Wiedmann

aus Mutlangen

2011

Erklärung

Diese Dissertation wurde im Sinne von § 13 Abs. 3 bzw. 4 der Promotionsordnung vom 29. Januar 1998 (in der Fassung der sechsten Änderungssatzung vom 16. August 2010) von Frau Prof. Dr. Angelika M. Vollmar am Lehrstuhl für Pharmazeutische Biologie betreut.

Ehrenwörtliche Versicherung

Diese Dissertation wurde selbständig, ohne unerlaubte Hilfe erarbeitet.

München, den 17.11.2011

Romina Madeleine Wiedmann

Dissertation eingereicht am:	17.11.2011
1. Gutachter:	Prof. Dr. Angelika M. Vollmar
2. Gutachter:	Prof. Dr. Stefan Zahler
Mündliche Prüfung am:	20.12.2011

meinen Eltern

CONTENTS

CONTENTS	I-V
INTRODUCTION	1
1.1. Background and aim of the study	2
1.2. Natural products	3
1.2.1. History and importance of natural products	3
1.2.2. Myxobacteria as source of natural compounds	3
1.3. V-ATPase as potential drug target	4
1.3.1. Function and relevance	4
1.3.2. Structure of the V-ATPase	4
1.3.3. V-ATPase inhibitors	5
1.3.3.1. The plecomacrolides Bafilomycin and Concanamycin	5
1.3.3.2. Benzolactone enamides	6
1.3.3.3. The novel class of macrolactones: the Archazolids	6
1.4. Metastatic cancer	7
1.4.1. Cell death - apoptosis	7
1.4.2. Formation of metastasis	9
1.4.3. The cell migration process	9
1.4.4. The signaling during cell migration	10
1.4.5. Endocytosis	13
MATERIAL AND METHODS	15
2.1. Materials	16
2.1.1. Compounds	16
2.1.2. Biochemicals, inhibitors, dyes and cell culture reagents	16
2.1.3. Technical equipment	17
2.2. Methods	18
2.2.1. Cell culture	18
2.2.2. Freezing and thawing	19
2.2.3. Flow cytometry	19
2.2.3.1. Quantification of apoptotic cell death with the Nicoletti assay	20
2.2.3.2. Cell cycle analysis	20
2.2.3.3. Measurement of mitochondrial potential change	21
2.2.3.4. Measurement of cytochrome c release	21
2.2.3.5. Measurement of EGF-R on the cell surface	22
2.2.4. Cell proliferation	22

2.2.5. Clonogenic assay	23
2.2.6. Measurement of caspase-activity	23
2.2.7. Gene expression profiling	24
2.2.7.1. RNA Isolation	24
2.2.7.2. Reverse Transcription	24
2.2.7.3. Quantitative Real-Time PCR	24
2.2.7.4. Polymerase-chain-reaction (PCR)	24
2.2.7.5. Microarray	25
2.2.8. Transfection of cells with siRNA or plasmids	26
2.2.8.1. Electroporation (Cell line nucleofactor kit V)	26
2.2.8.2. Liposome-based transfection (Fugene, Roche)	27
2.2.9. Transmission Electron Microscopy	27
2.2.10. Confocal microscopy (staining, LysosomeTracker)	27
2.2.11. Migration Assays	28
2.2.11.1. Wound healing assay	28
2.2.11.2. Boyden chamber assay	29
2.2.11.3. Chemotaxis	29
2.2.12. Cell adhesion/ruffle formation	30
2.2.13. Rac1 activation assay	31
2.2.14. Internalization assay (Transferrin-/EGF-rhodamine)	31
2.2.15. Western Blot	31
2.2.15.1. Protein sample preparations-total cell lysates	31
2.2.15.2. Protein quantification	32
2.2.15.3. SDS-PAGE	32
2.2.15.4. Tank blotting	33
2.2.15.5. Detection	34
2.2.15.6.1. Detection method-LICOR	34
2.2.15.7.2. Enhanced Chemiluminescence	34
2.2.16. T24 spheroids	35
2.2.17. Statistical analysis	36
RESULTS	37
3.1. Characterisation of the V-ATPase subunit c as potential drug target	38
3.1.1. Expression and localization of the V-ATPase subunit c	38
3.1.2. Archazolid B, a new potent inhibitor of the V-ATPase	39
3.1.3. Effects of Archazolid B on gene expression	40
3.2. Antitumor effects of Archazolid B	41
3.2.1. Archazolid B inhibits cell proliferation of highly invasive cancer cells	41
3.2.2. Archazolid inhibits clonogenic survival	42
3.2.3. Cell death features induced by Archazolid B	43

3.2.4. Archazolid B induces apoptosis	45
3.2.5. Effects of Archazolid B on the cell cycle	46
3.2.6. Archazolid B induces apoptosis caspase-dependently	47
3.2.7. Archazolid B affects the intrinsic apoptotic pathway	50
3.2.8. Effects of Archazolid B in a 3-D spheroid model	52
3.2.9. Impairment of proliferation, apoptosis and clonogenic survival by the downregulation of ATP6L	52
3.3. Antimetastatic properties of Archazolid B	54
3.3.1. Effects of Archazolid B on cell migration	54
3.3.1.1. Impairment of wound healing by Archazolid B	54
3.3.3.2. Impairment of migration by Archazolid B in the Boyden chamber assay	56
3.3.3.3. Effects of Archazolid B on cellular chemotaxis	57
3.3.2. Effects of Archazolid B on ruffle formation and the Rho-GTPase Rac1	59
3.3.3. The downregulation of ATP6L inhibits migration	60
3.3.4. The downregulation of ATP6L inhibits localization and activation of Rac1	62
3.3.5. Archazolid B increases EGF-R expression on the cell surface	63
3.3.6. Archazolid B affects EGFR signaling	64
3.3.7. Archazolid B affects the internalization process	66
3.3.7.1. Effects on internalization after short time treatment	66
3.3.7.2. Effects of Archazolid B on internalization after longtime treatment	66
3.3.8. Rab5-induced Rac1 activation is inhibited by Archazolid B	68
3.3.9. Endosomal localization of the Rho-GTPase Rac1	71
DISCUSSION	74
4.1. Cancer and treatment strategies	75
4.2. The V-ATPase as potential drug target	75
4.3. The role of V-ATPase in tumor cell growth	76
4.3.1. Anti-proliferative effect of Archazolid B	76
4.3.2. Inhibition of V-ATPase as attractive method to induce apoptosis	77
4.3.3. Effects of Archazolid B on T24 spheroid growth	79
4.3.4. The role of the subunit c	79
4.4. Impairment of V-ATPase in tumor cell migration	80
4.4.1. Rac1 signaling	81
4.4.2. EGF-R and its downstream players	82
4.4.3. Involvement of V-ATPase in endocytosis	83
4.4.4. The role of Rab5-recycling	84

SUMMARY AND CONCLUSIONS	86
5.1. Involvement of Archazolid B treatment in tumor cell growth	87
5.2. Involvement of V-ATPase inhibition by Archazolid B in cell migration and endocytosis	87
REFERENCES	89
APPENDIX	97
7.1. Abbreviations	98
7.2. Publications	100
7.2.1. Original publications	100
7.2.2. Poster presentations/abstracts	101
7.3. Grants	102
7.4. Curriculum vitae	103
7.5. Acknowledgement	104

INTRODUCTION

1.1. Background and aim of the study

Since it became clear that the reason of 90% of cancer deaths is due to the development of metastasis¹, it is important to improve nowadays available treatment options to prevent the metastatic process and to eliminate already existing metastasis.

Metastatic cancer cells are highly resistant against available chemotherapeutics and single cells are able to separate from a primary tumor and spread over the vascular system, the lymphatics or across body cavities throughout the body to form secondary tumors.²

Commonly used therapies are still surgery, radiotherapy and chemotherapy.³ The aim is to eliminate the tumor, repress cell proliferation, induce cell death, inhibit angiogenesis and cell migration. Known chemotherapeutics interfere for example in the oncogenic signaling pathways as antibodies, as ligand antagonists to oncogenic receptors, as inhibitors of small molecules like tyrosine kinases or vascular disrupting agents to prevent angiogenesis.²

As resistance features to new developed chemotherapeutics occur and also the drug efficiency often seems to be cell specific, it is still necessary to find new potential drug targets including new compounds. Our goal is to test various natural compounds from plants, marine organisms, fungi and bacteria as potential new drugs or as tools to further elucidate cancer signaling pathways.

One focus of our group are compounds of myxobacteria. Today myxobacteria are used as a major source of microbial secondary metabolites with pharmaceutical interest.⁴ One of these compounds is the vacuolar H⁺-ATPase (V-ATPase)-inhibitor Archazolid B.⁵ V-ATPases are described as attractive drug targets in the field of cancer in the last years.^{6,7} Archazolid B seems to be highly specific and inhibits the V-ATPase activity already in the nanomolar range.⁸

Thus, the aim of this study was

- 1. to investigate the effects of the V-ATPase inhibitor Archazolid B on tumor cell growth.**
- 2. to elucidate the cellular signaling induced by Archazolid B leading to cell migration inhibition of highly invasive cancer cells.**

1.2. Natural products

1.2.1. History and importance of natural products

Natural compounds offer an invaluable source of potential new therapeutic agents - directly or as lead structures. The high chemical diversity and the biochemical specificity made the natural-product structures attractive in the field of drug discovery. There are several examples of natural compounds being already in therapeutical use or in clinical trials for infectious diseases, neurological diseases, cardiovascular and metabolic diseases, immunological and oncological diseases. Anti-cancer agents were found in plants (Camptothecin-Topoisomerase-inhibitor, Paclitaxel-Tubulin-antagonist), in microorganism like actinomycetes (Doxorubicin-DNA-intercalating drug) or myxobacteria (Epothilone D-Tubulin-antagonist) and in marine organism like sponges (Spongistatin-Tubulin-antagonist).⁹ The fact, that many natural compounds being in various stages of clinical development underline the important source of natural compounds as potential new therapeutics.

1.2.2. Myxobacteria as source of natural compounds

The profound research of the group of Reichenbach and Hoeffle opened up the field of myxobacteria as new producers of bioactive compounds, with complete new structures and unique modes of action.¹⁰ Their various functions are for example effects on the electron transport, the damage of the cytoskeleton or inhibiting nucleic acid polymerase.¹¹ Examples for active compounds of myxobacteria as promising anti-cancer drugs are Tubulysin and Epothilones, which are both described as tubulin-antagonists.⁹ Ixabepilone, a semi-synthetic analogue of Epothilone B, has been recently approved by the Food and Drug Administration (FDA) for the treatment of chemotherapy-resistant breast cancer.¹²

The compound of our interest was Archazolid B, which is a vacuolar H⁺-ATPase (V-ATPase) inhibitor originally produced by *Archangium gephyra* and *Cystobacter violaceus*. In the following, the function of V-ATPase and its inhibitors will be explained in detail.

1.3. V-ATPase as potential drug target

1.3.1. Function and relevance

Vacuolar (V) H⁺-ATPases are heteromultimeric ATP-dependent proton pumps in eukaryotic cells.^{6,13} These pumps occur ubiquitous and regulate the pH in endomembrane systems, like endosomes, lysosomes, secretory vesicles and the Golgi apparatus. Furthermore it is reported that V-ATPases are also localized in specialized cells like osteoclasts, kidney intercalated cells and more important in the plasmamembrane of invasive tumor cells, where it acidifies the extracellular space.¹⁴ The acidic tumor microenvironment is favourable for the metastatic process.¹⁵ V-ATPases are involved in cellular processes like receptor-mediated endocytosis and membrane trafficking, the processing of proteins and cellular transport mechanisms.^{6,16} It is reported that the V-ATPase plays a crucial role in a number of diseases such as osteoporosis¹⁷, diabetes¹⁸, Alzheimer's¹⁹ or Parkinson's²⁰, cardiovascular disorders²¹ and cancer²².

1.3.2. Structure of the V-ATPase

The V-ATPase has structural and functional similarities with the mitochondrial F₀F₁-ATP-synthase (F-ATPase).²³ One functional difference is that F-ATPase produces ATP whereas V-ATPase uses ATP for the translocations of protons across endomembranes in eukaryotic cells.²⁴ Structurally, the V-ATPase is divided into two major domains: the peripheral V₁ domain is a complex localized to the cytoplasm and is performing the ATP hydrolysis. It consists of 8 subunits (A, B, C, D, E, F, G and H) and has a total mass of 650 kDa. The three altering copies of subunit A and B of the V₁ complex form a ring and represent the ATP binding side mediating its hydrolysis. The single copies of D and F represent a central rotational stalk and a peripheral stalk is made out of the subunits C, E, G and H. Both structures connect the V₁ complex with the intra-membrane V₀ complex. The membrane-bound V₀ subunit consist of the six subunits a, d, e and the proteolipids c, c' and c''. The c subunits with its isoforms form a H⁺-binding rotor ring. The V₀ subunit, which has a molecular weight of 260 kDa, is therefore responsible for the transport of protons from the cytoplasm to the lumen or the extracellular space or when the V₀ subunit is inserted in the plasma membrane into the extracellular fluid.^{25,26} Based on various models of the F-ATPases²⁷⁻²⁹ and V-ATPases^{30,31} the transfer of protons across membranes is proposed like shown in Figure 1. Two H⁺-half channels are formed by the subunit a close to the c-

ring. Through the inner half channel H^+ can enter and bind to one of the c-subunits. The rotation of the c ring is driven by the hydrolysis of ATP and the nearly 360° rotation of the c-ring allows the release of H^+ through the outer half of the channel.³²

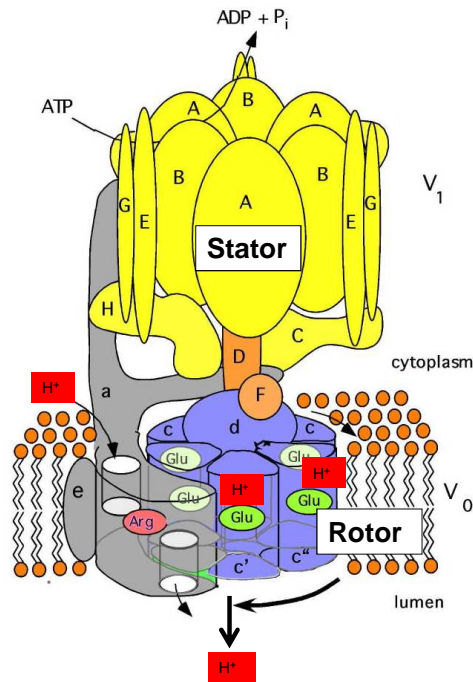


Figure 1.1: Structure and function of the V-ATPase. The V-ATPase consists of two main complexes V_1 and V_0 . V_1 consists of 8 subunits (A-H); the intramembrane subunit V_0 is composed of six different subunits (a, b, d and c, c', c''). The c subunits with its isoforms form a H^+ -binding rotor ring. One model of action would be that the central rotating shaft (subunit D, F) of the V_1 complex and the c-ring of the V_0 subunit form a rotor. ATP hydrolysis at the stator induces the rotation of the central shaft together with the c-ring. The subunit a of the V_0 subunit provides two H^+ half channels. When the c-ring rotates, H^+ pass from the inner channel to the outer half channel and bind intermediately on one of the c subunits.³² Image adapted from Fais *et al.*³³

1.3.3. V-ATPase inhibitors

1.3.3.1. The plecomacrolides Bafilomycin and Concanamycin

The first specific and highly potent discovered V-ATPase inhibitor was the plecomacrolide Bafilomycin³⁴, which was originally isolated from *Streptomyces griseus*. Together with another classical V-ATPase inhibitor Concanamycin, they were already identified and structurally described in the early 1980s.³⁵⁻³⁷ So far, two independent studies showed, that plecomacrolides bind foremost at the V_0 subunit c.^{38,39} In 2005, Wang *et al.* proposed a minor participation of the subunit a in the binding of plecomacrolides.⁴⁰ It is likely that the plecomacrolides bind at the interface between subunit a and c leading to a mechanical

blocking of the rotation of the c-ring and therefore inhibiting the translocation of protons across membranes.¹³

1.3.3.2. Benzolactone enamides

This group of V-ATPase inhibitors are found in various organisms like tunicates (Lobatamides), pseudomonas (Oximidines) and sponges (Salicylhalamides).¹³ For this group a clear binding site could not be distinguished, yet. Salicylhalamide seems to bind to the V_0 complex and together with Apicularen it doesn't interfere with the plecomacrolid binding site.^{8,41} Furthermore Apicularen does not interfere with the binding site of Archazolid.⁴²

1.3.3.3. The novel class of macrolactones: the Archazolids

The Archazolids are a novel group of V-ATPase inhibitors. Höfle *et al.* were the first isolating Archazolid A and B from cultivated myxobacteria *Archangium gephyra* Ar 3548. Also in *Cystobacter violaceus* Archazolids could be found.⁵ Structurally they are composed of a macrocyclic lactone ring with a thiazole side chain.⁴³ During competition assays with Concanamycin, using the radioactively labelled J-concanolide A, it could be clearly determined that Archazolid at least in part binds to the V_0 subunit c of the V-ATPase.⁸ Furthermore, Archazolid seems to specifically and very potently (IC_{50} values in the nanomolar range) inhibit the V-ATPase when compared with purified Na^+/K^+ -ATPases and mitochondrial F-ATPase.⁸

In contrast to the plecomacrolides, Archazolid does not penetrate in between two c subunits, more likely it binds to the membrane facing side of a single subunit c. Speculations of the functions therefore might be that Archazolid could act like a wedge between the subunit a and the c-ring, which would avoid the rotation. A further possibility would be that Archazolid masks the essential glutamate and therefore inhibits the proton binding.¹³

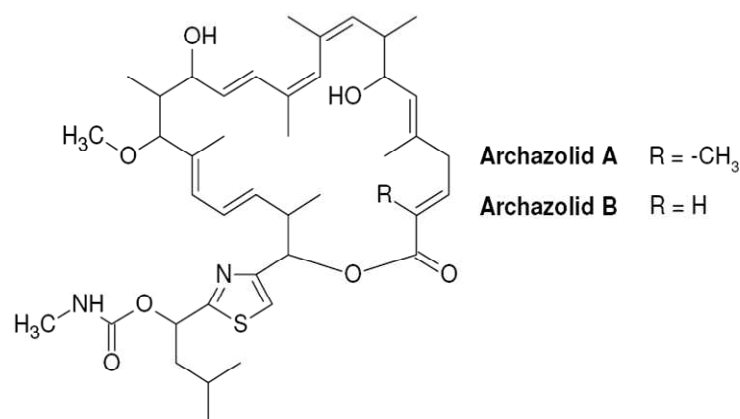


Figure 1.2: Structure of Archazolid A and Archazolid B. Chemical structure from Huss *et al.*⁸

1.4. Metastatic cancer

Nowadays, cancer is a major cause of mortality.⁴⁴ The first treatment option is still the surgical removal of the primary tumors usually followed by radiotherapy. But for the treatment of metastasis the use of chemotherapeutics is necessary.³ Even though the development of highly effective chemotherapeutics increased during the last years, the toxic side effects and the development of resistance are still main problems.¹ Affecting cell death, the metastatic process and trafficking processes like endocytosis would be key goals in the field of cancer research.

1.4.1. Cell death - apoptosis

One form of cell death is the programmed cell death, also called apoptosis. Apoptotic steps are important in development and tissue homeostasis; but its signaling is also shown to be important in many diseases such as cancer.⁴⁵ Apoptosis is usually described with a number of morphological features, like membrane blebbing, cytoplasmatic shrinkage, loss of phospholipids asymmetry, nuclear condensation and DNA fragmentation. Upon completion of apoptosis, cells break up into a series of membrane bound bodies called *apoptotic bodies* which contain normal but condensed chromatin.⁴⁶ Classically, the events of caspase-dependent apoptosis are divided in two major pathways:

1. The extrinsic or receptor-mediated apoptotic pathway.
2. The intrinsic or mitochondrial apoptotic pathway

The extrinsic pathway is induced by an extracellular event, usually the binding of ligands to its receptors on the cell surface, like TNF, Fas Ligands or Trail/Apo2L. Upon induction of this pathway a Death Inducing Signal Complex (DISC) is formed, leading to the activation of caspase-8, which then either directly activates caspase-3, leading to cell death or induces the mitochondrial pathway by the cleavage of the pro-apoptotic protein Bid.⁴⁷

The intrinsic pathway is a mitochondria-dependent signaling pathway, which is regulated by the Bcl-2 family and the activation of caspases. The balance of anti-apoptotic members (Bcl-2, Bcl-X_L, Ced-9, Bcl-w and Mcl-1) and pro-apoptotic members (like Bak or Bax) of the Bcl-2 family decides if cytochrome c is released from the mitochondria to activate caspases to finally induce cell death.

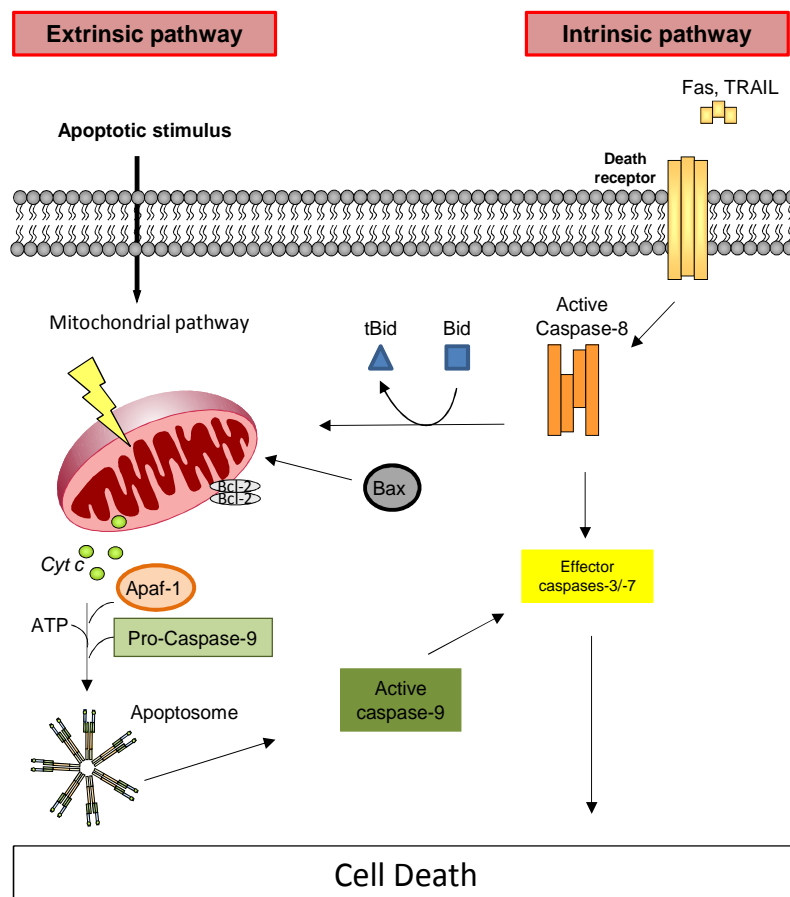


Figure 1.3: The caspase-dependent apoptotic pathways: the intrinsic and extrinsic signaling. When apoptotic cell death is induced due to internal stress response, cytosolic pro-apoptotic molecules like Bax oligomerize and translocate to the outer mitochondrial membrane. This initiates the permeabilization of the outer mitochondrial membrane, which causes the release of pro-apoptotic molecules like cytochrome c, AIF (apoptosis-inducing factor) or SMAC (second-mitochondria-derived activator of caspases). Cytochrome c forms together with Apaf-1 (apoptotic-protease-activating-factor-1) and the caspase-9, the apoptosome, which can activate the downstream caspase-3 and this leads finally to cell death.⁴⁸ If apoptosis is induced via the extrinsic pathway, the induction of a death receptor signal induces the activation of caspase-8, which can

directly activate caspase-3 or leads over the connection of the pro-apoptotic molecule tBid to the cell death signal via the mitochondria.⁴⁷

1.4.2. Formation of metastasis

The formation of metastasis are described as the high point of neoplastic progression.² During the metastatic process, single cells separate from the primary tumor and invade in the surrounding tissue to enter the microvascular system of the lymph and bloodstream. Invasive cancer cells are resistant to apoptosis and anoikis (cell death induction when cells are maintained in suspension) to be able to survive in the bloodstream. They get translocated to distant tissues and leave the bloodstream to finally adapt to the foreign microenvironment and start to proliferate forming a secondary tumor. Beside the resistance to apoptosis/anoikis, various survival signaling pathways are deregulated.^{1,49}

1.4.3. The cell migration process

The cellular migration can be described as a process in various steps. The first step is the polarization of the cell including the formation of lamellipodia and filopodia. The lamellipodia are highly dynamic and broad membrane protrusions of condensed F-actin and are assembled at the leading edge of the cell in a Rho - GTPase (Rac1) - dependent manner. In contrast to lamellipodia, filopodia are thin protrusions and act as tactic sensors to establish the directionality of the movement. By the formation of adhesion complexes under the leading edge, like integrins, the cell gets attached to the substratum and can extend and stretch the cell body in the direction of migration. To pull the rear of the cells forward, the actin-stress fibers contract in dependency of myosin II and the Rho - GTPase Rho A. Also adhesions at the rear of the cell have to be disassembled. After the contraction state this cycle starts again with the formation of the leading edge.⁴⁹

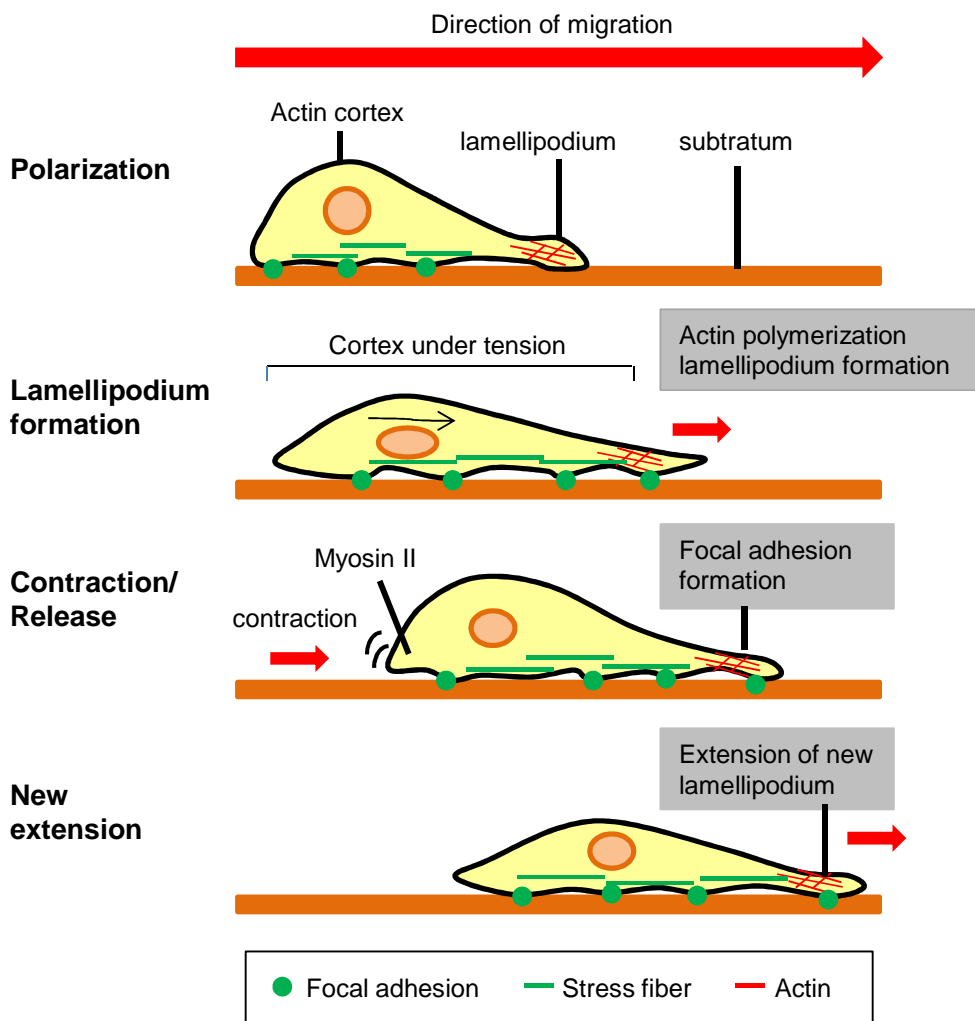


Figure 1.4: Cell migration process. For the forward movement, the cell polarizes due to the re-organisation of the cytoskeleton, like the formation of lamellipodia and filopodia. Also focal adhesions are formed to attach the cell to the substratum. The formation of stress fibers helps to contract the cells between the focal adhesions. The assembly and disassembly of focal contacts is necessary for the forward movement of the cell. Image adapted from Weinberg *et al.*⁴⁹

1.4.4. The signaling during cell migration

Upon chemically attraction like the binding of growth factors to its receptors, the cellular migration signaling is induced. The active growth factor receptor complex associates with the phosphoinositid-3-kinase (PI3K), which gets activated upon growth factor binding. It phosphorylates PtdIns-2,4-P₂ to PtdIns-2,4,5-P₃, which is bound to the cell membrane. By the binding of PtdIns-2,4,5-P₃ to AKT via its hydrophobic part, AKT gets localized to the plasma membrane. AKT is known to be a regulator in cell survival, growth, angiogenesis and metabolism.⁵⁰ Furthermore it plays a major role in the process of cell migration and recycling.^{51,52} AKT gets fully activated by the phosphorylation at two sites, the T308 and

more importantly the S473.^{52,53} Activated AKT as central mediator of the PI3K pathway has multiple downstream effectors all involved in the mentioned cellular processes.⁵²

The Rho-GTPases are a subgroup of the Ras superfamily of GTPases. They regulate the cell morphology and actin cytoskeleton and are therefore necessary during cell migration.⁵⁴ Rho GTPases are cycled between a GTP (guanosine triphosphate) - and a GDP (guanosine diphosphate) - bound state. The active GTP – bound - conformation can be promoted by guanine - nucleotide exchange factors (GEFs) but also the activation involving the recycling molecule Rab5 could be recently shown.^{55,56} Furthermore the GTP hydrolysis is performed by the GTPase - activating protein (GAP), which converts the protein in its inactive conformation. The cycle of GDP - to GTP - bound stage can be induced by growth factors receptor or integrin activation.⁵⁷ The most characterized members of the Rho - GTPase family are Rac1, Rho and Cdc42. Rac1 is a main regulator to induce actin polymerization and the formation of lamellipodia at the cell front of migrating cells. Cdc42 provokes the formation of filopodia, which act as tactic sensors. Whereas Rho is involved in the contraction of the cell and induces the formation of stress fibers.⁵⁷ The regulation during the migration process is also visualized in more detail in the Figure below.

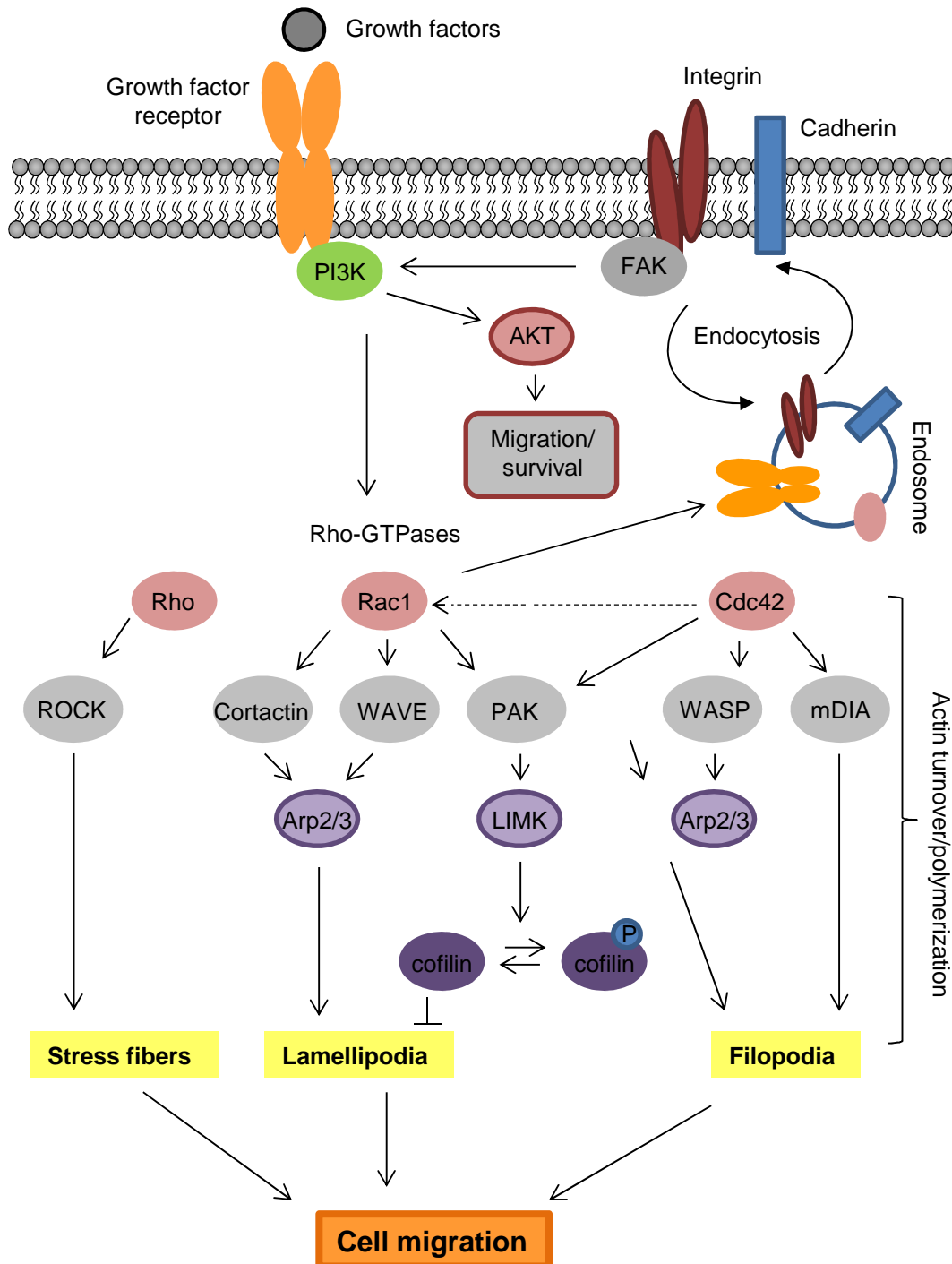


Figure 1.5: Signaling during the process of cell migration. PI3K gets activated by a growth factor stimulus and accumulates at the leading edge. The AKT-pathway and the Rho-GTPases get activated and further downstream signaling is induced. Localized at the leading edge, Rac1 is involved in the induction of actin polymerization and lamellipodia formation. Filopodia, are especially regulated by Cdc42 and act as sensors of the extracellular environment. By disassembly of adhesions and the shortening of the microtubule, Rho A is activated, which regulates the formation of stress fibers and cell contraction, which finally translocates the nucleus and the cell body in the direction of migration. During the migration process adhesion-molecule, like integrin and cadherin are expressed, helping to attach the cell to the substratum. During the forward movement adhesion molecules as well as the Rho-GTPase Rac1 need to be recycled or degraded via endocytotic processes.

1.4.5. Endocytosis

Many years the process of endocytosis was regarded as the simple internalization of nutrient and membrane-associated molecules. However, nowadays knowledge describes endocytosis as a main regulator of cellular signaling, by which signals not only get extended but foremost increase their diversity and specificity. The signaling persists during the endocytotic route and the intracellular endocytotic stations attenuate the signals in space and time.⁵⁸ Especially the recycling of receptors and re-localization at the plasma membrane seem to be major mechanisms in processes like cell migration, apoptosis, mitosis or cell fate determination. All these processes are important players in the development of invasive cancer.^{58,59}

Classically, soluble molecules like nutrients or cell-surface receptors and their bound ligands get internalized via the well characterized clathrin-mediated endocytosis (CME). The non-clathrin-mediated endocytosis is still quite undefined. After ligand binding, adaptor proteins like AP-2 or β -arrestin help to recruit the receptors close to clathrin. Clathrin polymerizes and the endocytotic pit is formed, which will be released in the cytoplasm. This process is regulated by the GTPase dynamin and dependent on the endocytotic regulator Rab5. In further steps the receptor is shuttled to early endosomes, where they continue to signal in an endosome-specific manner. The recycling in the endosomal system is controlled by the small GTP-binding proteins Rab and Arf (ADP-ribosylation factor) families. In early endosomes the decision is made if the receptor will be either recycled back to the cell surface or will get ubiquitinated, shuttled to late endosomes and degraded in lysosomes.⁵⁹ The endocytotic process is dependent on the acidic pH in endosomes and lysosomes which is mainly regulated by the V-ATPase.¹⁶

The activation of for example the Rho GTPase Rac1 is related to the described recycling process. Rac1 gets activated in the early endosomes via its GTP exchange factor Tiam in a Rab5-dependent manner. Since Rac1 is a main regulator of the actin cytoskeleton, its recycling and re-localization is important for the process of cell migration.⁵⁶

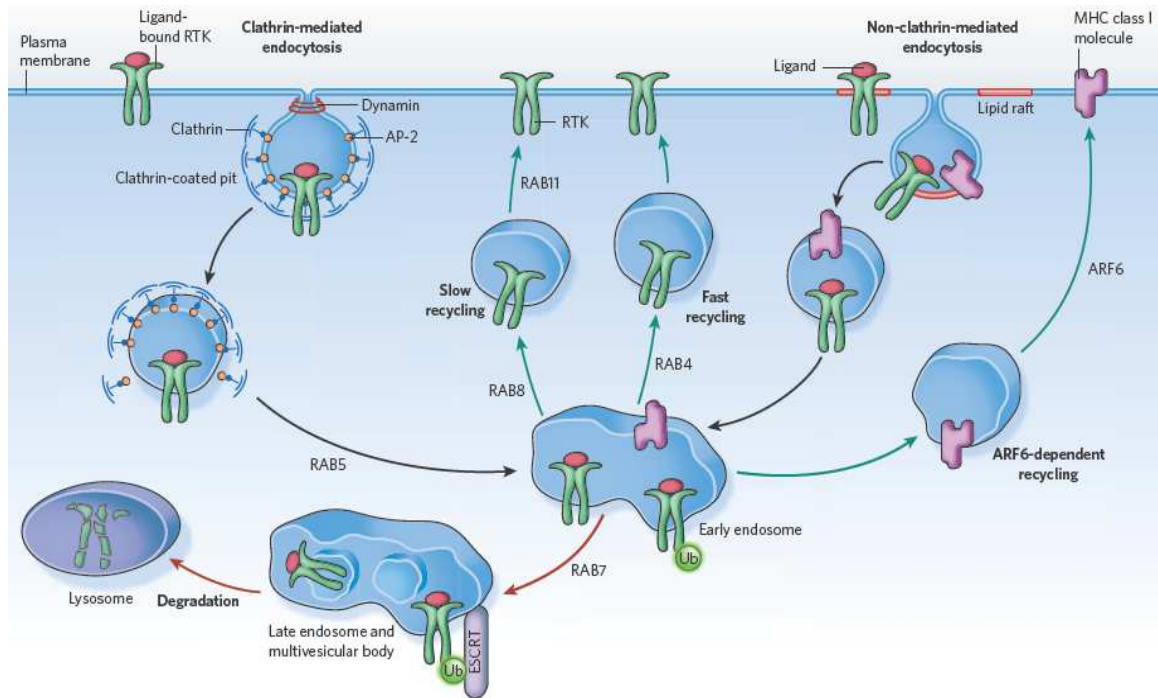


Figure 1.6: The endocytotic process. During clathrin-mediated endocytosis foremost plasma membrane signaling receptors such as receptor tyrosine kinases get internalized in clathrin coated pits. Receptors are shuttled to early endosomes where the decision of recycling or degradation of the receptor is made. One non-clathrin mediated endocytotic pathway, the recycling of the major histocompatibility complex (MHC) class I molecules is described to be recycled in an Arf6-dependent manner. Image adapted from Scita *et al.*⁵⁹

In the following study we wanted to characterize the new V-ATPase inhibitor Archazolid B as potential new drug to inhibit tumor cell proliferation, to induce apoptosis and to inhibit tumor cell migration. Moreover we wanted to elucidate in detail the signaling leading to the inhibition of cell migration.

MATERIAL AND METHODS

2.1. Materials

2.1.1. Compounds

Archazolid B as well as its precursor molecule were generously donated by Prof. Dr. Dirk Trauner (Department of Biochemistry, LMU Munich). Concanamycin A was purchased from Enzo Life Sciences GmbH (Lörrach, Germany)

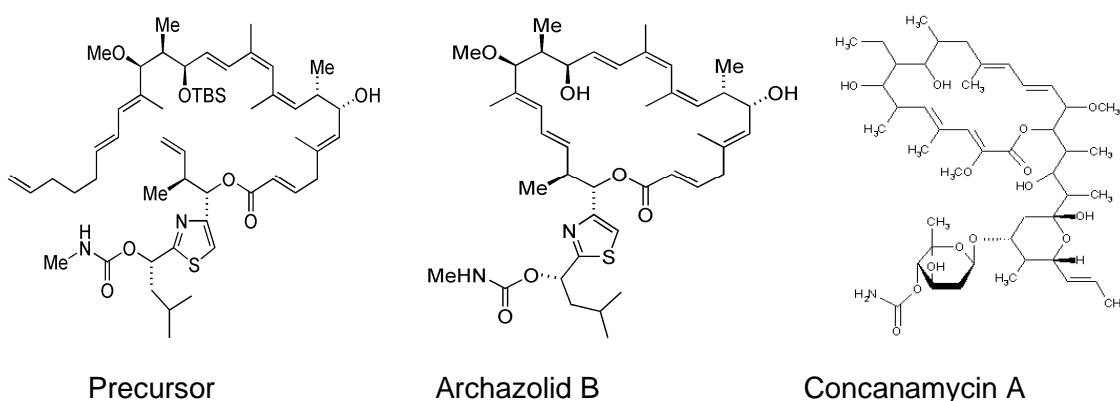


Figure 2.1: Chemical structures of precursor molecule of Archazolid B synthesis, Archazolid B⁶⁰ and Concanamycin A (Enzo Life Sciences, Lörrach, Germany).

2.1.2. Biochemicals, inhibitors, dyes and cell culture reagents

Table 2.1: Biochemicals, inhibitors, dyes and cell culture reagents

Reagent	Producer
Accustain® formaldehyde	Sigma Adrich, Taufkirchen, Germany
Ac-DEVD-AFC (Caspase-3)	Bachem, Bubendorf, Germany
Ac-LETD-AFC (Caspase-8)	Bachem, Bubendorf, Germany
Bradford Reagent TM	Bio-Rad, Munich, Germany
Collagen G	Biochrome AG Berlin, Germany
Complete®	Roche Diagnostics, Penzberg, Germany
DMEM	PAA Laboratories, Cölbe, Germany
DMSO	Sigma-Aldrich, Taufkirchen, Germany
FCS gold	PAN Biotech, Aidenbach, Germany
Formaldehyde, 16% ultrapure	Polysciences Europe GmbH, Eppelheim
Glutamine	Sigma-Aldrich, Taufkirchen, Germany
Glycine	Sigma-Aldrich, Taufkirchen, Germany
JC-1 iodide	Axxora, Lörrach, Germany

McCoy's medium	PAA Laboratories, Cölbe, Germany
M199 Medium	PAN Biotech, Aidenbach, Germany
Matrigel™	BD Discovery Labware, Bedford, MA, USA
Na ₃ VO ₄	ICN Biomedicals, Aurora, Ohio, USA
NaF	Merck, Darmstadt, Germany
Non-essential amino acids	PAA Laboratories, Cölbe, Germany
Page Ruler™ Prestained Protein Ladder	Fermentas, St. Leon-Rot, Germany
Polyacrylamide	Roth GmbH, Karlsruhe, Germany
Propidium iodide	Sigma-Aldrich, Taufkirchen, Germany
PermaFluor mounting medium	Beckman Coulter, Krefeld, Germany
PMSF	Sigma Aldrich, Taufkirchen, Germany
Pyruvate	Merck, Darmstadt, Germany
Q-VD-OPh	R&D Systems, Wiesbaden, Germany
Rhodamin-phalloidin	Invitrogen, Karlsruhe, Germany
RPMI 1640	PAA Laboratories, Cölbe, Germany
Tris-HCl	Sigma-Aldrich, Taufkirchen, Germany
Triton X-100	Merck, Darmstadt, Germany

Table 2.2: Commonly used buffers

PBS + Ca²⁺/Mg²⁺ (pH 7.4)		PBS (pH 7.4)	
NaCl	137 mM	NaCl	132.2 mM
KCl	2.68 mM	Na ₂ HPO ₄	10.4 mM
Na ₂ HPO ₄	8.10 mM	KH ₂ PO ₄	3.2 mM
KH ₂ PO ₄	1.47 mM	H ₂ O	
MgCl ₂	0.25 mM		
H ₂ O			

2.1.3. Technical equipment

Table 2.3: Technical equipment

Name	Device	Producer
AB7300 RT-PCR	Real-time PCR system	Applied Biosystems, Fosterer City, CA, USA
Axiovert 200	Inverted microscope	Zeiss, Jena, Germany

Culture flasks, plates, dishes	Disposable cell culture material	TPP, Trasadingen, Switzerland
Curix 60	Tabletop film processor	Agfa. Cologne, Germany
Custom-made climate chamber	Life cell observation on LSM 510 Meta	EMBLEM Heidelberg, Germany
FACSCalibur	Flow cytometry	Becton Dickinson, Heidelberg, Germany
FACSCanto II	Flow cytometry	Becton Dickinson, Heidelberg, Germany
IBIDI™ μ -slide	Microscope slide	Ibidi GmbH, Munich, Germany
LSM 510 Meta	Confocal laser scanning microscope	Zeiss, Jena, Germany
Mikro 22 R	Table centrifuge	Hettich, Tuttlingen, Germany
Nanotrop R ND-1000	Spectrophotometer	Peqlab, Wilmington, DE, USA
Odyssey 2.1	Infrared Imaging System	Li-Cor Biosciences, Lincoln, NE, USA
SpectraFluor Plus™	Microplate multifunctional reader	Tecan, Männedorf, Switzerland
Sunrise™	Microplate absorbance reader	Tecan, Männedorf, Switzerland
Transwell plates	Boyden chamber assays	Corning Inc., Life Sciences, Lowell, MA, USA
Vicell™ XR	Cell viability analyzer	Beckman Coulter, Fullerton, CA, USA

2.2. Methods

2.2.1. Cell culture

The human urinary bladder carcinoma cell line T24 was kindly provided by PD Dr. Barbara Mayer (Klinikum Grosshadern, LMU Munich, Germany). The human pancreatic cancer cell line L3.6pl was obtained as a generous gift by Christine J. Bruns (Department of Surgery, Klinikum Grosshadern, LMU Munich, Germany). T24 cells were maintained in McCoy's medium (PAA Laboratories, Cölbe, Germany) respectively supplemented with 10% heat-inactivated fetal calf serum (FCS) (PAA Laboratories, Cölbe, Germany), 1% Glutamin (Sigma-Aldrich, Taufkirchen, Germany). The L3.6pl cells were cultivated on

0.001% collagen G - coated culture flasks in RPMI 1640 medium (PAA Laboratories, Cölbe, Germany) respectively supplemented with 10% FCS, 1% pyruvate (Merck) and 1% non-essential amino acids (PAA Laboratories, Cölbe, Germany). Hela cells (from ATCC) were grown in DMEM medium supplemented with 10% South American serum (EuroClone) and 1% L-glutamine. All cell lines were kept at 37°C in a humidified 5% CO₂ atmosphere.

For splitting (1:10) and seeding, cells were washed once with pre-warmed PBS, which was removed completely with a sterile pipette. 3 ml Trypsin/EDTA (T/E) was added (75 cm² flask) and cells were incubated for a few minutes at 37°C (T24: 1-2 min; L3.6pl/Hela: 5 min). To terminate the trypsin reaction 7 ml medium containing FCS was added. Further, cells were centrifuged for 5 minutes at 1,000 rpm to remove the T/E. The supernatant was discarded and cells were resuspended in growth medium and seeded into flasks or well plates. (In case of L3.6pl all plates and flasks were coated with 0.0001% collagen G). Cell concentration and viability was measured using the VICELL™ cell viability analyzer (Beckman Coulter, Krefeld, Germany).

Table 2.4: Trypsin/EDTA and collagen G composition

Trypsin/EDTA		Collagen G	
Trypsin	0.05%	Collagen G	0.001%
EDTA	0.20%	PBS	
PBS			

2.2.2. Freezing and thawing

To prepare nitrogen stocks of all cell lines, cells were trypsinized and centrifuged (180 x g, 10 min, 4°C). Cells were resuspended in freezing medium and transferred to cryovials (2 x 10⁶ cells in 1.5 ml). Cells were first frozen overnight at -20°C and then transferred to -80°C. Cell stocks were either kept in -80°C or transferred to nitrogen (-196°C) for long-term storage.

2.2.3. Flow cytometry

This method was used to analyze cell death, mitochondrial membrane potential change or the determination of cell surface molecules, like epidermal growth factor receptor (EGFR). Measurements were done with two different FACS machines, the FACSCanto II or FACSCalibur (Becton Dickinson, Heidelberg, Germany).

Table 2.5: Facs buffer for Facs Calibur

Sheat fluid	
NaCl	8.12 g
KH ₂ PO ₄	0.26 g
Na ₂ HPO ₄	2.35 g
KCl	0.28 g
Na ₂ EDTA	0.36.g
LiCl	0.43 g
NaN ₃	10 mM
H ₂ O	ad 1.0 l, pH 7.37

2.2.3.1. Quantification of apoptotic cell death with the Nicoletti assay

T24 or L3.6pl cells were seeded in 24 well plates (50,000 cells/well). The next day cells were treated with Archazolid B in various concentrations for various time periods. The caspase-inhibitor QVD-OPh (R&D Systems, Inc.) was added 2 hours before treatment with Archazolid B in a concentration of 10 μ M. The propidiumiodide staining was performed as described by Nicoletti *et al.*⁶¹

After the treatment points, medium of each well was collected and still adherend cells were trypsinized with T/E. Trypsinized cells were pooled with their according medium and centrifuged (600 x g, 10 min, 4°C). Supernatant was discarded and cells were once washed with PBS (600 x g, 10 min, 4°C). For the staining, cells were resuspended in HFS - solution containing 50 μ g/ml PI and incubated overnight at 4°C followed by analysis via flow cytometry. Cells containing hypoploid DNA were considered as dead.

Table 2.6: HFS solution

HFS-solution	
Sodium citrate	0.1%
Triton X-100	0.1%
PBS	ad 1 ml

2.2.3.2. Cell cycle analysis

Using the fluoresecence channel 2 (FL2, em585) the fluorescence intensity was measured in the logarithmic mode using the flow cytometry. Propidiumiodide intercalates in the DNA. Since iodide-fluoresecence depends on the status of cellular chromatin, the different cell cycle status can be distinguished. Most cells are in the G₀/G₁ cell cycle phase with 2n chromosome set, lacking the sister chromatids. Cells in the G₂/M phase are in the process

of cell division. This means that these cells have $2n$ chromosome set, but furthermore the sister chromatids as duplicates. This sister chromatide duplication allows the differentiation of the G_2/M -phase to G_0/G_1 -phase. Via flow cytometry this can be distinguished by the higher fluorescence peak due to the increased amount of propidium-iodide intercalation. The S-phase is the synthesis-phase. In this phase cytosol is accreted and chromatids become duplicated. This fluorescence peak is located between the fluorescence peaks of G_0/G_1 and G_2/M -phase. Furthermore, during apoptotic processes DNA becomes condensed and fragmented, generating a peak which is located left of the G_0/G_1 fluorescence. Using the Flow cytometry analysis software FlowJo 7.6, regions for each fluorescence peak according to their chromatin states (percentages of cells in the single cell cycle states) were measured and set into relation of the total cell number.

2.2.3.3. Measurement of mitochondrial potential change

T24 and L3.6pl were treated with Archazolid B for 24 hours. Cells were harvested as described (2.2.3.1.) and washed once with 0.5% BSA/PBS. Subsequently, 5, 5', 6, 6'-tetraethylbenzimidazol-carbocyanine iodide (JC-1) was directly added into the vials with a final concentration of $1.25 \mu\text{M}$. Then, cells were incubated for 15 minutes, 37°C . After centrifugation ($600 \times g$, 5 min, RT) samples were resuspended in 0.5% BSA/PBS and analyzed by flow cytometry using FACSCanto II (Nectin Dickinson, Heidelberg, Germany). The increase in green fluorescence (FITC-A channel) indicates loss of mitochondrial membrane potential.

2.2.3.4. Measurement of cytochrome c release

Cytochrome c release was performed as described in Waterhouse *et al.*⁶² Cells were seeded and treated with Archazolid B for 48 hours. Supernatant and trypsinized cells were centrifuged ($600g$, 4°C , 10 min) and washed once with ice cold PBS. Cells were permeabilized using the digitonin-containing buffer and incubated for 30 minutes on ice. Cells were centrifuged ($600 \times g$, 4°C , 10 min) and fixed with 4% PFA for 20 minutes. Samples were washed twice with PBS and incubated with blocking buffer for 1 hour, RT. $50 \mu\text{l}$ of 1:200 diluted cytochrome c antibody (Cell Signaling Technology, Danvers, MA, USA) was added and samples were incubated at gentle agitation overnight at 4°C . The next day, samples were washed twice with PBS and incubated with the fluorescein isothiocyanate (FITC)-labeled second antibody (1:200) for 1 hour, RT. Samples were washed again with PBS and redissolved in $500 \mu\text{l}$ PBS. Using the FACS Calibur, the amount of cytochrome c in remaining in the mitochondria was measured.

Table 2.7: Buffer for cytochrome c release measurement

Digitonin-containing buffer		Blocking buffer	
Na-EGTA	0.2 mM	BSA	3 %
KCl	100 mM	Saponine	0.05 %
Digitonin	50 µg/ml	PBS	
PBS			

2.2.3.5. Measurement of EGF-R on the cell surface

T24 and L3.6pl were treated with Archazolid B for 24 hours. Cells were harvested as described (2.2.3.1.) and washed twice with 0.5% BSA/PBS. The EGF-R-FITC antibody (R&D Systems, Wiesbaden, Germany) was diluted 1:5 in 0.5% BSA/PBS and 50 µl were added per sample. Samples were carefully mixed and incubated for 30 - 45 minutes at 4°C. After the incubation period, samples were centrifuged (600 x g, 5min, 4°C). Cell pellet was washed twice with 500 µl of 0.5% BSA/PBS. Finally, cell pellet was carefully resuspended in 200 µl of 0.5% BSA/PBS and analyzed via flow cytometry (FL-1) using the FACSCalibur (Becton Dickinson, Heidelberg, Germany). The mean fluorescence was calculated using the Cellquest Pro software of BD Bioscience. The histogram overlays were done with the Flow cytometry analysis software FlowJo 7.6.

2.2.4. Cell proliferation

1500 cells/well were seeded in 96 well plates. The next day, various concentrations of Archazolid B/Concanamycin A were added. After 72 hours of incubation, supernatant was removed and cells were stained with crystal violet for 10 minutes, RT. Carefully, wells were rinsed with water to remove unbound crystal violet and cells were dried. Crystal violet was resolved with sodium citrat and the absorbance of crystal violet, which correlates with the cell number, was measured at 550 nm at the SpectraFluor Plus™ (Tecan, Männedorf, Austria). For statistical analysis, untreated cells were set to 100% viable cells.

Table 2.8: Crystal violet and sodium citrat solution

Crystal violet		Sodium citrat solution	
Crystal violet	0.5 %	Na ₃ citrate	0.05 M
Methanol	20 %	Ethanol	50 %
H ₂ O		H ₂ O	

2.2.5. Clonogenic assay

L3.6pl/T24 cells were seeded as usual and treated the next day for 24 hours with Archazolid B in various concentrations. After treatment, cells were trypsinized and 10,000 L3.6pl/5,000 T24 cells were seeded in a 6-well plate. In case of transfection with siRNA-ATP6L (V-ATPase subunit c), cells were freshly seeded after 24 hours of transfection. The cells were allowed to grow for 6 days. Similar to the proliferation assay, cells were stained with crystal violet for 10 minutes. Wells were rinsed carefully with water to remove unbound crystal violet. Pictures of the wells were taken and finally crystal violet was redissolved with sodium citrate solution to measure absorption at 550 nm in a SpectraFluor Plus™ (Tecan, Männedorf, Austria). For statistical analysis, untreated cells were set to 100% viable cells.

2.2.6. Measurement of caspase-activity

Cells were seeded and treated for 48 hours with Archazolid B. Supernatant was discarded and adherend cells were washed twice with ice cold PBS. Lysis buffer was added and samples were frozen at -80°C overnight. The next day, cells were harvested using a cell scraper and the collected lysate was centrifuged (10,000 rpm, 4°C, 10 min). Protein concentrations were determined using the method of Bradford *et al.*⁶³ (described in the chapter 2.2.15.2 Protein quantification)

For the measurement 10 µl of each sample was pipetted into a black 96-well plate. 90 µl of freshly prepared substrate solution was added to each well. In case of activated caspases, the substrates were cleaved indicated by a fluorometric shift. Measurements were done at the time points 0 and after 5 hours using the SpectraFluor Plus™ (Tecan, Männedorf, Austria).

Table 2.9: Buffer for caspase-activity measurement

Lysis buffer		Buffer B (pH 7.5)	
MgCl ₂	203.4 mg	HEPES	50 mM
EGTA	76 mg	Sucrose	1%
Triton X-100	200 µl	CHAPS	0.1 %
HEPES	25 mM	H ₂ O	
H ₂ O	up to 400 ml		

Table 2.10: Caspase-substrate solution

Substrate solution	
Buffer B	8 ml
Caspase-3/-8 substrate	45 μ l
DTT 16 %	100 μ l

2.2.7. Gene expression profiling

2.2.7.1. RNA Isolation

Total RNA was isolated using the RNeasy Kit (Qiagen, Hilden, Germany) according to the manufacture's instruction. RNA was eluted in TE/water. RNA concentrations were determined using the NanoDrop spectrophotometer (NanoDrop Technologies, Wilmington, Germany).

2.2.7.2. Reverse Transcription

For the reverse transcription of the RNA into cDNA, 2 μ g RNA were used and re-transcribed using the high capacity cDNA Reverse Transcription Kit (Applied Biosystems, Foster City, CA, USA), which includes random primers. The reaction was run for 2 hours at 37 °C. cDNA was stored at 4°C until qRT-PCR/microarray was performed.

2.2.7.3. Quantitative Real-Time PCR

For the Quantitative Real-Time PCR the ABI 7300 RealTime PCR system with the TaqMan Universal PCR Mastermix (Life Technologies Corporation, Carlsbad, CA, USA) was used. Probe and primers for the V-ATPase subunit c (ATP6L) were supplied as mix (Life Technologies Corporation, Carlsbad, CA, USA). As housekeeping gene, GAPDH was used (forward/reverse primer, probe sequence, biomers, Ulm, Germany). For the comparison of the ATP6L-expression level in T24 and MCF-10A cells the 18S rRNA (Life Technologies Corporation, Carlsbad, CA, USA). Fluorescence development was analyzed using the ABI 7300 system software. Calculation of relative mRNA was done according to Pfaffel⁶⁴

2.2.7.4. Polymerase-chain-reaction (PCR)

To compare the level of V-ATPase subunit c expression in various cell lines, a PCR was performed using cDNA of various cell lines which are characterized by different invasive

potential. For each reaction 2 μg of cDNA was used. The PCR Mastermix contained 10 x Reaction buffer (Invitrogen, Darmstadt, Germany), TaqPolymerase (Invitrogen, Darmstadt, Germany) and the forward and reverse primer for the V-ATPase subunit c (ATP6L) (biomers, Ulm, Germany). Following PCR program was used. To analyze the result of the PCR, samples were loaded on a 2% Agarose gel.

Tab.2.11: PCR conditions

PCR conditions	
94°C	5 min
(30 Zyklen)	
94°C	30 sec
55°C	30 sec
72°C	30 sec
72°C	5 min
4°C	∞

2.2.7.5. Microarray

The microarray was done in collaboration with the group of Prof. Dr. Efferth, University of Mainz, Germany. The procedure is described briefly as followed.

1) Probe Labeling and Illumina Sentrix BeadChip array Hybridization

The labeling of cRNA was performed based on the modified Eberwine protocol.^{65,66} 250-500 ng of RNA was used for the synthesis of complementary DNA (cDNA). This was followed by an amplification/labeling step (in vitro transcription) to synthesize biotin-labeled cRNA according to MessageAmp II aRNA Amplification kit (Ambion, Inc., Austin, TX) and Biotin-16-UTP (Roche, Penzberg, Germany). The cRNA was purified using the Total Prep RNA Amplification Kit. To control the quality of the RNA, a RNA Nano Chip Assay and Agilent 2100 Bioanalyzer was used and furthermore RNA was quantified spectrophotometrically using the NanoDrop.

100 ng cRNA/ μl diluted in GEX-HCB buffer (Illumina Inc.) was used to perform the hybridization at 58°C, 20 hours in a wet chamber. Spike-in controls for low, medium and highly abundant RNAs were added, as well as mismatch control and biotinylation control oligonucleotides. The microarrays were washed once in High Temp Wash buffer (Illumina Inc.) at 55°C, followed by two washing steps in E1BC buffer (Illumina Inc.) for 5 minutes, RT. In

between microarrays were washed with ethanol. Microarrays were blocked for 5 min in 1% (wt/vol) Blocker Casein in phosphate buffered saline Hammarsten grade (Pierce Biotechnology, Inc., Rockford, IL). For the development of the signals, microarrays were incubated for 10 min in 2 ml of 1 µg/ml Cy3-streptavidin (Amersham Biosciences, Buckinghamshire, UK) solution and 1% blocking solution, followed by a last washing step in E1BC. Finally, the microarrays were dried and scanned.

2) Scanning and data analysis

To scan the arrays, the Beadstation array scanner was used. The setting was adjusted to a scaling factor of 1 and PMT settings at 430. Data extraction was done for all beads individually, and outliers are removed when > 2.5 MAD (medium absolute deviation). All remaining data points were used for the calculation of the mean average signal for a given probe, and standard deviation for each probe was calculated, too.

Using the quantile normalization algorithm without background subtraction, measured signals were normalized and differentially regulated genes are defined by calculating the standard deviation differences of a given probe in an one-by-one comparison of samples or groups.

3) Microarray data analysis

The expression data were analyzed using Chipster (<http://chipster.csc.fi/>); genes were filtered, which vary in expression and significance. 250-900 genes were filtered and a subsequent assessment of significance using empirical Bayes t-test was done. All considered genes have assigned p-values < 0.05 . Filtered data was applied to Ingenuity pathway analysis for Core analysis. Here networks and pathways influenced by drug treatments were determined (<http://www.ingenuity.com/>).

2.2.8. Transfection of cells with siRNA or plasmids

2.2.8.1. Electroporation (Cell line nucleofactor kit V)

T24/L3.6pl cells were trypsinized and cell number was determined with the VICELL™. For transfection with siRNA 1×10^6 T24 or 1.5×10^6 L3.6pl were centrifuged. Supernatant was discarded and cells were resuspended in 95 µl of transfection buffer. 10 µl of 20µM siRNA Stock (Dharmacon) was added and cell suspension was added in the kit's cuvettes to be electroporized in the AMAXA machine (Program for T24: A-23; L3.6pl: C-19). 500 µl of culture medium with FCS was added directly to the cuvette, helping the cells to recover.

Depending on the experiment either all cells or equal amounts of transfected cells were seeded according to the assay's protocol in normal culture medium. By Real-time PCR the downregulation of the V-ATPase subunit c (ATP6L) was tested. After 24 hours of transfection the best downregulation was achieved. Therefore experiments (Boyden chamber assay, Rac1 pulldown-assays) were continued after 24 hours of transfection.

2.2.8.2. Liposome-based transfection (Fugene, Roche)

250,000 T24 cells were seeded in 6 well plates. After cells have attached properly, cells were transfected with the according plasmids (pCMV-BamHI, pCMV-ATP6L-myc, pCMV-Rab5, pCDNA3-Rac1-HA, pGFP-Rac1-C1, 1014 pRaichu-CRIB/CFP-CRIB-YFP). A transfection mix per sample was prepared containing 1-3 µg of plasmid in 100 µl sterile water. 5 µl of Fugene (Roche, Penzberg, Germany) was added and gently mixed. After incubation (15 min, RT) transfection mix was added to the already seeded cells. After 16 hours of transfection the treatment with Archazolid B followed.

2.2.9. Transmission Electron Microscopy

T24 cells were treated with 10 nM Archazolid B for various time points (0, 5, 15, 30 hours). Cells were collected, centrifuged and resuspended in a fixation solution (2.5% glutaraldehyde in fixative buffer: 75 mM cacodylate, 75 mM NaCl, 2 mM MgCl₂, pH 7.0). After incubation of 1 hour, cells were washed several times in fixative buffer and postfixed in 1 % OsO₄ (diluted in fixative buffer). Finally cells were washed with aqua dest before dehydrated in a graded series of acetone. Finally cells were embedded in Spurr low-viscosity epoxyresin and polymerized at 65°C. Several pictures were taken with a Zeiss EM 912 transmission electron microscope with integrated Ω -filter (in "zero-loss-mode").

2.2.10. Confocal microscopy (staining, LysosomeTracker)

Cells were seeded on IBIDI slides (IBIDI, Martinsried, Germany) (scratch assay: 80,000/well; Lysosome staining: 40,000/well) one day before treatment. After treatment cells were fixed with 4%-paraformaldehyde, 10 minutes, RT. To permeabilize, 0.2% Triton/PBS was added for 2 minutes, RT. For blocking 0.1% Triton, 1% BSA/PBS was added for 10 minutes, RT. Antibodies were diluted in 0.1% Triton, 1% BSA/PBS. Cell samples were incubated with the primary antibodies for one hour, RT. Before the secondary antibody was added, cells were washed three times with PBS+ before adding the secondary

antibody for another hour, RT. Cells were washed three times with PBS+ and once with distilled water. Cell samples were covered with a coverslip using mounting medium.

If cells shouldn't be permeabilized (EGF-R surface staining), no Triton was used and antibodies were diluted in PBS without Triton.

For the lysosome staining 75 nM LysoTracker (Invitrogen) was added into the culture medium and incubated for 30 minutes. To stain the nuclei, Hoechst was added in a final concentration of 0.05 µg/ml and incubated for 5 minutes. Cells were analyzed by confocal microscopy (Zeiss, Oberkochen, Germany) without fixation. Therefore a climate chamber was used (37°C, 5% CO₂).

Table 2.12: Primary antibodies used for confocal microscopy

Antigen	Isotype	Dilution	Provider
Actin	goat	1:100	Santa Cruz
Cortactin	rabbit	1:100	Cell signaling
Ductin (ATP6L)	rabbit	1:100	Millipore
EGF-R	mouse	1:100	Santa Cruz
pAkt (S473)	mouse	1:200	Cell signaling
Rab5A	rabbit	1:100	Santa Cruz
Rac1	mouse	1:100	Upstate

Table 2.13: Secondary antibodies used for confocal microscopy

Antigen	Conjugate	Dilution	Provider
Donkey-anti-goat	AlexaFluor @543	1:300	Molecular Probes
Goat-anti rabbit	AlexaFluor @488	1:300	Molecular Probes
Goat-anti rabbit	AlexaFluor @543	1:300	Molecular Probes
Goat anti-mouse	AlexaFluor @633	1:300	Molecular Probes
Phalloidin-rhodamin	AlexaFluor @543	1:300	Molecular Probes
Phalloidin-FITC	FITC	1:100	Sigma-Aldrich

2.2.11. Migration Assays

2.2.11.1. Wound healing assay

T24 and L3.6pl cells were seeded one day before treatment (Direct treatment: 250,000 cells/well; pre-treatment: 100,000 cells/well). In case of the direct treatment, the 100%

confluent cell layer was scratched using a yellow pipette tip and directly treated with according concentrations of Archazolid B diluted in normal culture medium. In case of the pre-treatment cells were treated at 70% confluence for 24 hours. After that, cells were scratched as described and normal culture medium without Archazolid B was added. The migration assay was run for 16 hours followed by fixation with 3% PFA, 10 minutes, RT. Pictures were taken at the microscope (Axiovert, Zeiss, Oberkochen, Germany). The analysis was done by the WimScratch software (Wimasis, Munich, Germany).

2.2.11.2. Boyden chamber assay

T24/L3.6pl cells were seeded as for other experiments and treated with Archazolid B at a confluence of 70% for 24 hours/16 hours. 100,000 cells/Boyden chamber well (for siRNA experiments with T24: 75,000 cells/ Boyden chamber well) were redissolved in McCoy's culture medium without FCS. Boyden Chambers (Corning Inc., Life Sciences) themselves were coated with 0.0001% collagen G. Transwell chambers with a pore size of either 8.0 μm for L3.6pl cells or 5 μm for T24 cells were used. The bottom of the Boyden chamber contained normal culture medium with 10% FCS (L3.6pl: in addition 100 ng/ml EGF). Cells were allowed to migrate at 37°C, 5% CO₂ (T24: 4 hours; L3.6pl: 20 hours). Cells were fixed and stained with crystal violet. Not-migrated cells on the top of the Boyden chamber were removed with a q-tip.

Pictures of the bottom part of the chamber membrane (migrated cells) were taken using the microscope (Axiovert, Zeiss, Oberkochen, Germany). Counted cells were calculated in comparison to 10% FCS non-treated cells, which represent in this time frame 100% migration.

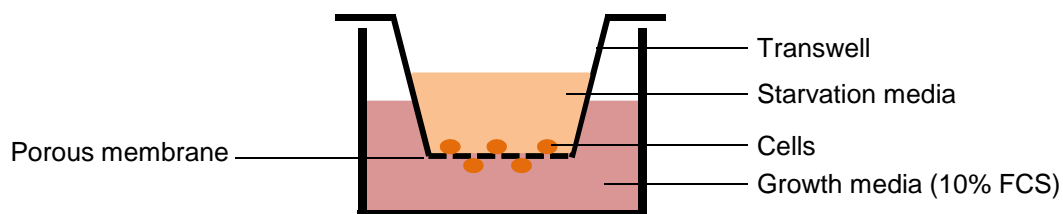


Figure 2.2: Boyden chamber assay. Cells, redissolved in starvation medium, were seeded on top of the Boyden chamber. Cells migrate in direction of the growth medium containing FCS. Migrated cells on the bottom of the porous membrane were fixed and counted.

2.2.11.3. Chemotaxis

For the chemotaxis assay, T24 cells were seeded in "μ-slides Chemotaxis" (IBIDI, Martinsried, Germany). Trypsinized T24 cells were centrifuged (1000 rpm, 5 min) and redissolved in McCoy's medium (PAA) containing 2% FCS to a final concentration of 5×10^6

cells per ml. Cells were seeded as described in the ‘ μ -slide Chemotaxis’ protocol provided by the manufacturer. In case of treatment, Archazolid B was directly added during the seeding process. After 16 hours treatment at 37°C, 5% CO₂, upper and lower reservoirs were filled with culture medium without FCS. To generate a FCS-gradient from 0-10%, culture medium with 30% FCS was filled in the upper reservoir. Chemotaxis was observed over 24 hours by live cell imaging. Thereby, a picture was taken every 10 minutes. Migrating cells were tracked using the manual tracking plug-in Image J (NIH, Bethesda, MD). Furthermore with the chemotaxis and migration tool (IBIDI) of ImageJ tracked cells could be further analyzed. Parameters like the accumulative and the euclidean distance, velocity as well as the y-forward migration index were determined.

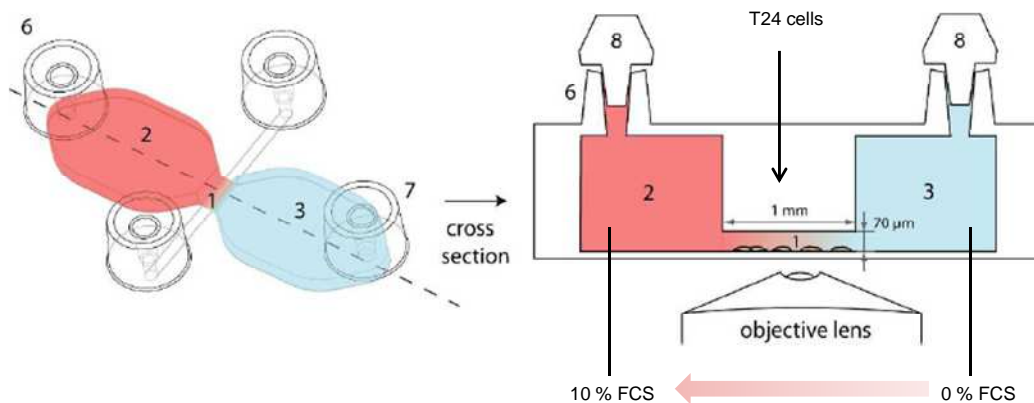


Figure 2.3: Chemotaxis chamber. T24 cells were seeded into the channel (1) and a FCS gradient 1 - 10% was established to allow migration of T24 in direction of the highest FCS concentration. (Image adapted of chemotaxis protocol from IBIDI (Martinsried, Germany))

2.2.12. Cell adhesion/ruffle formation

T24 cells were treated for 24 hours with Archazolid B as described before. μ -slides (IBIDI, Martinsried, Germany) were coated with fibronectin (BD Biosciences, Heidelberg, Germany). 40,000 T24 cells/well were allowed to adhere for 30 minutes at 37°C. Supernatant was discarded and adherend cells were washed with PBS+ once to remove any unbound cells. In a next step, cells were fixed using 4% PFA. Pictures were taken (Axiovert, Zeiss) and cells were counted. Furthermore, the amount of peripheral ruffle formation was calculated relating to the total amount of adherend cells.

In Hela cells, it is possible to distinguish between peripheral, circular dorsal ruffles and invadopodia. Palamidessi *et al*⁶. described that Rab5 overexpression in addition to hepatocyte growth factor (HGF) induce ruffle formation. We overexpressed 2 μ g pCMV-Rab5WT in Hela cells for 24 hours. In addition, transfected Hela cells were treated with

10 nM Archazolid B for 24 hours. Ruffle formation was induced with 10 ng/ml HFG and 10% FCS for 5 minutes. Cells were fixed with 4% PFA and stained with phalloidin-FITC (Sigma-Adlrich) and Rab5 (Santa Cruz) antibody. Pictures were taken at the wide-field microscope (Upright Olympus AX70) and the number of ruffles in Rab5-overexpressing Hela cells was counted.

2.2.13. Rac1 activation assay

For the Rac1 Assay 250,000 T24 cells/well were seeded in 6 well plates. The next day, cells were treated with Archazolid B in starvation medium for 24 hours. Rac1 activation was induced with 100 ng/ml epidermal growth factor (EGF) for 5 minutes. Cells were harvested and the Rac1 assay was performed using the Rac1 pulldown kit (PIERCE). In the kit the downstream target of Rac1, called PAK, was used. Only active GTP-bound Rac1 can bind to PAK. After the pulldown, samples were either frozen at -20 °C or directly loaded onto a 12 % gel to perform Western Blot analysis as described in 2.2.15.

2.2.14. Internalization assay (Transferrin-/EGF-rhodamine)

T24/L3.6pl cells were seeded on μ -slides (IBIDI, Martinsried, Germany). The next day, cells were treated with Archazolid B for various time periods. Treated cells were starved for 2 hours in DMEM medium. Then, transferrin- / EGF-rhodamine was added for 5/15 minutes, 37°C. Cells were washed once with PBS + and fixed with 4% PFA (10 min, RT). Samples were covered with mounting media and a coverslip and pictures were taken using confocal microscopy (Zeiss, Oberkochen, Germany).

2.2.15. Western Blot

2.2.15.1. Protein sample preparations-total cell lysates

For Western Blot analysis, cells were seeded in 6 well plates and treated as described. Supernatant and trypsinized cells were pooled and centrifuged (600 x g, 5min, 4°C). After washing the cell pellet with cold PBS, cells were lysed in the lysis buffer for 30 min at 4°C. Cellular debris was removed by centrifugation at 10,000 x g, 10 minutes, 4°C. Supernatants were transferred to new tubes.

Table 2.14: RIPA and triton protein lysis buffer

RIPA Buffer		Triton lysis buffer	
Tris/HCl	0.79 g	Tris/HCl, pH 7.5	30 mM
NaCl	0.87 g	NaCl	150 mM
Nonidet NP40	1.0 ml	EDTA	2 mM
Deoxycholic acid	0.25 g	Triton X-100	1 %
Tris/HCl	0.10 g	Complete®	1:25
Complete®	1:25	H ₂ O	
PMSF	1.0 mM		
Na ₃ VO ₄	1.0 mM		
NaF	1.0 mM		
H ₂ O	up to 250ml		

Table 2.15: Sample buffer.

5x SDS sample buffer		3 x Laemmli buffer	
Tris/HCl 3.125 M	100 µl	Tris/HCl 187.5 mM	
SDS 20%	250 µl	SDS	6 %
Glycerol	500 µl	Glycerol	30 %
DTT 16%	125 µl	Bromophenolblue	0.025 %
Pyronin Y 5%	5 µl	β-Mercaptoethanol	12.5 %
H ₂ O		H ₂ O	

2.2.15.2. Protein quantification

Protein samples were quantified according to Bradford *et al.*⁶³ The standard calibration curve was generated using samples which contain defined concentrations of BSA suspended in H₂O (50 µg/ml-500 µg/ml). 190 µl of the Bradford reagent (Bradford reagent stock was diluted 1:5 in H₂O) was added to each 10 µl aliquot of the diluted protein samples (diluted 1:10 in H₂O) and calibration samples in a 96-well flat bottom plate. All measurements were performed in triplicates. Probes were incubated for 5 minutes and absorbance was measured using the SpectraFluor PlusTM (Tecan, Männedorf, Austria).

2.2.15.3. SDS-PAGE

The SDS-PAGE was performed according to Laemmli *et al.*⁶⁷. Here the Mini Protean III system from Bio-Rad (Munich, Germany) was used. Prior to loading the samples, the apparatus was assembled as described by the producer, and the chamber was filled with ice-cold electrophoresis buffer. Before loading, samples were boiled at 95°C for 5

minutes. Equal protein amount/per sample was loaded onto the SDS-gel. 2 μ l of the Fermentas page ruler™ prestained protein ladder was loaded on each gel to estimate the molecular weights of the separated proteins. Proteins were separated in a discontinuous electrophoresis: Proteins were focused by running the probes through the stacking gel, pH 6.8 (100 V, 20 minutes) and then separated in the separating gel, pH 8.8 (200 V, 35-45 minutes).

Table 2.16: Electrophoresis buffer

Electrophoresis buffer	
Tris base	3.0 g
Glycine	14.4 g
SDS	1.0 g
H ₂ O	up to 1 l

Table 2.17: Preparation of SDS-PAGE

Stacking gel		Seperating gel	
30 % PAA solution	1.28 ml	30 % PAA solution	5.0 ml
1.25 M Tril HCl pH 6.8	0.75 ml	1.25 M Tril HCl pH 6.8	3.75 ml
10 % SDS	75 μ l	10 % SDS	150 μ l
H ₂ O	5.25 ml	H ₂ O	6.1 ml
APS	75 μ l	APS	75 μ l
TEMED	20 μ l	TEMED	20 l

2.2.15.4. Tank blotting

After separating the samples in the SDS-PAGE, proteins were transferred to a nitrocellulose membrane (Hybond-ECL™, Amersham Bioscience, Freiburg, Germany) via tank blotting. A blotting sandwich was prepared in a box filled with 1 x Tank Buffer as follows: cathode-pad, blotting paper, separating gel (from SDS-PAGE)-nitrocellulose membrane, blotting paper-pad-anode. Pads, papers, and the membrane were equilibrated with 1 x Tank buffer 15 minutes prior to running the tank blot. Sandwiches were mounted on the Mini Trans-Blot® system (Bio-Rad, Munich, Germany), and the system was filled up with ice cold 1 x Tank buffer. Transfers were carried out at 4°C at 23 V overnight.

Table 2.18: Tank buffer

5 x Tank buffer		1 x Tank buffer	
Tris base	15.2 g	5x Tank buffer	200 ml
Glycine	79.2 g	Methanol	200 ml
H ₂ O	up to 1 l	H ₂ O	up to 1 l

2.2.15.5. Detection

After the transfer, sandwiches were disassembled and gels were stained with coomassie blue (see below). Membranes were incubated in 5 % blotto for 1 hour, RT to block unspecific binding reactions. After one washing step with 1x TBS-T, membranes were incubated with the primary antibody dilution overnight at 4°C. The next day, membranes were washed three times 10 min with 1x TBS-T and then incubated with the secondary antibody for either 1 hour (IR-dye, light protection) or 2 hours (HRP-dye) at room temperature.

2.2.15.6.1. Detection method-LICOR

Secondary antibodies coupled to IRDye™ 800 and Alexa Fluor® 680 with emission maxima at 800 and 700 nm were used. Membranes were incubated for one hour, RT in appropriate dilutions. After the incubation period, membranes were washed three times for 10 minutes with TBS-T. Membranes were scanned and analyzed using the Odyssey imaging system (LICOR Biosciences, Lincoln, NE). Thus, the intensity of each protein band could be determined.

2.2.15.7.2. Enhanced Chemiluminescence

Proteins coupled to peroxidase-conjugated antibodies were detected with ECL solution. After incubation with the secondary antibody, membranes were washed three times for 10 minutes with TBS-T. Then the membrane was incubated protected from light in ECL Plus™ Western Blotting detection reagent (Amersham Bioscience) for 1 minute, and layered between two plastic sheets. Chemiluminescence was detected by exposing the membranes to a X-ray film (Super RX, Fuji, Düsseldorf, Germany) for the appropriate time period in a darkroom. X-ray films were developed in a Curix 60 developing system (Agfa-Gevaert AG, Cologne, Germany)

Table 2.19: Primary antibodies for Western Blot analysis

Antigen	Isotype	Dilution	Provider
Actin	mouse	1:1000	Santa Cruz
Akt (tot)	rabbit	1:1000	Cell signaling

pAkt (S473)	mouse	1:1000	Cell signaling
Ductin (ATP6L)	rabbit	1:500	Millipore
EGF-R	rabbit	1:500	Cell signaling
pEGF-R	rabbit	1:1000	Cell signaling
ERK (tot)	rabbit	1:1000	Cell signaling
pERK	mouse	1:1000	Cell signaling
Rab5A	rabbit	1:1000	Santa Cruz
Rac1	mouse	1:1000	Upstate

Table 2.20: Secondary antibodies for Western Blot

Antigen	Dilution	Provider
AlexaFluor ® 680 Goat anti-mouse	1:10.000	Molecular Probes
IRDye™ 800CW Goat anti-mouse	1:10.000	Li-COR Biosciences
AlexaFluor ® 680 Goat-anti rabbit	1:10.000	Molecular Probes
IRDye™ 800CW Goat-anti rabbit	1:10.000	Invitrogen
Goat anti-mouse IgG ₁ : HRP	1:5000	Biozol
Goat anti-mouse IgG _{2b} : HRP	1:5000	Biozol
Goat-anti rabbit IgG: HRP	1:5000	Dianova

To verify a homogenous loading, polyacrylamid gels were stained for 30 minutes with coomassie-blue, and destained with coomassie-destaining solution. After protein detection, membranes were stained with Ponceau S (0.2% Ponceau S in 5% acetic acid) for 5 minutes and destained with distilled water. Membrane was scanned (Canon, Krefeld, Germany).

Table 2.21: Coomassie staining solutions

Coomassie staining solution		Coomassie destaining solution	
Coomassie blue	3.0 g	Glacial acetic acid	100 ml
Glacial acetic acid	100 ml	Ethanol	333 ml
Ethanol	450 ml	H ₂ O	up to 1 l
H ₂ O	up to 1 l		

2.2.16. T24 spheroids

T24 cells were trypsinized and counted. 40,000 cells/ml cells were seeded in 50 mg/ml PolyHEMA coated plates. Cells were grown in conditioned medium for 7 days before us-

ing them for an experiment. All formed spheroids were collected. To determine the cell number one half of the cell suspension was digested with T/E into a single cell suspension. Cell number was calculated. According to the determined cell concentration, 5000 cells/well of the undigested spheroid suspension were seeded in PolyHEMA coated plates. A treatment with Archazolid B for 72 hours followed. In parallel, T24 cells were seeded in 2D as usual and treated for 72 hours. For the analysis, a CellTiter-Glo Luminescent Cell Viability Assay (Promega Cooperation, Madison, WI, USA) was performed.

2.2.17. Statistical analysis

All experiments were performed at least three times in duplicates/triplicates. Results are expressed as mean value \pm SEM. One-way ANOVA/Dunnett's or unpaired Students t-tests were performed using GraphPadPrism™. P-values < 0.05 were considered as significant.

RESULTS

3.1. Characterisation of the V-ATPase subunit c as potential drug target

3.1.1. Expression and localization of the V-ATPase subunit c

In some cancer cells, subunits of the V-ATPase seem to be overexpressed⁷ and expression may correlate with the invasiveness of these cancer cells⁶⁸.

To proof these facts, we first compared the mRNA-level of the V-ATPase subunit c (ATP6L) in highly invasive urinary bladder cancer cells (T24) to the level in non-cancerous breast cells of epithelial origin (MCF-10A). We could show that the highly invasive cancer cells T24 express almost 50% more of the V-ATPase subunit c than the non-cancerous breast cells MCF-10A. As standard, the expression level of the 18S rRNA was used. This experiment was kindly performed by Lina Schneiders during her Master thesis (Figure 3.1 A).

Next, we were interested in comparing the levels of ATP6L in various cancer cell lines. By PCR we amplified the V-ATPase subunit c from the cDNA of various cell lines using ATP6L-specific primers. We could see that the urinary bladder cancer cell line T24 and the pancreatic cancer cell line L3.6pl express more ATP6L than for example the low invasive liver cancer cells HepG2 (Figure 3.1 B). Since the expression level of housekeeping genes differ a bit between cell lines⁶⁹, the shown ATP6L levels should be more considered as tendencies.

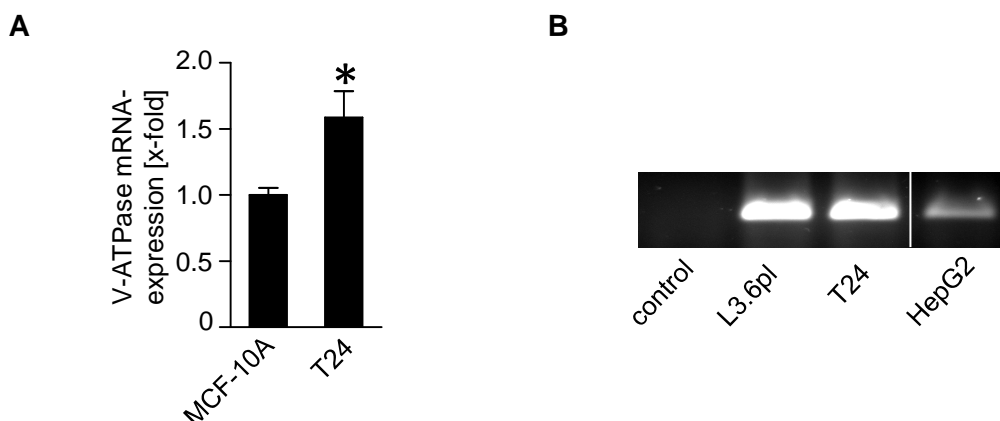


Figure 3.1: ATP6L is overexpressed in highly invasive cancer cell lines. (A) A Real-time PCR detecting the V-ATPase subunit c (ATP6L) was performed. Bars represent the mean \pm S.E.M. of three independent experiments performed in duplicates. (t-test, unpaired). (B) Via PCR ATP6L of

cDNA of various cell lines was performed. One representative experiment out of three independent experiments is shown.

In the breast cancer cell line MDA-MB-231 it could be shown that the V-ATPase subunit A is localized in the plasma membrane.¹⁵ As we saw a high expression of the V-ATPase subunit c (ATP6L) in the urinary bladder cancer cell line T24, we were interested in its distribution during the migration. A wound healing assay with T24 cells was performed and cells were stained for confocal microscopy using an antibody which detects the V-ATPase subunit c. Indeed, we see a localization of this subunit in the plasma membrane of polarized T24 cells (Figure 3.2).

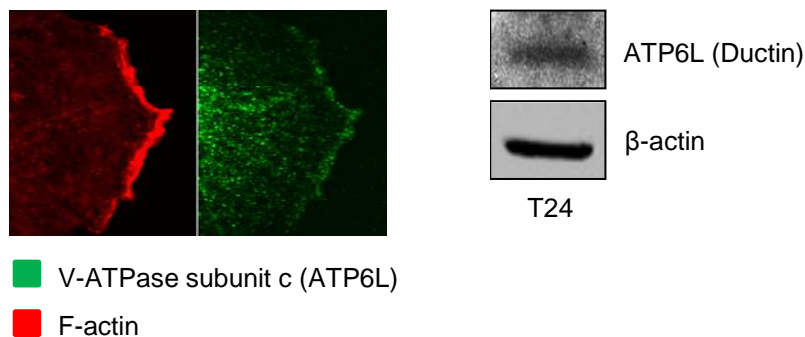


Figure 3.2: The V-ATPase subunit c (ATP6L) is localized at the leading edge of migrating T24 cells. A wound healing assay with T24 cells was performed and cells were stained with antibodies raised against ATP6L. In a Western Blot ATP6L could be detected. One representative image out of three independent experiments is shown.

3.1.2. Archazolid B, a new potent inhibitor of the V-ATPase

V-ATPases are foremost localized in membranes of acidic organelles, like lysosomes⁸. To test the functionality of Archazolid B (Arch B) as V-ATPase-inhibitor, a lysosome staining was performed. Acidic lysosomes were stained with a LysoTracker. If the V-ATPase is inhibited, the pH in the lysosomes will increase and the fluorescence of the pH-sensitive LysoTracker is decreased. We compared our results with the effects of an already known V-ATPase inhibitor Concanamycin A (Conc A), which binds to the same subunit of the V-ATPase⁸. Indeed we see for both V-ATPase inhibitors an increase of the pH in the lysosomes, shown by a decrease of the LysoTracker fluorescence (Figure 3.3).

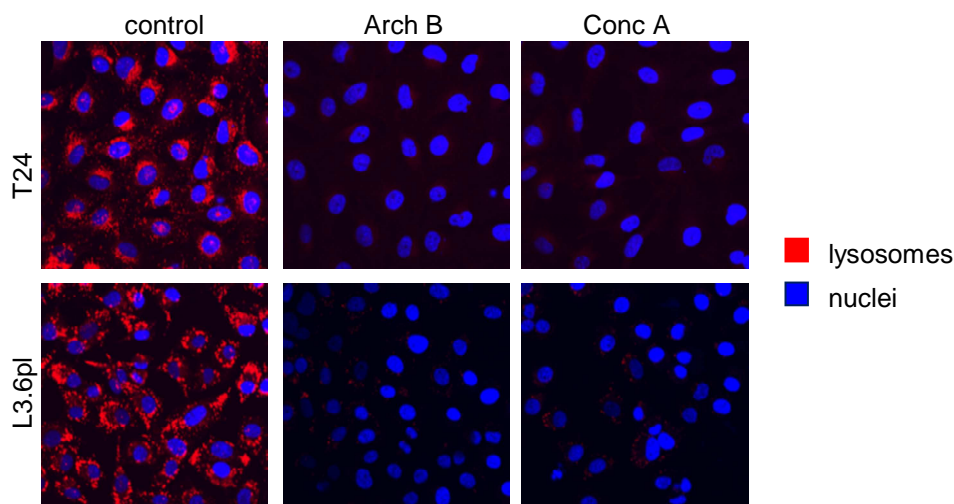


Figure 3.3: Archazolid B inhibits the V-ATPase-activity in lysosomes. Acidic lysosomes were stained with LysoTracker (red) and the nuclei with Hoechst (blue) after 2 hours of treatment with the V-ATPase inhibitors Concanamycin A (5 nM) or Archazolid B (5 nM). Representative images out of three independent experiments are shown.

3.1.3. Effects of Archazolid B on gene expression

By its increased expression and different localization in invasive cancer cells, it is assumed that the V-ATPase plays a crucial role in the process of tumor development and metastasis.^{7,15,68} To elucidate the gene expression which may be affected by the inhibition of the V-ATPase using Archazolid B, a microarray was performed (Cooperation with Prof. Efferth, University of Mainz).

The microarray showed that in general genes in the field of cell death, cell proliferation and cancer are affected by Archazolid B treatment (Figure 3.4).

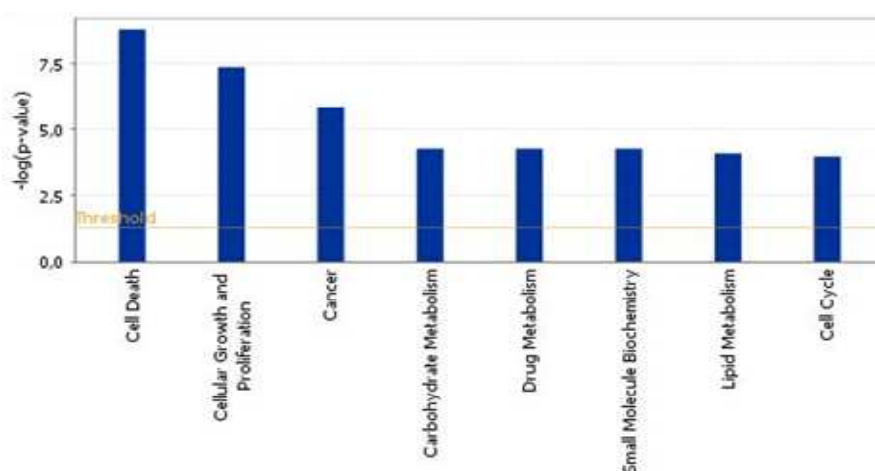


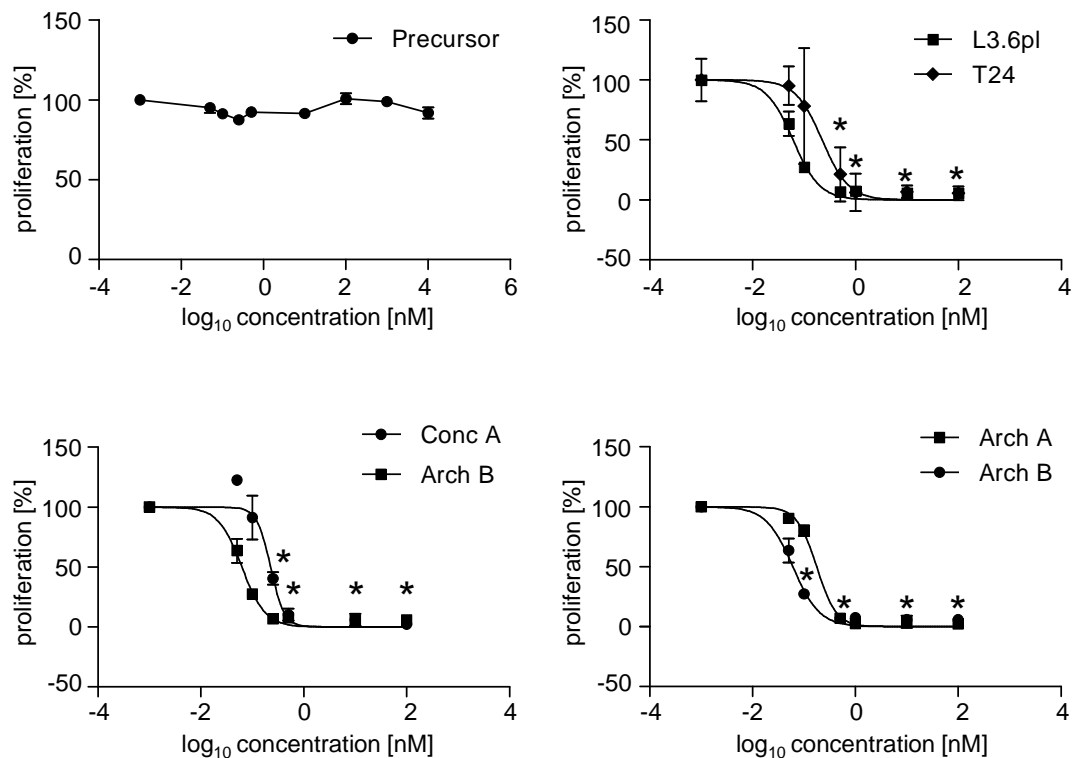
Figure 3.4: Archazolid B affects genes involved in cell death, cellular growth, proliferation and cancer. T24 cells were treated for 24 hours with Archazolid B (10 nM). mRNA was isolated

and after cDNA synthesis, a microarray was performed (Cooperation with the group of Prof. Dr. Efferth, University of Mainz, Germany)

3.2. Antitumor effects of Archazolid B

3.2.1. Archazolid B inhibits cell proliferation of highly invasive cancer cells

In the tumor cell lines T24 and L3.6pl the effect on cell proliferation by V-ATPase inhibitors was tested. Using a precursor molecule of the synthesis of Archazolid B⁶⁰, no effect on the cell proliferation could be determined in L3.6pl cancer cells. Whereas Archazolid B inhibited the cell proliferation already in picomolar ranges in both cell lines. Generally, Archazolid B was slightly more potent than Archazolid A or the already known V-ATPase inhibitor Concanamycin A (Figure 3.5).



cells/compound	IC ₅₀ [nM]
T24 (Arch B)	0.22
L3.6pl (Arch B)	0.06
L3.6pl (Arch A)	0.18
L3.6pl (Conc A)	0.22

Figure 3.5: Inactivation of the V-ATPase by inhibitors binding to the subunit c represses proliferation of highly invasive cancer cells. T24/L3.6pl cells were treated with according compounds for 72 hours. A crystal violet staining followed and its absorbance was measured, which correlates with the cell number. Bars represent the mean \pm S.E.M. of three independent experiments performed in triplicates. * $p < 0.05$ (One Way ANOVA, Dunnett's)

3.2.2. Archazolid inhibits clonogenic survival

One characteristic of chemoresistant and metastatic tumor cells is that they don't undergo apoptosis upon a short-time treatment with a chemotherapeutic or that some cells are able to recover. In a clonogenic assay, cells are allowed to grow over an extended time period after a shorter treatment time of the according compound. L3.6pl cells were treated at high confluence with Archazolid B for 24 hours. After the treatment cells were seeded at very low density and cultivated for another 6 days. As shown in Figure 3.6, 1 nM of Archazolid B reduced the clonogenic survival by approximately 60% in comparison to the untreated cells (Figure 3.6).

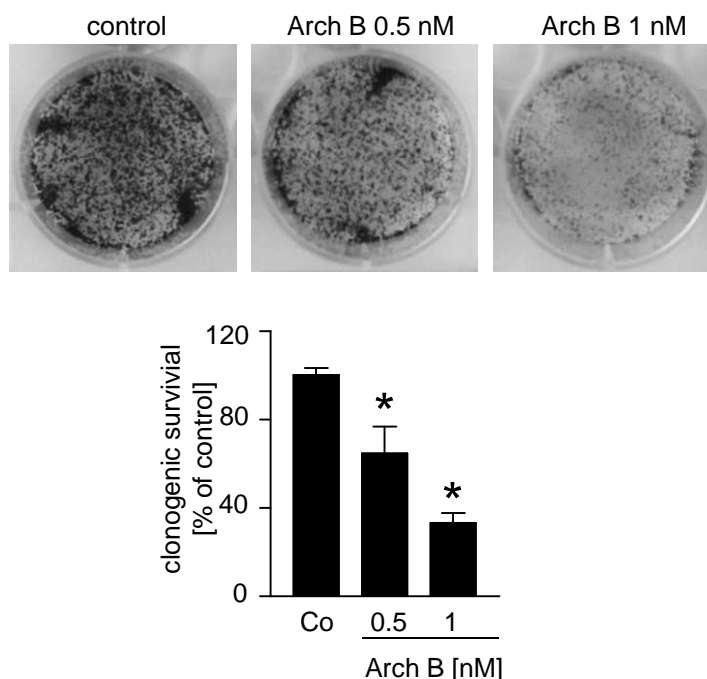


Figure 3.6: Archazolid B reduces clonogenic survival. 70% confluent L3.6pl cells were treated with Archazolid B for 24 hours. Cells were freshly seeded in very low confluence and cultivated for 6 days. To analyze the clonogenic survival, cells were stained with crystal violet and the absorbance, which correlates with the number of cells, was measured. Bars represent the mean \pm S.E.M. of three independent experiments performed in triplicates. * $p < 0.05$ (One Way ANOVA, Dunnett's)

3.2.3. Cell death features induced by Archazolid B

During the process of apoptosis different features can be observed, which include cell shrinkage, formation of apoptotic bodies, changes in size and shape of the cell and DNA condensation and -fragmentation.^{46,70}

T24 cells treated with Archazolid B for 48 hours show a characteristic morphological change. T24 cells shrink and look spindle-shaped. Compared to classical induced apoptosis, no clear formation of apoptotic bodies can be determined. However, staining with the vital dye Hoechst 33342 clearly indicates DNA condensation in Archazolid B treated cells shown here by bright Hoechst staining compared to faint staining in the control cells (Figure 3.7 B).

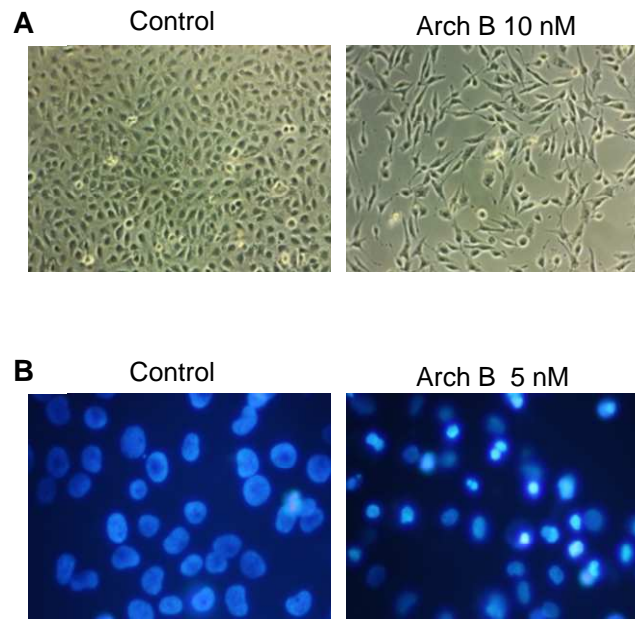


Figure 3.7: Archazolid B induces morphological changes and DNA condensation in T24 cells. (A) T24 cells were treated for 48 hours with 10 nM Archazolid B. Pictures were analyzed by light microscopy. (B) T24 cells were stained with the vital dye Hoechst 33342 48h after Archazolid B treatment. Cells were analyzed by fluorescence microscopy.

To elucidate the effect of Archazolid B more precisely, cell sections were analyzed by transmission electron microscopy. T24 cells were treated with 10 nM Archazolid B for various timepoints and samples were prepared for electron microscopy. Pictures were taken in collaboration with Prof. Dr. Wanner, Department of Physiology, LMU Munich.

For each timepoint, two pictures are shown in Figure 3.8. After 5 hours of Archazolid B treatment, small vacuoles seem to be formed in the cytoplasm. After 15 hours the nuclei membrane already seems to be separated. Furthermore, the determined vacuoles get bigger and show some content. Vaccari *et al.*⁷¹ described this vacuoles with content as multivesicular bodies (MVBs) The morphology of mitochondria and the endoplasmatic reticulum look relatively normal. After 30 hours, the cytoplasm is more and more filled with vacuoles, some with content some without.

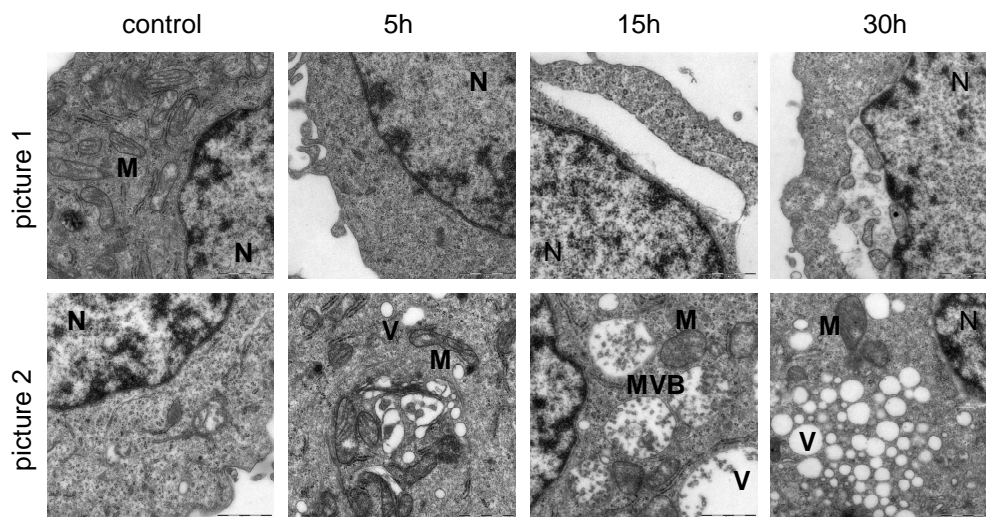
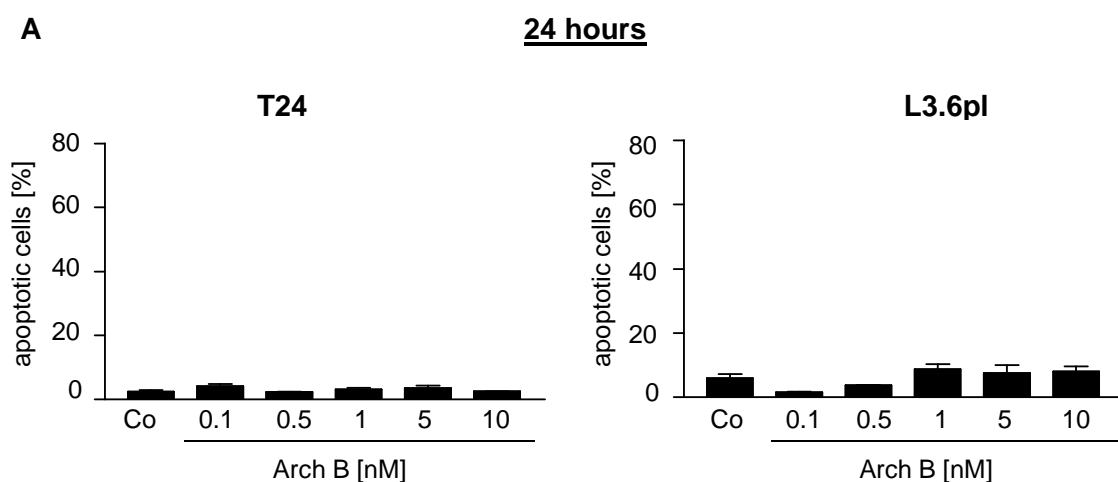


Figure 3.8: Morphological changes by Archazolid B determined by electron microscopy. T24 cells were treated with 10 nM Archazolid B for various time points. Cells were embedded in paraffin and sections were done. Cells were further prepared for electron microscopy and pictures were taken. (Cooperation with the group of Prof. Dr. Wanner, Department of Physiology, LMU Munich). (N-nuclei, M-mitochondria, V-vacuoles, MVB-multivesicular bodies)

3.2.4. Archazolid B induces apoptosis

To quantify apoptosis the amount of DNA condensation and fragmentation was measured via flow cytometry. Archazolid B induces apoptosis time- and dose-dependent. But interestingly, the induction of apoptosis started after a quite late treatment time. After 48 hours, about 20-25 % of cells treated with 10 nM Archazolid B underwent apoptosis. This rate increased up to 50-60 % after a treatment for 72 hours (Figure 3.9).



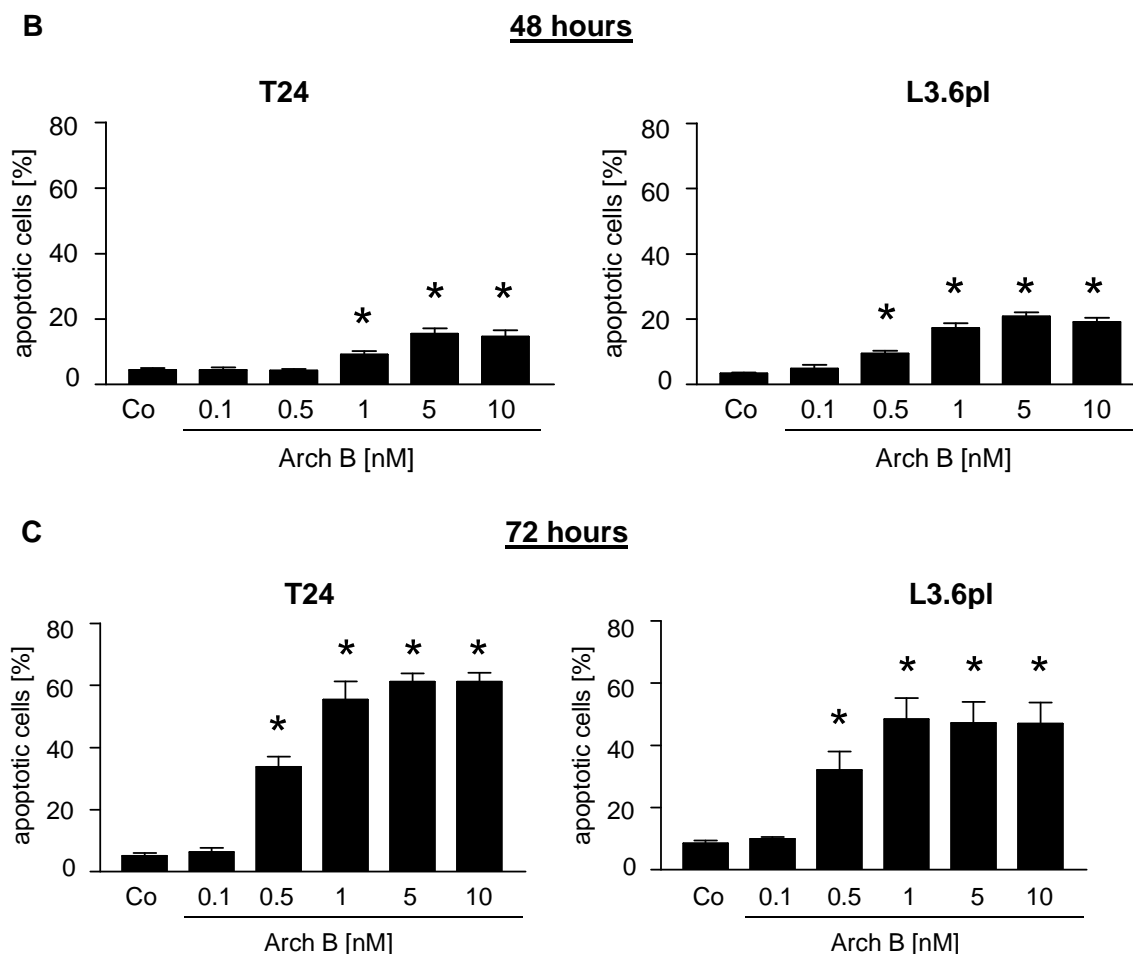
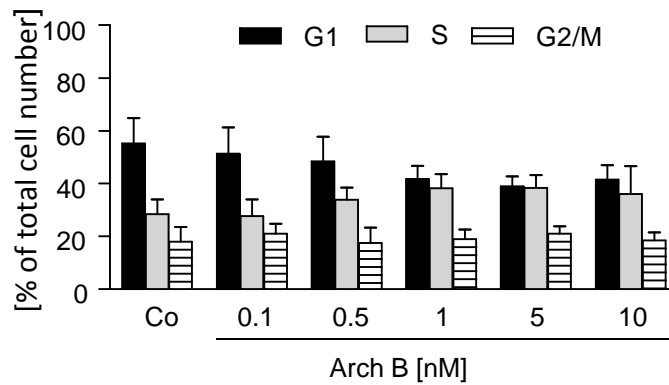


Figure 3.9: Archazolid B induces dose- and time-dependent apoptosis. T24/L3.6pl cells were treated with various concentrations for 24 hours (A), 48 hours (B), 72 hours (C). Cells were permeabilized and stained with propidium iodide using the method described by Nicoletti *et al.*⁶¹ DNA condensation/apoptotic cells, were quantified by flow cytometry. Bars represent the mean \pm S.E.M. of three independent experiments performed in triplicates. * $p < 0.05$ (One Way ANOVA, Dunnett's)

3.2.5. Effects of Archazolid B on the cell cycle

Some chemotherapeutics induce a cell cycle arrest. The cell cycle is defined as a number of events during cell replication, distinguished between the interphase and the mitosis, the subdividing G_1/G_0 (single DNA content), S and G_2/M (double DNA content) phases, all depending on the amount of DNA per cell. As shown in Figure 10, there is almost no effect on the G_1/G_0 or G_2/M -phase in both cell lines. There is a slight increase of the amount of cells in the S-phase, which seems to be more obvious in the T24 cells.

T24



L3.6pl

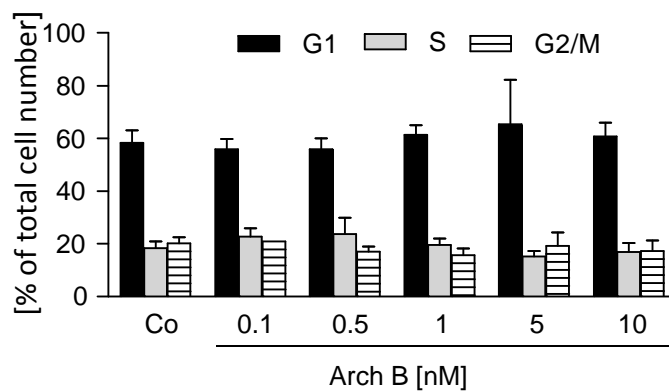


Figure 3.10: Archazolid B doesn't affect the cell cycle significantly. T24/L3.6pl cells were treated for 48 hours and a propidiumiodide staining using the method described by Nicoletti *et al.*⁶¹ was performed. The cell cycle analysis was done with the FlowJo 7.4 program. Bars represent the mean ± S.E.M. of three independent experiments performed in triplicates. *p < 0.05 (One Way ANOVA, Dunnett's)

3.2.6. Archazolid B induces apoptosis caspase-dependently

The pan caspase-inhibitor Q-VD-OPh inhibits the activation of all caspases. In combination of this pan caspase-inhibitor Q-VD-OPh with Archazolid B no apoptosis could be measured. Therefore, Archazolid B induces apoptosis caspase-dependently.

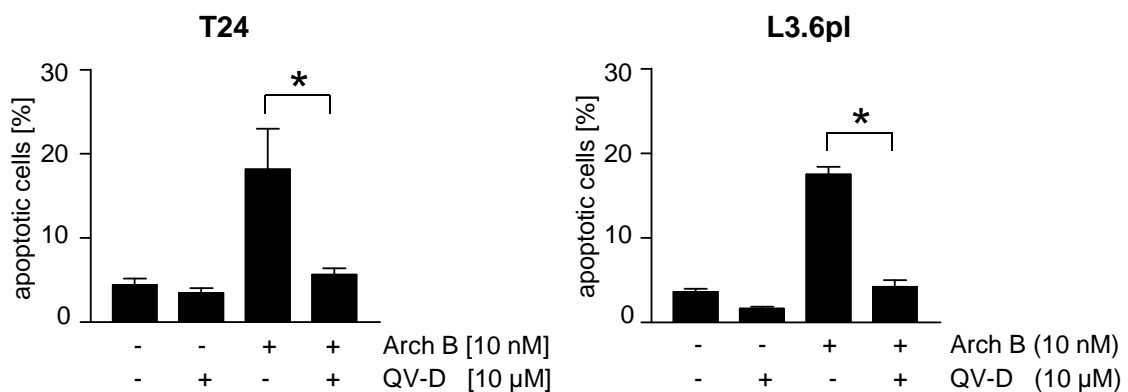
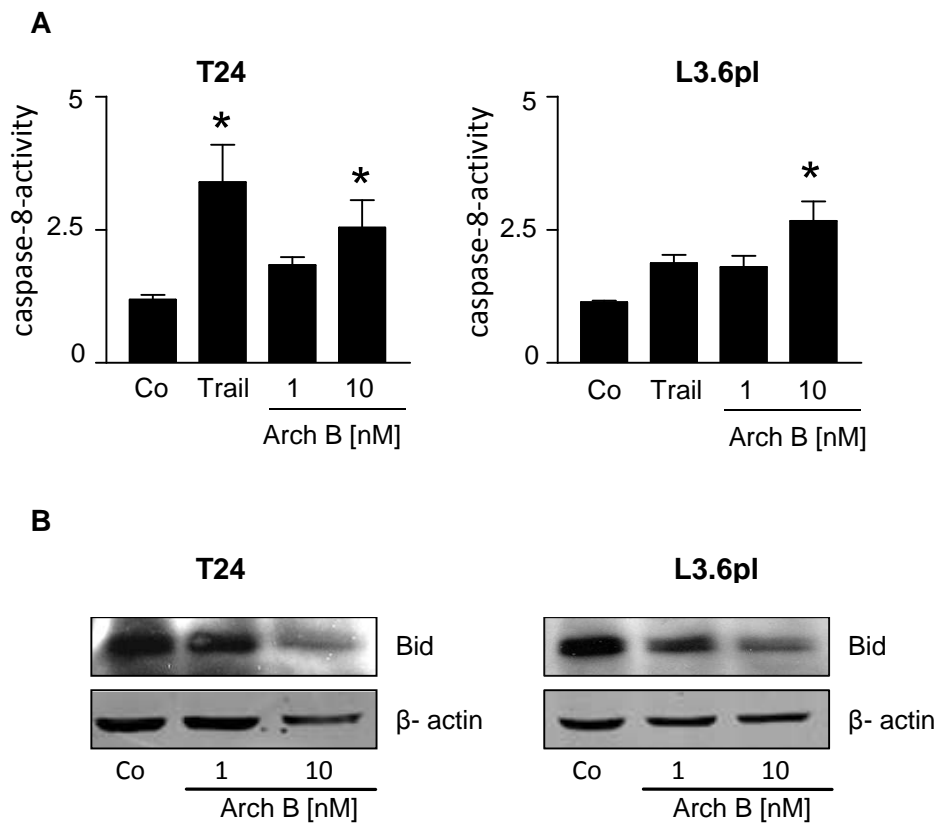


Figure 3.11: Archazolid B induces caspase-dependent apoptosis. T24/L3.6pl cells were treated with Archazolid +/- the caspase-inhibitor Q-VD-OPh for 48 hours. Cells were permeabilized and stained with propidiumiodide using the method described by Nicoletti *et al.*⁶¹ DNA condensation was quantified by flow cytometry. Bars represent the mean \pm S.E.M. of three independent experiments performed in triplicates. * $p < 0.05$ (t-test, unpaired)

To underline the results, the activity of various caspases was measured. Generally, caspases are separated in initiator caspases, such as caspases-8 and-9, which in turn promote activation of downstream caspases and effector caspases (caspases-3,-6, and-7). Really prominent is the activation of caspase-8 upon treatment of the cells with Archazolid B in both cell lines, followed by a reduced Bid expression after Archazolid B treatment. Furthermore, we can determine caspase-3 activation (Figure 3.12). These experiments were kindly performed by Isabella Stapff during her Master thesis.



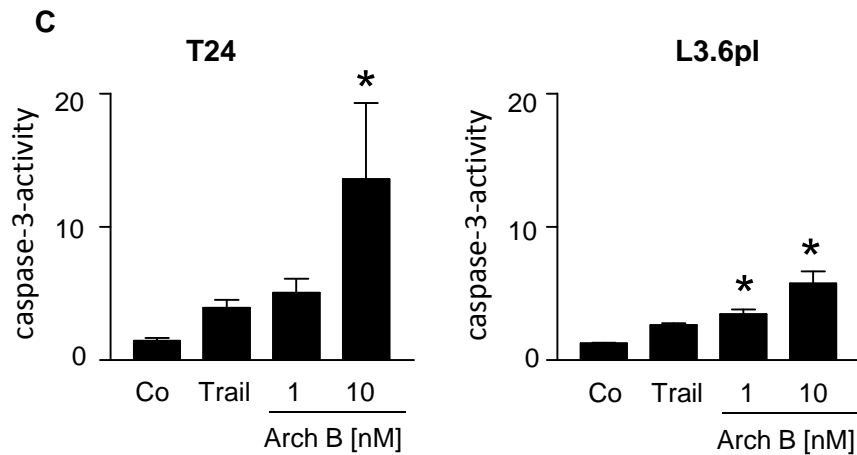
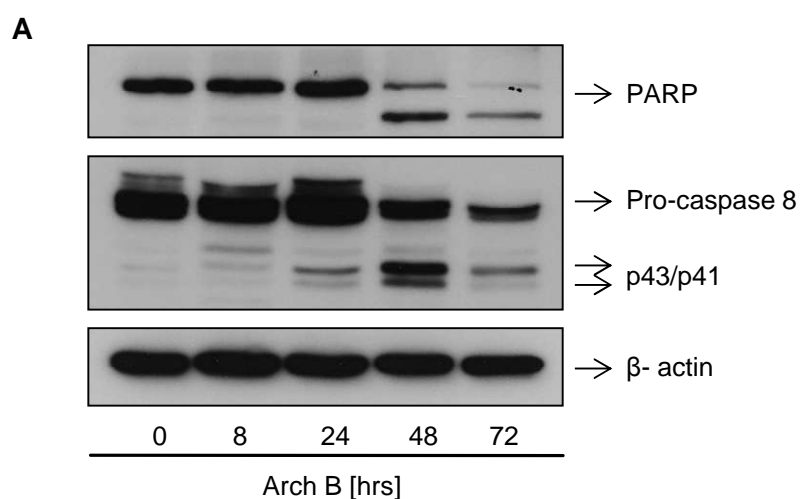


Figure 3.12: Archazolid B induces the activation of caspase-8 and caspase-3. T24/L3.6pl cells were treated for 48 hours and caspase-8 (A) or caspase-3 (C) - activity was measured using the specific caspase substrate. Cleavage of the caspase-substrate can be measured as fluorimetric shift. Bars represent the mean \pm S.E.M. of three independent experiments performed in triplicates. * $p < 0.05$ (One Way ANOVA, Dunnett's). (B) After 48 hours Archazolid B treatment, a Western Blot was performed and proteins were detected using specific antibodies. One experiment out of three independent experiments is shown.

On protein levels the induction of caspase-8 could also be shown. Beside that, we could determine the activation of the effector caspase-9 by Archazolid B, which is involved in the formation of the apoptosome in the intrinsic pathway. Caspase-3 is involved in cleavage of a variety of proteins such as poly (ADP-ribose) polymerase (PARP) a DNA repair enzyme which is active in presence of DNA damage. PARP cleavage is therefore an indicator for DNA strand breaks leading to apoptosis and it is induced by Archazolid B treatment (Figure 3.13).



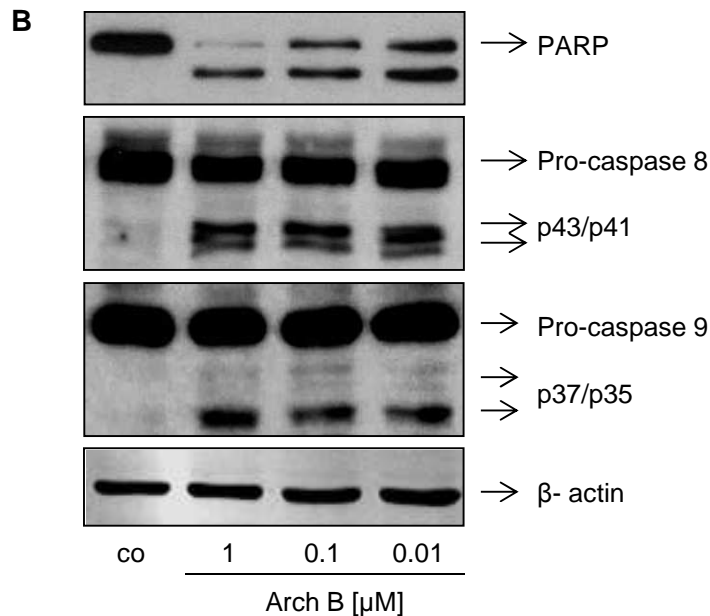


Figure 3.13: Archazolid induces the activation of caspase-8/9 and the cleavage of PARP induced by caspase-3 in a time and dose-dependent manner. (A) L3.6pl cells were treated with 10 nM Archazolid for various timepoints. (B) L3.6pl cells were treated with various concentrations of Archazolid B for 48 hours. Western Blot was performed and proteins were detected using specific antibodies. One experiment out of three independent experiments is shown.

3.2.7. Archazolid B affects the intrinsic apoptotic pathway

Two classical signaling pathways of caspase-dependent apoptosis can be distinguished: the extrinsic and the intrinsic pathway. The intrinsic pathway is mitochondria-dependent and regulated by the Bcl-2 family and leads to the activation of caspase family members.

To distinguish which pathway is influenced by Archazolid B, we determined if Archazolid B causes a loss of the mitochondrial potential in treated cells. Indeed, we see after 24 hours of treatment with Archazolid B that the mitochondrial potential is affected (Figure 3.14 A).

Furthermore, we see a downregulation of the anti-apoptotic molecule Bcl-2 after 48 hours of Archazolid B treatment, which is involved in the inhibition of apoptosis via the intrinsic pathway (Figure 3.14 B).

Via flow cytometry we could detect cytochrome c release from the mitochondria, which is a further hint that Archazolid B induces apoptosis via the intrinsic pathway (Figure 3.14 C). The measurement of the cytochrome c was kindly performed by Isabella Stapff during her Master thesis

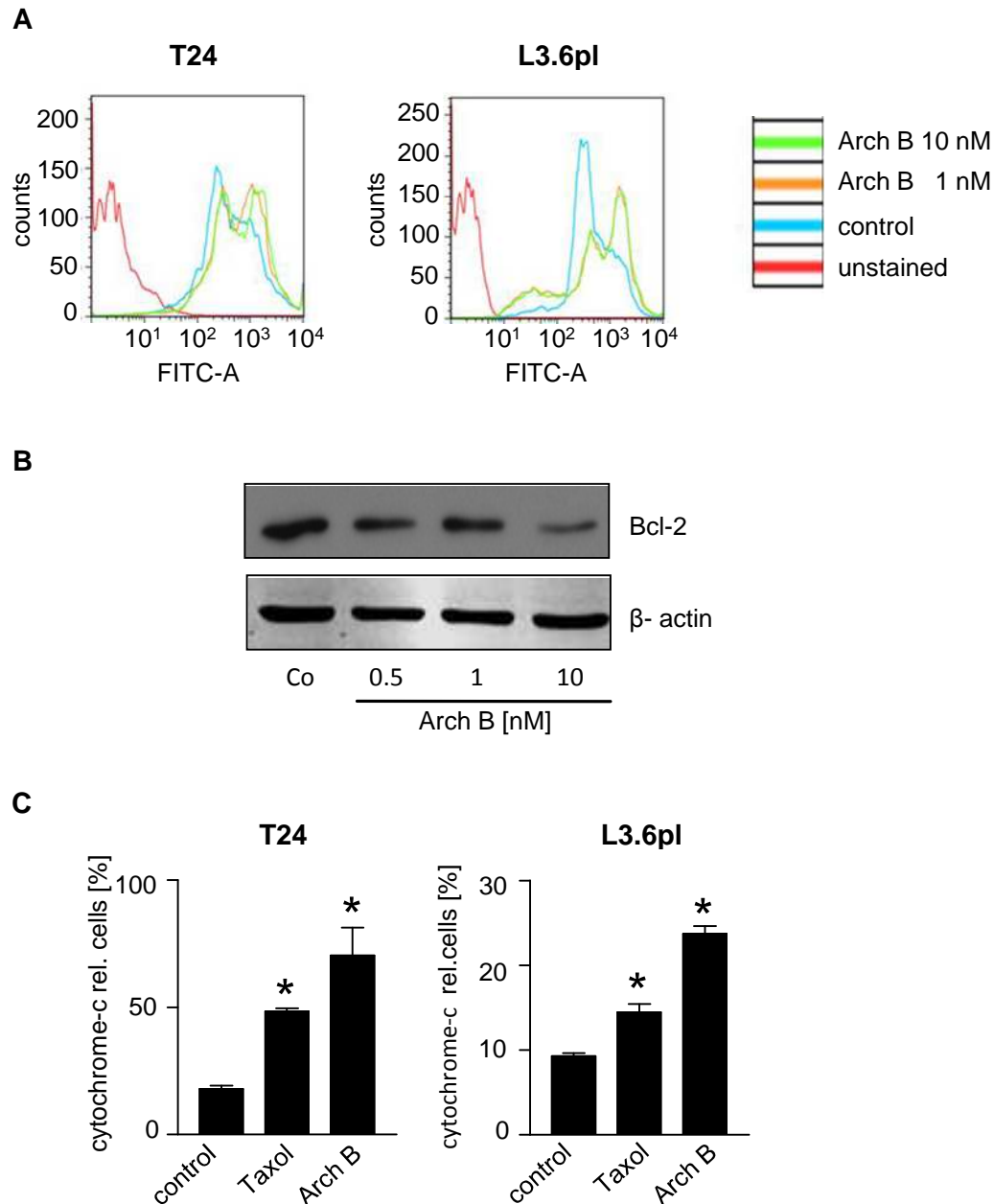


Figure 3.14: Archazolid B induces loss of the mitochondrial potential, downregulates the anti-apoptotic protein Bcl-2 and induces cytochrome c release. (A) T24/L3.6pl cells were treated for 24 hours with Archazolid B. Cells were stained with JC-1 and analyzed via flow cytometry. One representative histogram out of three independent experiments performed in triplicates is shown. (B) L3.6pl cells were treated with various concentrations of Archazolid B for 48 hours. Western Blot of total cell lysate was performed. One experiment out of three independent experiments is shown. (C) After 48 hours of treatment with Archazolid B, cytochrome c release was determined via flow cytometry. Bars represent the mean \pm S.E.M. of one experiment performed in triplicates. * $p < 0.05$ (One Way ANOVA, Dunnett's)

3.2.8. Effects of Archazolid B in a 3-D spheroid model

Spheroids exhibit an *in vitro* 3D model and therefore fill a gap between the consideration of effects in 2D *in vitro* assays and *in vivo* assay. Grown spheroids were treated with Archazolid B for 72 hours. As we can show in Figure 3.15, the cell viability of T24 cells in 2D is almost completely inhibited at nanomolar concentrations. But also the viability of the spheroids is clearly diminished (Figure 3.15). This experiment was kindly performed in cooperation with the group of Prof. Dr. Wagner, LMU Munich.

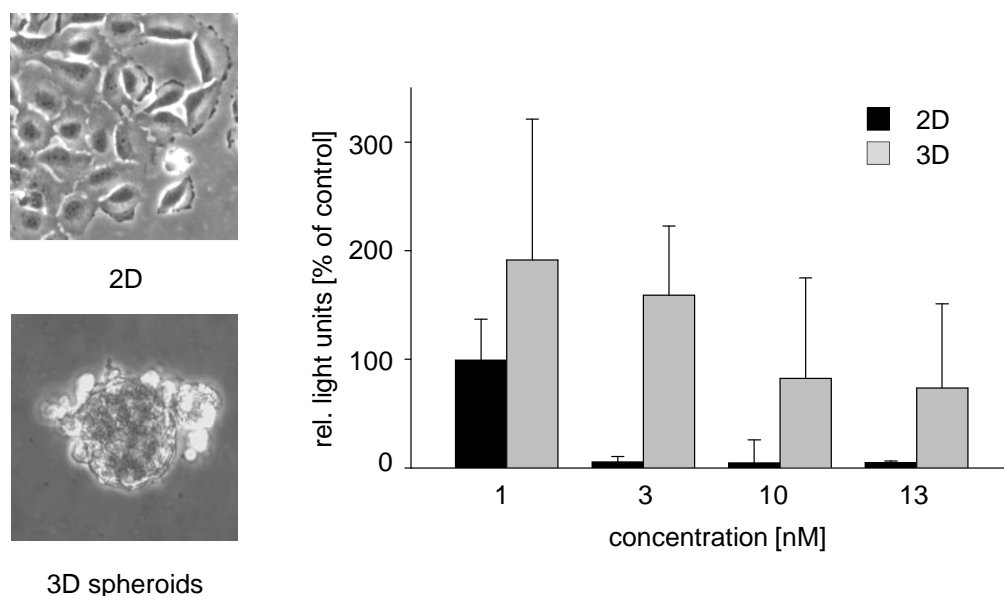


Figure 3.15: Archazolid B diminishes the cell viability of T24 spheroids. Spheroids were grown for 7 days before the treatment with Archazolid B. After 72 hours of Archazolid B treatment cell viability was determined. Bars represent the mean \pm S.E.M. of triplicates of one representative experiment, * $p < 0.05$ (One Way ANOVA, Dunnett's). The experiment was repeated three times in total.

3.2.9. Impairment of proliferation, apoptosis and clonogenic survival by the downregulation of ATP6L

Archazolid B binds to the V_0 subunit c of the V-ATPase. To prove, that the effects on proliferation, apoptosis and clonogenic survival are due to the inhibition of the V-ATPase, we downregulated this subunit (ATP6L) using siRNA. Surprisingly, the downregulation of ATP6L did not show an inhibition of cell proliferation after 72 hours, also no apoptosis is induced by the downregulation of ATP6L itself. However, the apoptosis rate is even increased by the combination of siRNA transfection and Archazolid B treatment in T24 cells

(Figure 3.16). The level of ATP6L-downregulation was tested via real time PCR (see Figure 3.17).

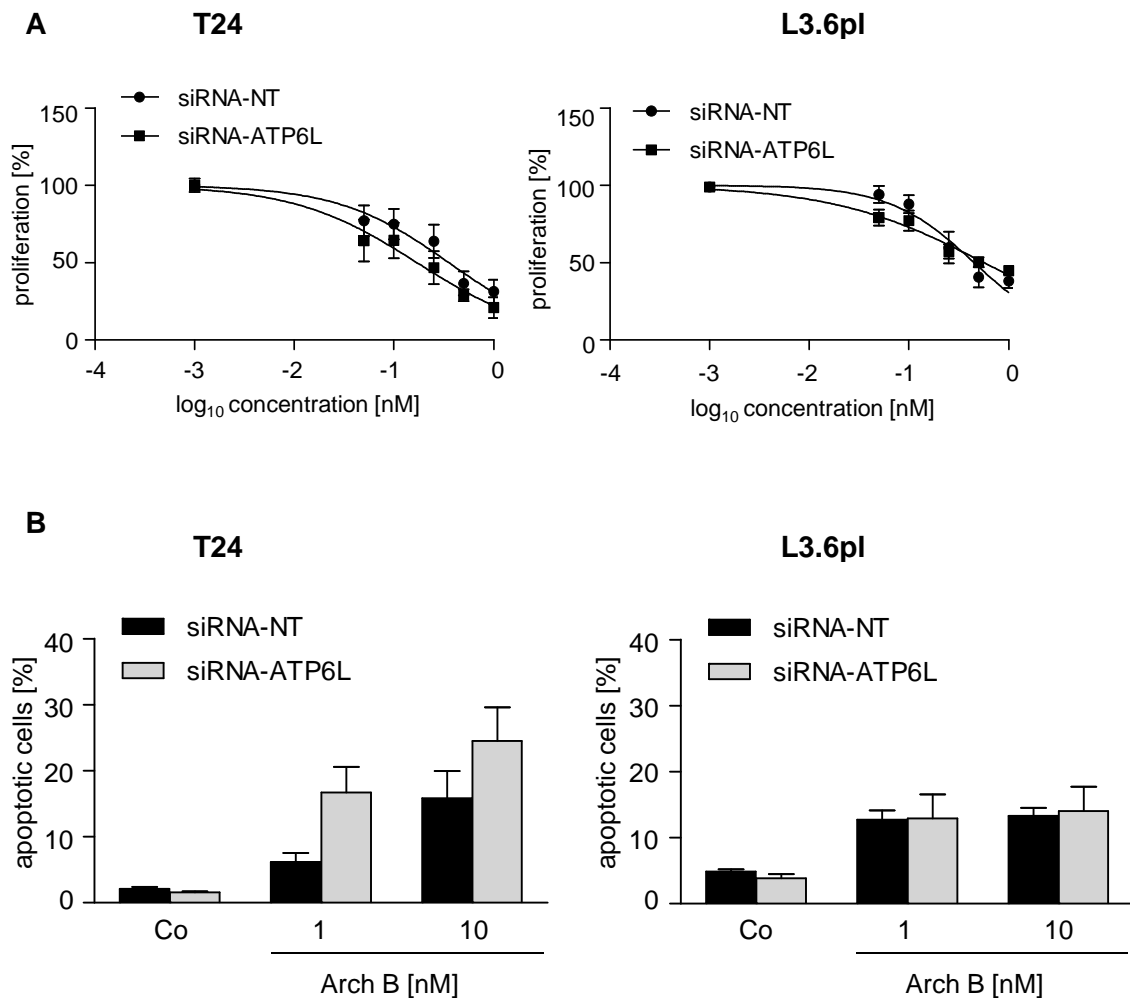


Figure 3.16: Downregulation of ATP6L via siRNA does not affect cell proliferation and apoptosis. T24/L3.6pl cells were transfected with siRNA-ATP6L for 24 hours, followed by a treatment of Archazolid B for another 48 hours. (A) Cells were stained with crystal violet to determine cell proliferation. (B) Cells were permeabilized and stained with propidiumiodide (Nicoletti *et al*⁶¹.) and analyzed by flow cytometry. Bars represent the mean \pm S.E.M. of three independent experiments performed in triplicates. * $p < 0.05$ (One Way ANOVA, Dunnett's)

But interestingly, the clonogenic survival of T24/L3.6pl cells was inhibited. After a transfection for 24 hours with siRNA, cells were seeded in very low density and cultured for 6 days. Clearly, the longtime proliferation of the siRNA-ATP6L transfected cells was inhibited (Figure 3.17).

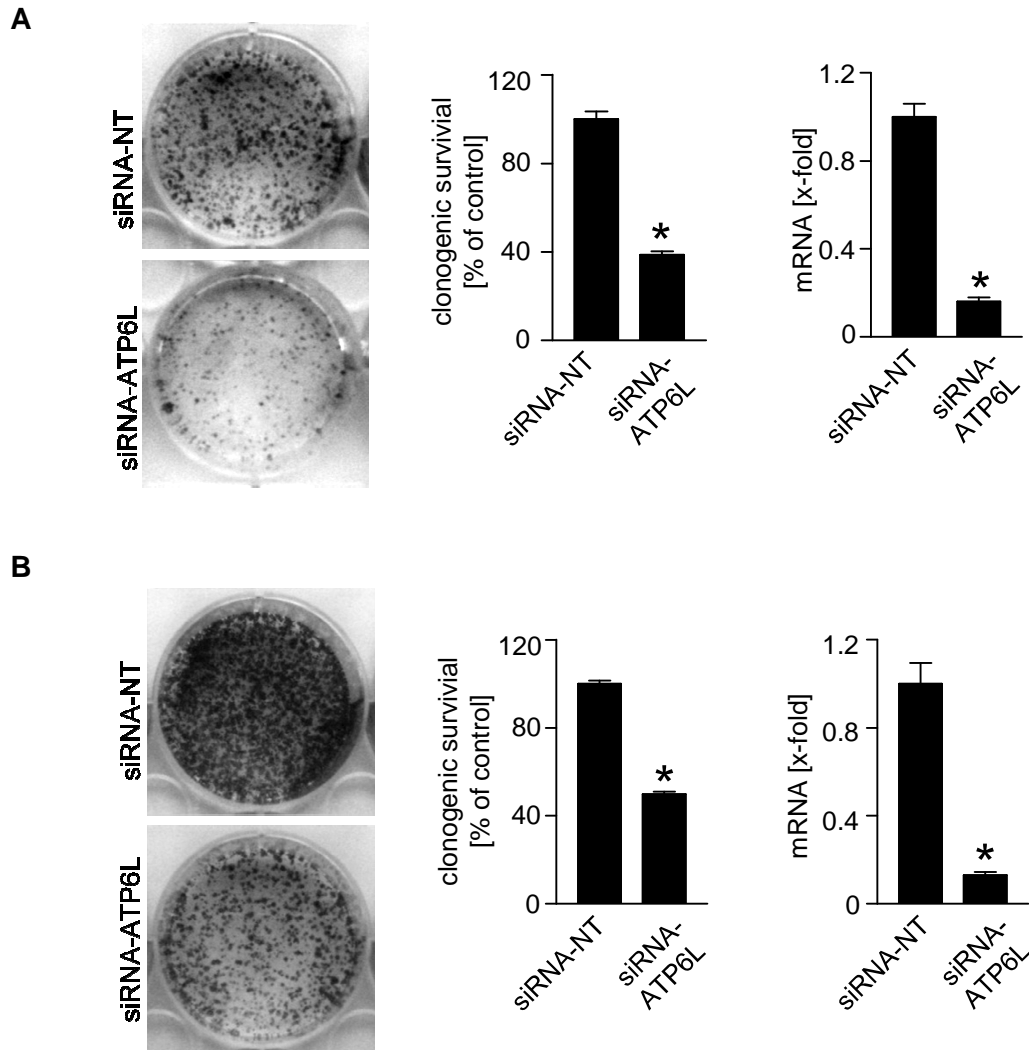


Figure 3.17: The downregulation of the V_0 subunit c of the V-ATPase (ATP6L) inhibits the clonogenic survival. T24 (A) and L3.6pl (B) cells were transfected for 24 hours with siRNA. Cells were seeded at very low density and cultured for 6 days. A staining with crystal violet followed. The absorbance of the crystal violet correlates with the cell number. Bars represent the mean \pm S.E.M. of three independent experiments performed in triplicates. * $p < 0.05$ (t-test, unpaired)

3.3. Antimetastatic properties of Archazolid B

3.3.1. Effects of Archazolid B on cell migration

3.3.1.1. Impairment of wound healing by Archazolid B

To first test the ability of Archazolid B to inhibit the migration in T24 cells and L3.6pl cells a wound healing assay was performed. In this assay, direct treatments versus pre-treatments were tested. As seen in Figure 3.18, the direct treatment with Archazolid B after scratching a wound into the confluent cell layer, led only for the L3.6pl cells to a sig-

nificant inhibitory effect on cell migration (Figure 3.18 B). The T24 cells, which seem to be more resistant and show a higher migration potential, appear almost not affected (Figure 3.18 A).

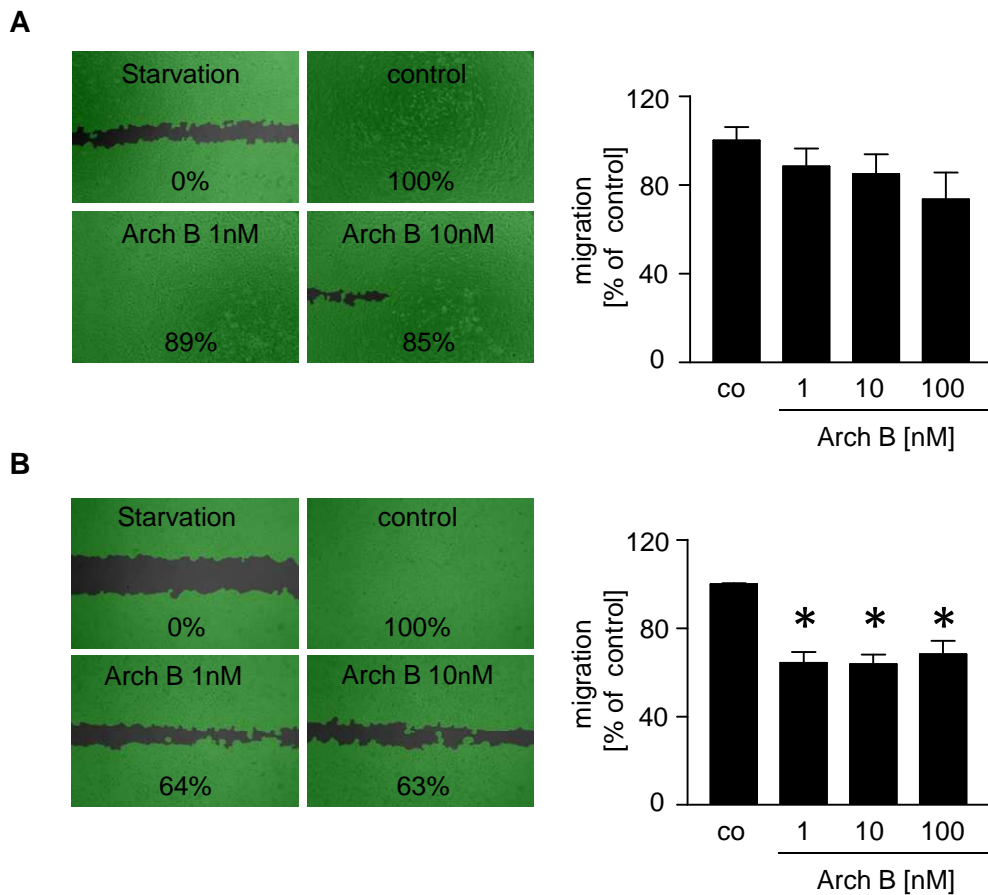


Figure 3.18: Direct Archazolid B treatment shows slight inhibitory effects on the wound healing. The confluent cell layer of T24 (A) and L3.6pl (B) was scratched with a pipette tip. Cells were allowed to migrate while directly being exposed to Archazolid B treatment. Cells were fixed and analyzed. Bars represent the mean \pm S.E.M. of three independent experiments performed in triplicates. * $p < 0.05$ (One Way ANOVA, Dunnett's)

Since we didn't see a significant reduction of cell migration for the direct treatment of T24 cells with Archazolid B, we tried to pre-treat the cells for 24 hours followed by the procedure of a scratch assay. During the actual migration no additional Archazolid B was added. Since the treatment and migration time did not take longer than 40 hours, we could be sure that no more than 20 % of the cells undergone apoptosis (Figure 3.20).

Indeed, the effect of Archazolid B on cell migration of T24 and L3.6pl cells was more pronounced when the cells were pre-treated (Figure 3.19).

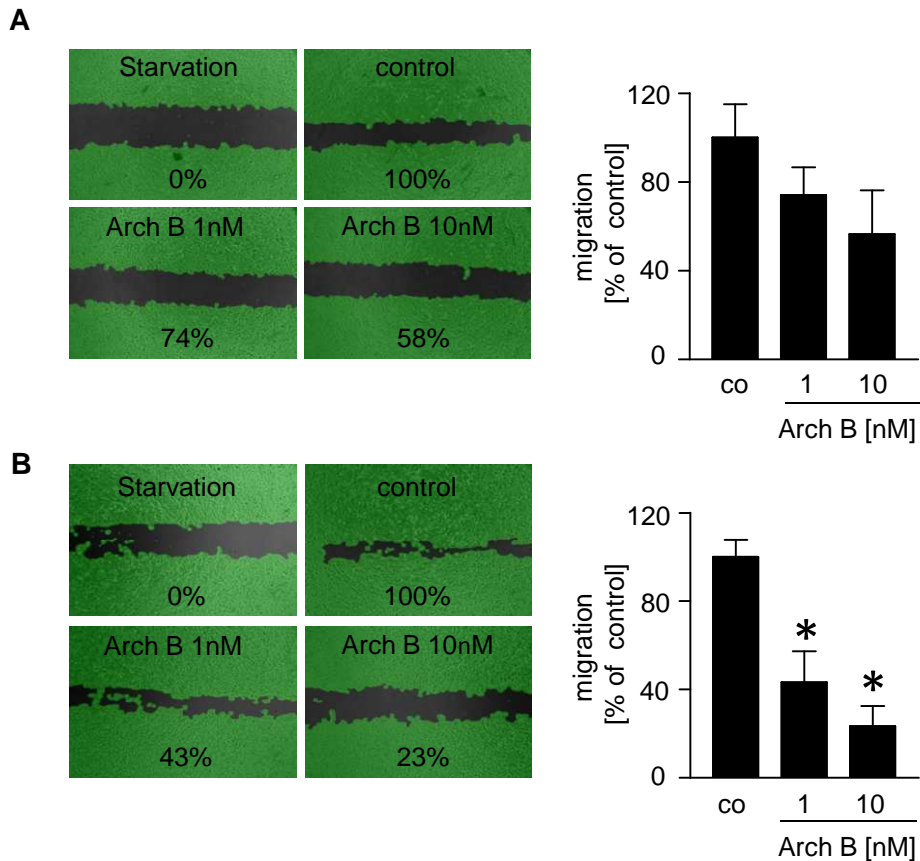


Figure 3.19: Pre-treatment of Archazolid B inhibits the wound healing significantly. The 70-80% confluent cell layer of T24 (A) and L3.6pl (B) was treated for 24 hours. The confluent cell layer was scratched with a pipette tip. Cells were allowed to migrate without additional treatment with Archazolid B. Cells were fixed and analyzed. Bars represent the mean \pm S.E.M. of three independent experiments performed in triplicates. * $p < 0.05$ (One Way ANOVA, Dunnett's)

3.3.3.2. Impairment of migration by Archazolid B in the Boyden chamber assay

During the migration process, cancer cells have to pass different barriers. To mimic this barrier a migration assay using Boyden chambers was performed. In this assay cells have to migrate through a porous membrane in direction to FCS.

As described in the material and methods, T24 and L3.6pl cells were pre-treated before seeded in collagen-coated Boyden chambers. As shown in Figure 20, a clear inhibition of migration started with a concentration of 1 nM Archazolid B and became even more prominent with a concentration of 10 nM. The results are similar in both cell lines. During the assay time almost no apoptosis (for the L3.6pl cells max. 20% apoptosis) was induced (Figure 3.20).

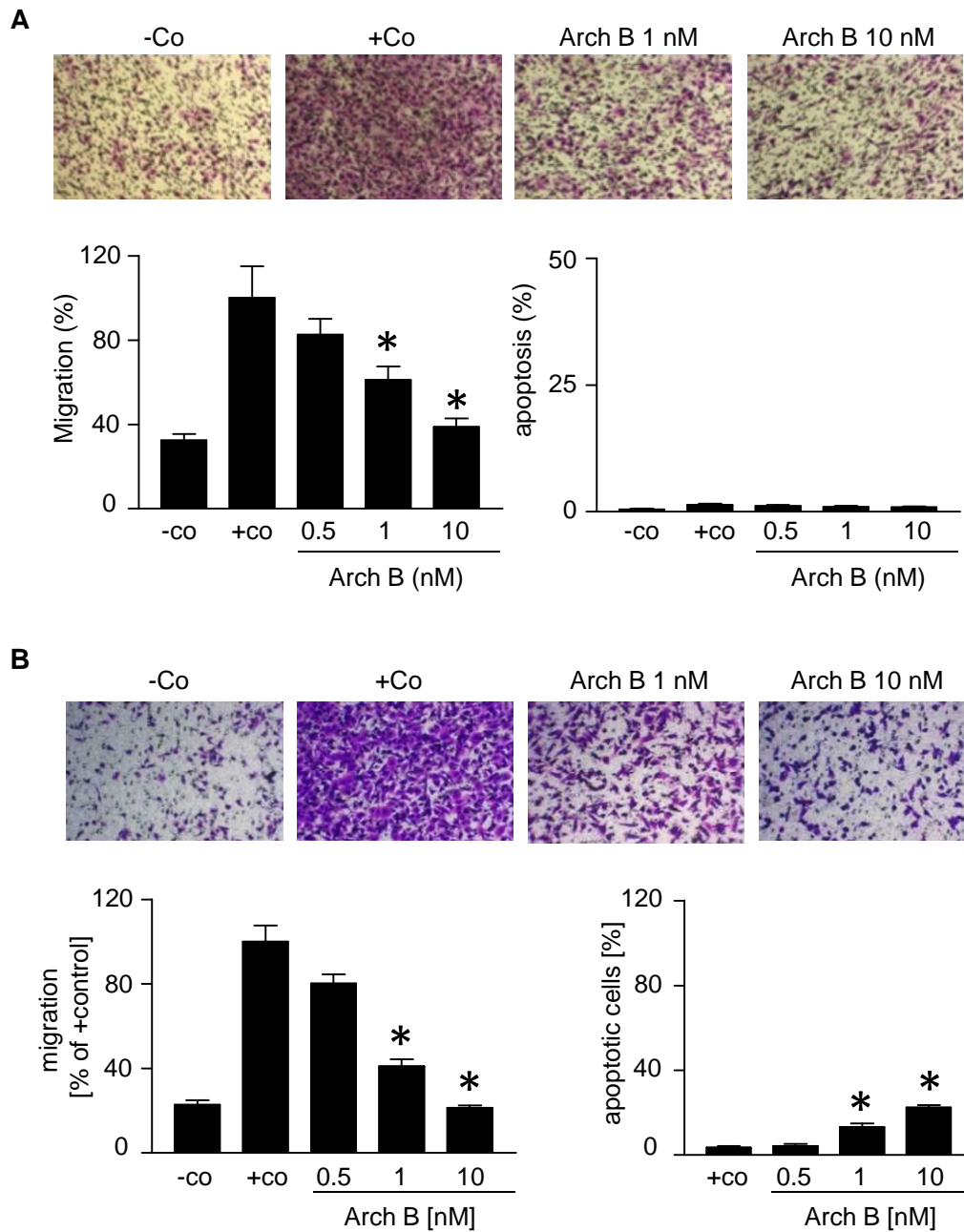


Figure 3.20: Archazolid B inhibits the migration of highly invasive cancer cells. (A) T24 cells were pre-treated for 24 hours and allowed to migrate in Boyden chambers for 4 hours. (B) For the L3.6pl cells the migration inhibition looks similar. L3.6pl cells were pre-treated for 16 hours and allowed to migrate in Boyden chambers for 20 hours. Bars represent the mean \pm S.E.M. of three independent experiments performed in triplicates. * $p < 0.05$ (One Way ANOVA, Dunnett's)

3.3.3.3. Effects of Archazolid B on cellular chemotaxis

To further analyze the migration process inhibited by Archazolid B, a chemotaxis assay was performed. Here, it can be distinguished if Archazolid B blocks cell migration via inhibiting cell motility per se (chemokinesis) or if the effects are caused by a loss of orientation. In a chemotaxis assay a FCS gradient is prepared and a directional migration to 10%

FCS is induced. Cells pre-treated with 10 nM Archazolid B were still able to move (intact accumulative distance), but without the right orientation in direction to FCS (reduced Euclidean distance and reduced distance direction y-forward migration index) (Figure 3.21).

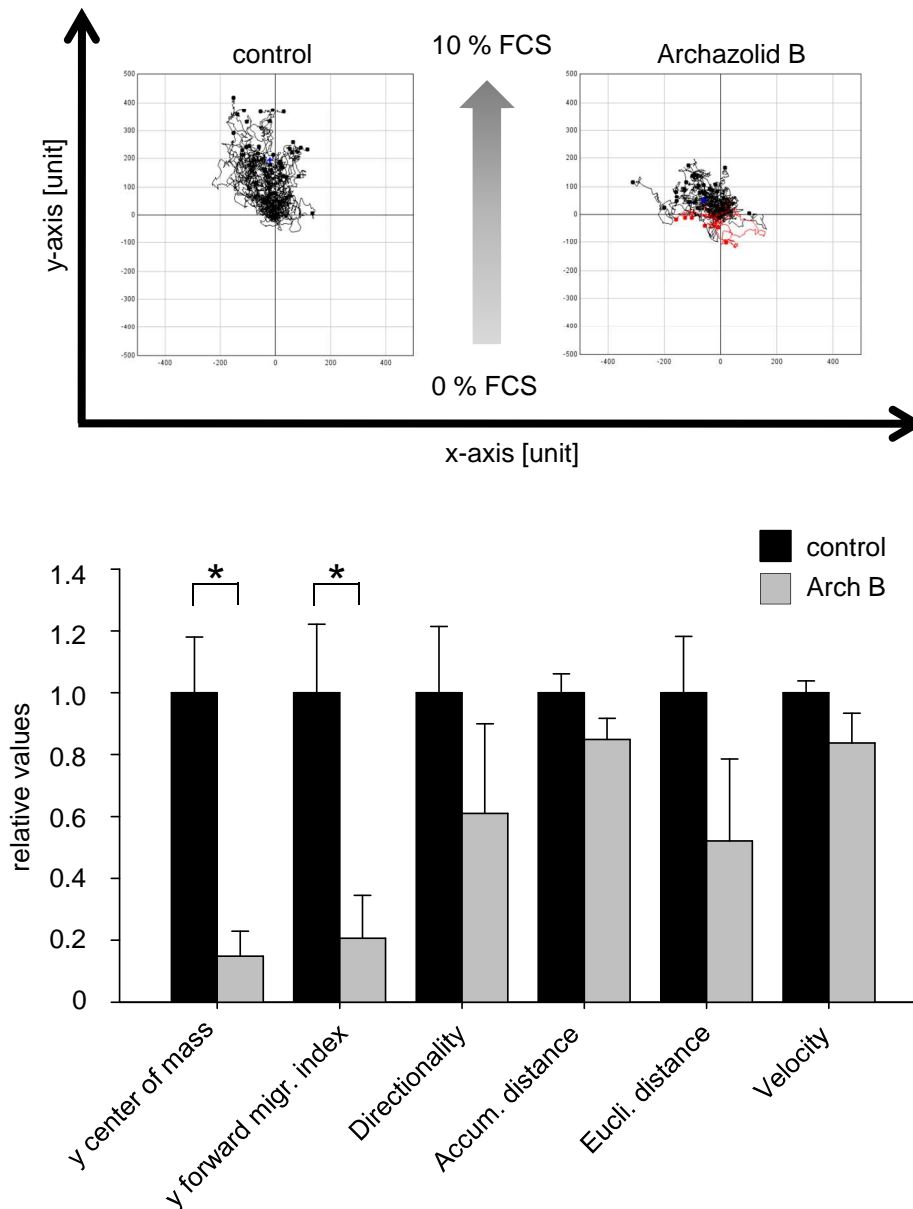
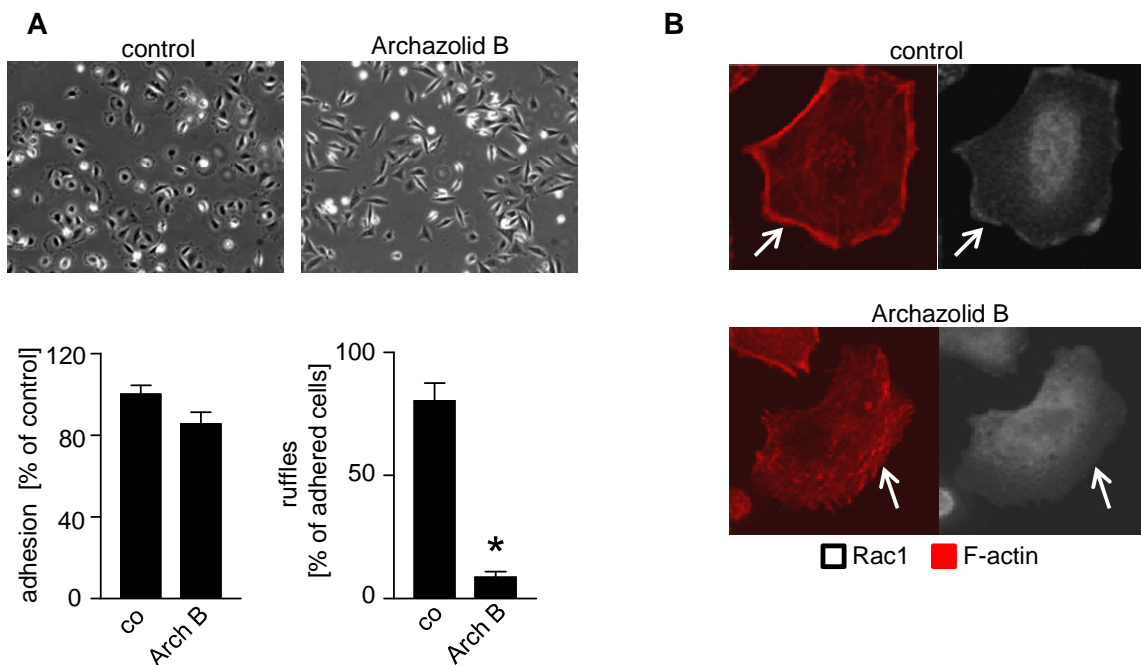


Figure 3.21: Archazolid B inhibits the migration of highly invasive cancer cells. T24 were treated with 10 nM Archazolid B for 16 hours. A FCS-gradient was created and life cell imaging was performed over 24 hours. Bars represent the mean \pm S.E.M. of three independent experiments. * $p < 0.05$ (t-test, unpaired)

3.3.2. Effects of Archazolid B on ruffle formation and the Rho-GTPase Rac1

Since the migration process in T24 cells seems to be inhibited, the effect on the adhesion was determined. T24 cells were treated with Archazolid B for 24 hours and then freshly seeded on fibronectin-coated IBIDI-slides. After 30 minutes of adhesion, cells were fixed with paraformaldehyde. Counting the adherent cells, no significant difference could be determined of Archazolid B-treated cells in comparison to control cells. But the morphological change of the Archazolid B-treated cells was obvious; since control cells show a prominent ruffle formation at the plasma membrane, no ruffles could be seen in Archazolid B treated cells (Figure 3.22 A). In the ruffles usually the active Rho-GTPase Rac1 is localized. After Archazolid B treatment, Rac1 is no longer localized at the plasma membrane during the adhesion process (Figure 3.22 B). Furthermore, during the migration process, no Rac1 is localized at the leading edge of T24 cells (Figure 3.22 C). In order to analyze if beside the localization, the activation of Rac1 itself is affected, we performed a Rac1-pulldown assay using a downstream target (Pak) of the active Rac1 (Rac1-GTP). Indeed, also the Rac1 activation is inhibited by Archazolid B treatment (Figure 3.22 D).



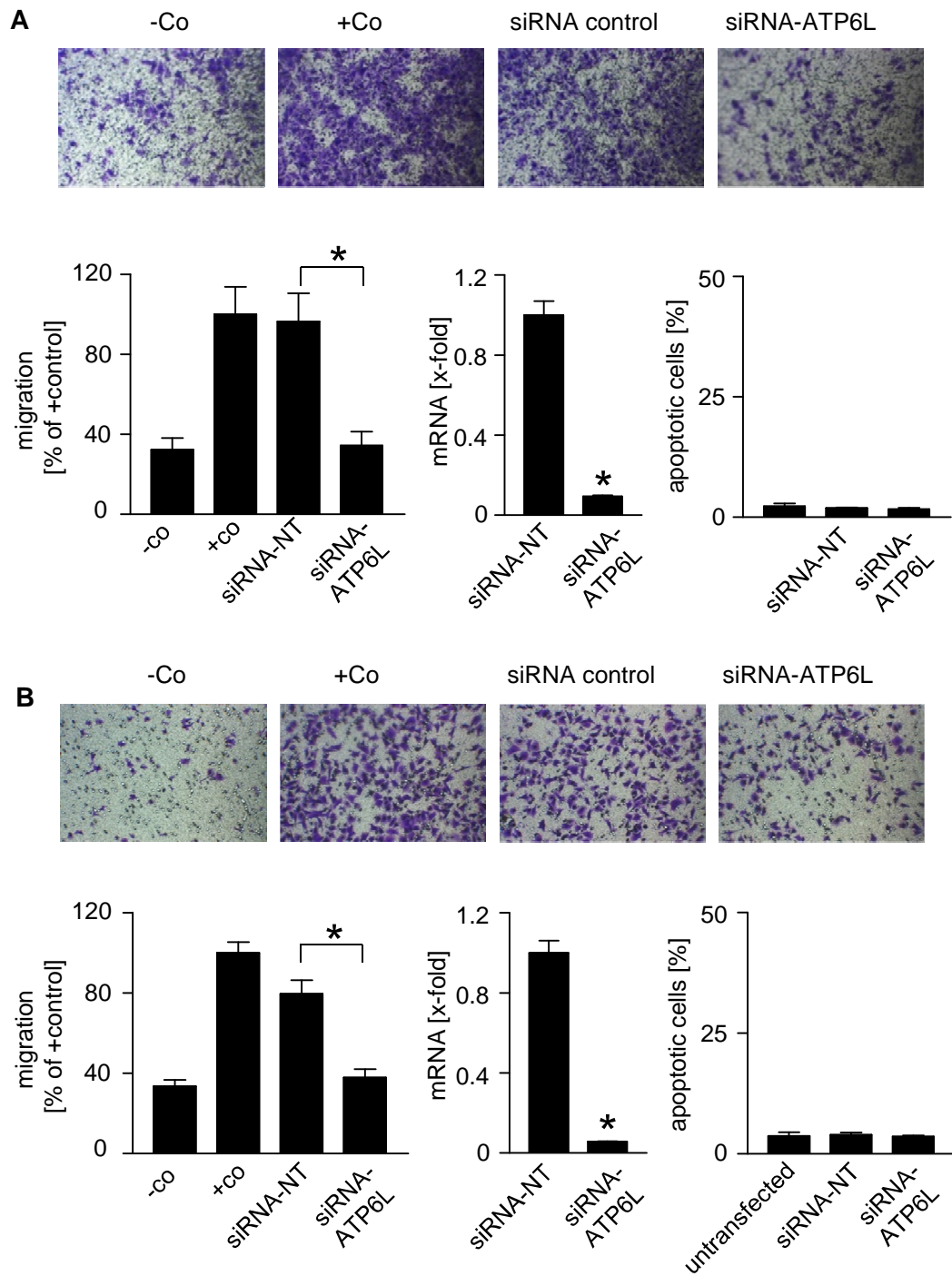


Figure 3.23: The migration of T24 (A) and L3.6pl (B) cells is inhibited by the downregulation of the Archazolid B binding site, the V-ATPase subunit c, by siRNA. Cells were transfected with siRNA for 24 hours, followed by a Boyden chamber assay. As a control, real-time PCR was performed. Furthermore, a cytotoxic effect induced by the siRNA-transfection was excluded by performing propidium iodide staining (Nicoletti *et al*⁶¹.) 24 hours after transfection (starting point of the Boyden chamber assay). Bars represent the mean \pm S.E.M. of three independent experiments performed in duplicates. * $p < 0.05$ (t-test, unpaired).

3.3.4. The downregulation of ATP6L inhibits localization and activation of Rac1

The described effects on the Rho-GTPase Rac1 could also be determined by downregulation of the V_0 subunit c of the V-ATPase (ATP6L). Generally, adhesion and the amount of ruffle formation were already decreased in cells transfected with control siRNA. But compared with the siRNA-ATP6L transfected cells, a decrease of ruffle formation could be determined. Furthermore in a scratch assay we could show, that ATP6L and Rac1 are not localized at the leading edge anymore. Also, the activation of Rac1 is affected by the downregulation of the V_0 subunit c of the V-ATPase (Figure 3.24).

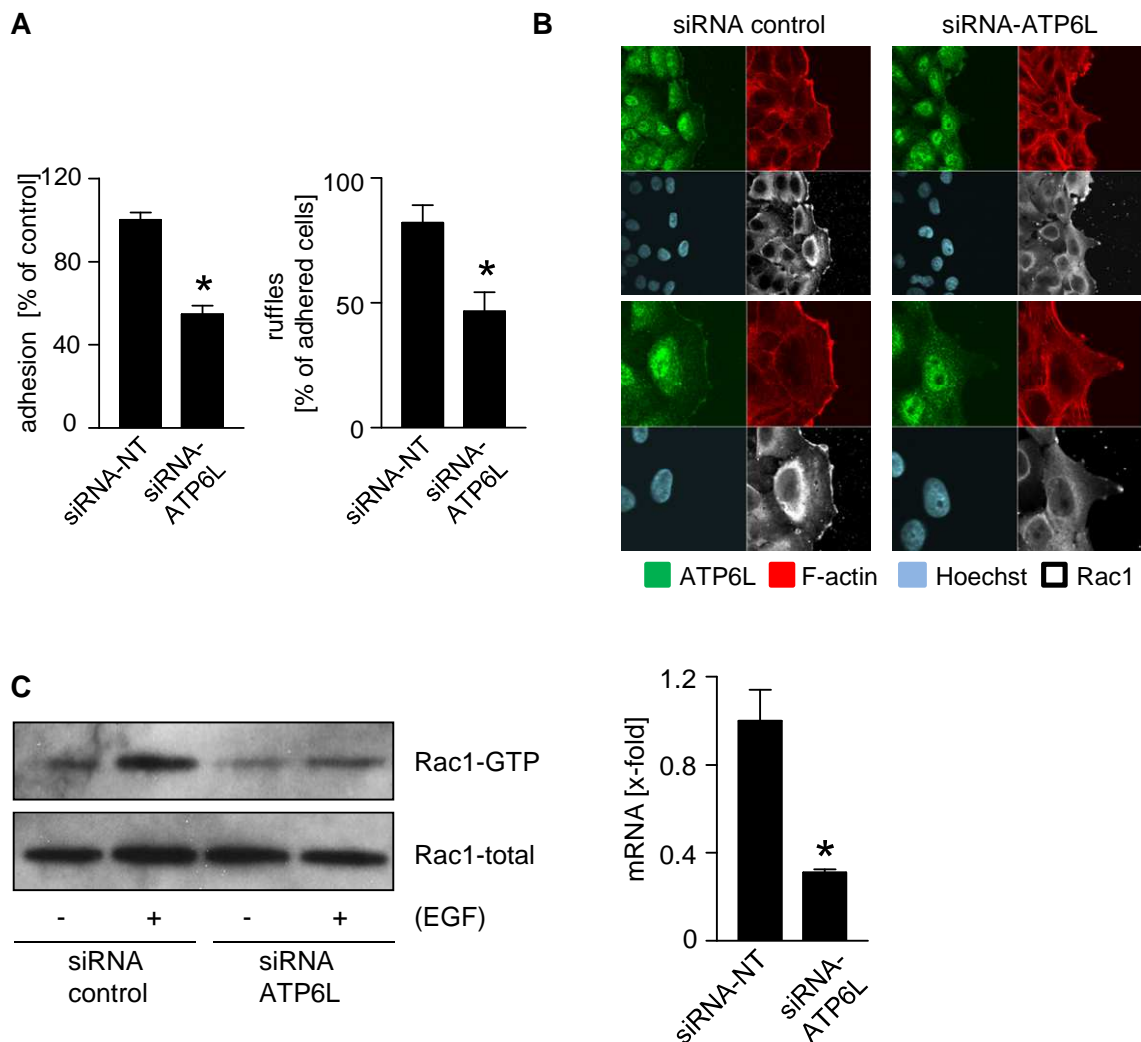
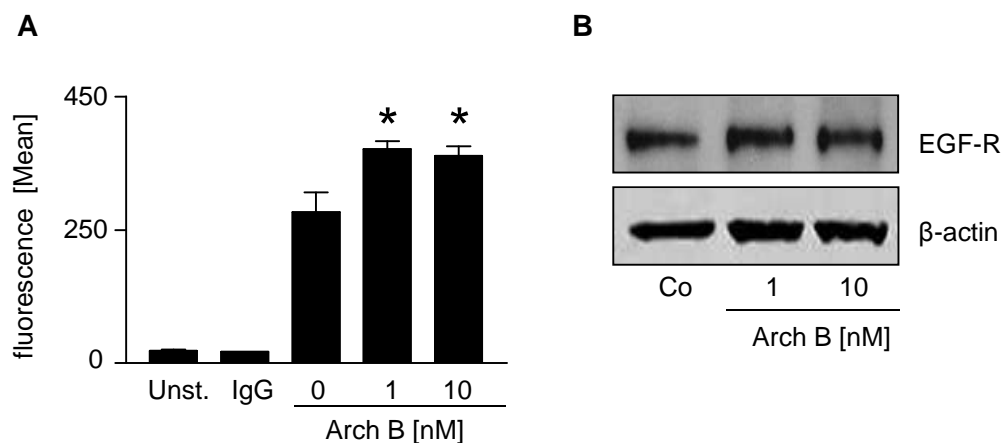


Figure 3.24: Downregulation of ATP6L affects Rac1 localization and activation (A) T24 cells were transfected 24 hours with siRNA-ATP6L and freshly seeded. Phase-contrast pictures were taken and cells were counted. Bars represent the mean \pm S.E.M. of three independent experiments performed in duplicates. * $p < 0.05$ (t-test, unpaired). (B) T24 cells were transfected for 24 hours with siRNA-ATP6L followed by a wound healing assay and fluorescent staining with antibodies

raised against ATP6L and Rac1 and the dye phalloidin-rhodamine. (C) A Rac1 pulldown assay (PIERCE) was performed 24 hours after transfection with siRNA-ATP6L. Downregulation of ATP6L via siRNA was proved for each single experiment by real-time PCR. Representative experiments of three independent experiments are shown.

3.3.5. Archazolid B increases EGF-R expression on the cell surface

Beside the Rho-GTPases, growth factor receptors play a crucial role in the migration process. With growth factor receptors, cells can detect the direction of nutrition and get therefore polarized. We measured the amount of epidermal growth factor receptor (EGF-R) on the cell surface. We could detect an increase of EGF-R on the cell surface after a treatment of 10 nM Archazolid B for 24 hours. Furthermore the total amount of protein did not change (Figure 3.30 A/B). Since this was quite surprising we were interested in the distribution of EGF-R on the cell surface. During migration, more EGF-R should be localized at the leading edge. In not-permeabilized cells we saw that the distribution of EGF-R changed after Archazolid B treatment. In control cells, a big amount of EGF-R seems to be localized at the leading edge. In Archazolid B-treated cells in contrast, EGF-R seems to be localized all over the cell surface and no longer at the leading edge (Figure 3.30 C). But the EGF-R seems to be still active, shown here by its phosphorylation at Tyr1068 (Figure 3.31 D).



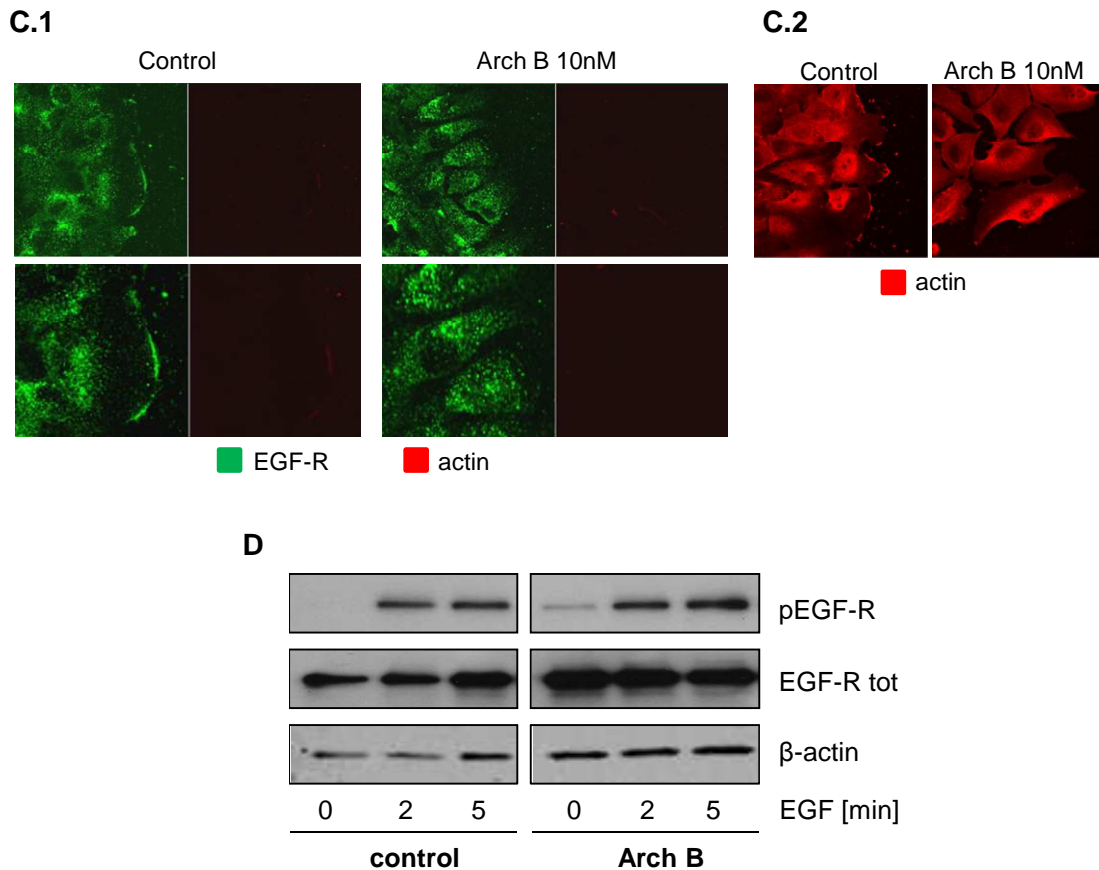


Figure 3.30: Archazolid B increases EGF-R expression on the cell surface and changes its localization. (A) T24 cells were treated for 24 hours with Archazolid B. Using an EGF-R-FITC antibody, surface EGF-R was labeled and its amount was measured via flow cytometry. Bars represent the mean \pm S.E.M. of three independent experiments performed in triplicates. * $p < 0.05$ (One Way ANOVA, Dunnett's). (B) A Western blot of total cell lysate was performed (C.1) Cells were treated for 24 hours with Archazolid B, scratched and after 5 hours of migration, fixed and stained for EGF-R without permeabilization (shown here by negative actin-staining). (C.2) As control T24 samples were permeabilized and stained with an antibody raised against actin. (D) T24 cells were treated for 24 hours with Archazolid B. After starvation period, EGF (100ng/ml) was added for various timepoints to induce EGF-R phosphorylation. A Western blot was performed.

3.3.6. Archazolid B affects EGFR signaling

Classical signaling pathways affected during the migration process are: the PI3K/AKT signaling pathways and the mitogen-activated protein kinases (MAPK) extracellular-signal-regulated kinases (ERK 1/2) pathway.

The extracellular signal-regulated kinases 1 and 2 (ERK 1/2) are the most prominent members of the family of mitogen-activated protein kinases (MAPK). MAPKs influence cell proliferation, differentiation, survival, apoptosis and development.⁷² Interestingly, the phosphorylation of ERK 1/2 was increased by a pre-incubation with Archazolid B (Figure 3.31 A).

AKT is a kinase important in various cellular processes like apoptosis, survival, cell growth and proliferation.⁷³ Since we induced the Rac1 activation with epidermal growth factor (EGF), we tested if the phosphorylation of AKT at Ser473, which is induced by EGF, can be inhibited by pre-treatment of Archazolid B. Performed was a time-course of EGF-treatment. We can see that the phosphorylation and therefore full activation of AKT is inhibited by Archazolid B pre-treatment (Figure 3.31 A). Furthermore, during migration, the binding of a growth factor activates PI3K, which induces PtdIns-2,4,5-P₃ production. By the binding of AKT to PtdIns-2,4,5-P₃ it is localized at the plasma membrane. In Figure 3.31 B it is shown that Archazolid B treatment inhibits the localization of AKT at the plasma membrane during the migration process (Figure 3.31 B).

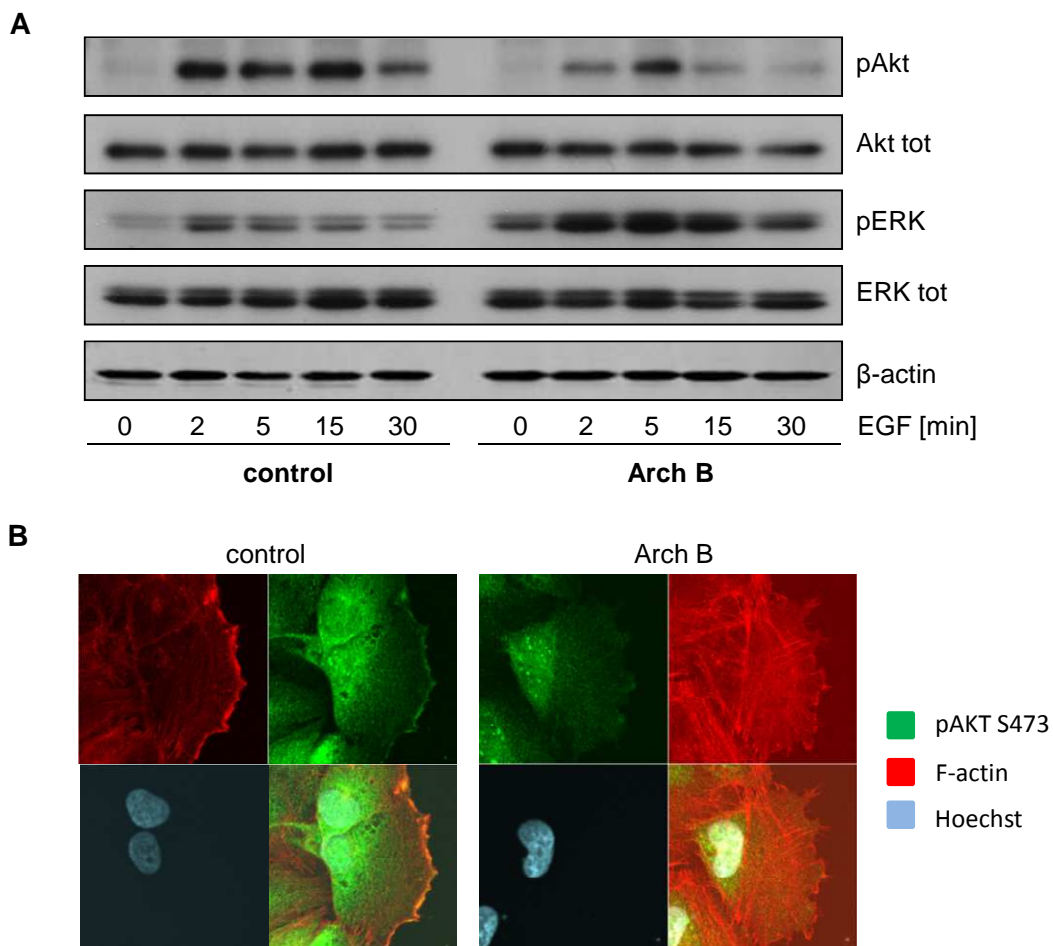


Figure 3.31: Archazolid B treatment reduces EGF-induced activation and localization of AKT but increases phosphorylation of ERK. (A) T24 cells were treated for 24 hours with 10 nM Archazolid B. Cells were starved for 2 hours and 100ng/ml EGF was added for various time periods. Finally, a Western blot was performed. One representative experiment out of three independent experiments is shown. (B) T24 cells were treated for 24 hours and a wound healing assay was performed. A staining for fluorescence microscopy was performed using antibodies raised against pAKT-S473. The actin-cytoskeleton was stained with phalloidin-rhodamine. One representative experiment out of three independent experiments is shown.

3.3.7. Archazolid B affects the internalization process

3.3.7.1. Effects on internalization after short time treatment

In the literature it could be reported that V-ATPase inhibition leads to defects in the cellular trafficking and recycling processes.^{16,74,75} Most of the effects induced by Archazolid B were determined after a longtime treatment. Baravalle *et al.* could show that Bafilomycin A₁ inhibits the recycling and degradation of dextran already after 1 hour treatment.⁷⁵ To prove that this known phenomenon can be achieved with Archazolid B as well, we treated T24 cells with Archazolid B for 1 hour and allowed dextran-rhodamine to internalize for 10 minutes. Cells were fixed and analyzed via confocal microscopy. Indeed, we can show that also Archazolid B inhibits the transfer of dextran from early to late endosomes already after this short-time treatment (Figure 3.27).

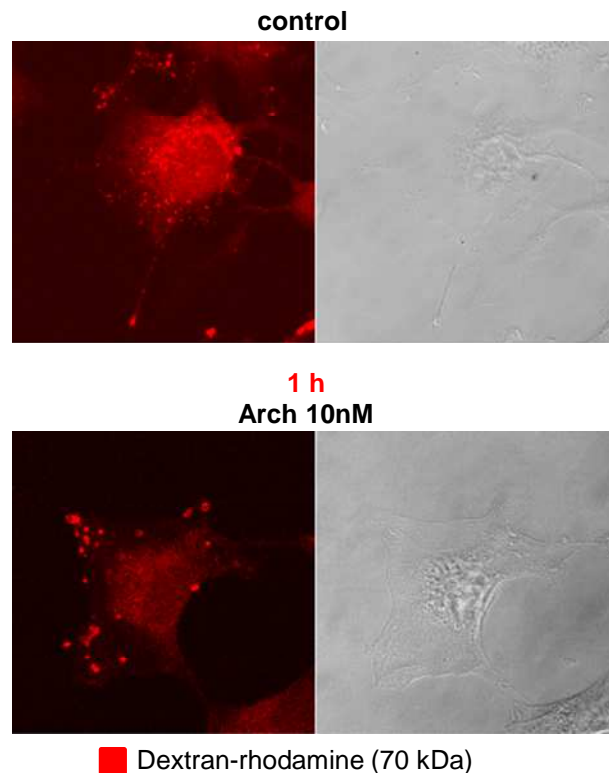


Figure 3.27: Archazolid B affects dextran uptake after short-time treatment. T24 cells were starved for 2 hours. After 1 hour, 10 nM Archazolid B was added. After Archazolid B treatment, dextran-rhodamine was added for 10 minutes. Finally cells were fixed and analyzed via confocal microscopy. Representative images out of three independent experiments are shown.

3.3.7.2. Effects of Archazolid B on internalization after longtime treatment

Furthermore, Baravalle *et al.* reported that they don't see an effect of 1 hour Bafilomycin A₁ treatment on the transferrin-uptake.⁷⁵ With Archazolid B we also don't see effects

on the transferrin uptake after shorttime treatments. But treating the cells for longer times, like 20 hours or 24 hours clearly evokes an inhibition of transferrin uptake. Since no acid wash was carried out, which removes extracellular bound transferrin to its receptor, we can see, that transferrin-rhodamine binds to its receptor but the uptake is inhibited (Figure 3.28).

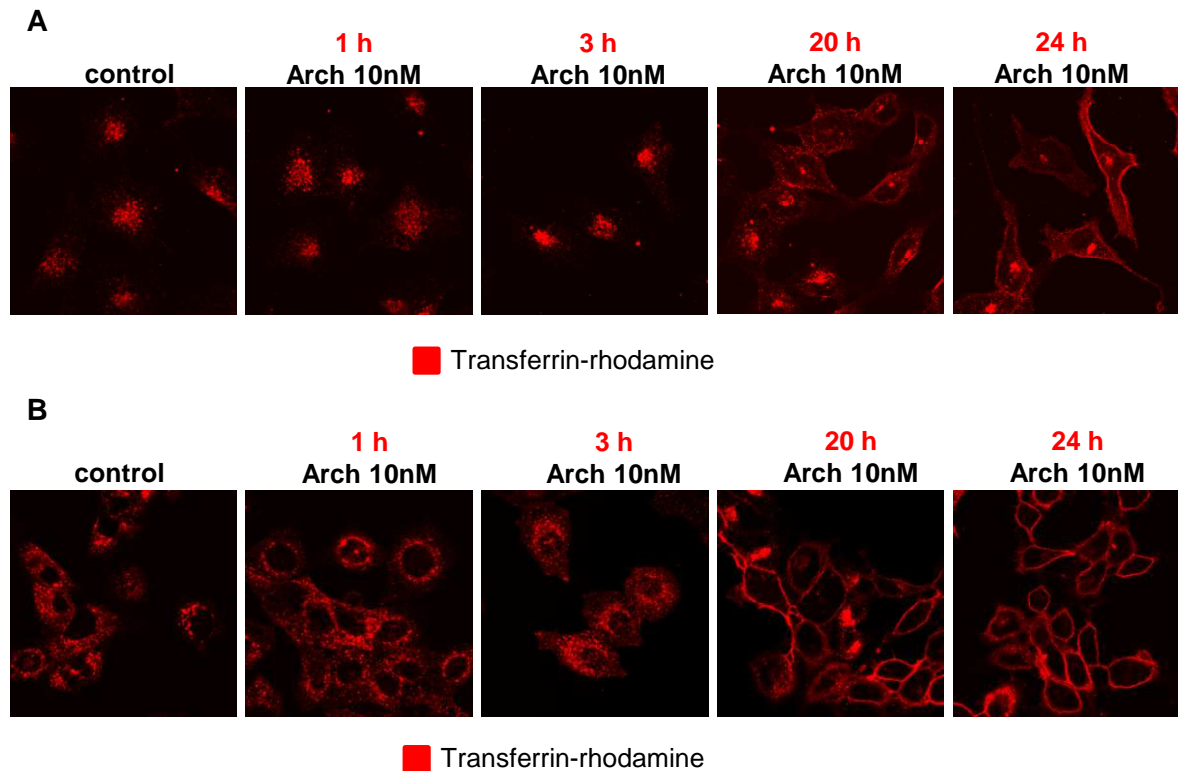


Figure 3.28: Archazolid B inhibits the uptake of transferrin-rhodamin after longtime treatment. T24 (A) and L3.6pl (B) cells were treated for various times with 10 nM Archazolid B. Transferrin-rhodamine was added for 10 minutes and cells were fixed with paraformaldehyde and analyzed via confocal microscopy. Representative images out of three independent experiments are shown.

The epidermal-growth factor receptor (EGF-R) is also described to get internalized upon ligand binding. After a 24 hour treatment with Archazolid B, the internalization of EGF-R is clearly reduced, shown by a reduced uptake of EGF-rhodamine (5 minutes EGF-rhodamine exposure). But after a longer exposure to EGF-rhodamine (15 minutes), some internalization is still possible (Figure 3.29).

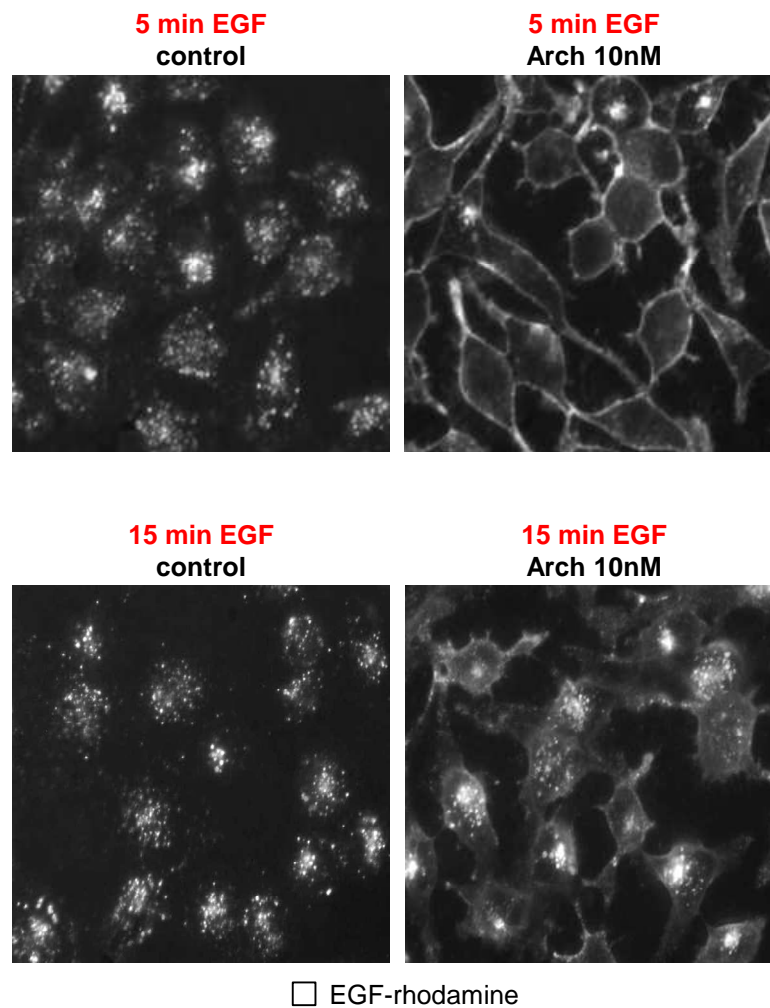


Figure 3.29: Archazolid B delays the uptake of EGF-rhodamine after longtime treatment. T24 cells were treated for 24 hours with 10 nM Archazolid B. EGF-rhodamine was added for 5 or 15 minutes and cells were fixed with paraformaldehyde and analyzed wide-field-microscopy. Representative pictures out of three independent experiments are shown.

3.3.8. Rab5-induced Rac1 activation is inhibited by Archazolid B

Palamidessi *et al.* reported that for the activation of the Rho GTPase Rac1 also the recycling molecule Rab5 is responsible.⁵⁶ Since we saw that Archazolid B inhibits the localization and activation of Rac1 and furthermore saw that the classical recycling pathways seems to be affected, we were wondering if Archazolid B influences Rab5-induced Rac1 activation. Firstly, we were testing if the ruffle formation in Rab5WT overexpressing cells is also inhibited upon Archazolid B treatment. Furthermore, we distinguished between the formation of peripheral ruffles, which are linked to the migration process and the formation of circular dorsal ruffles (internalization) as well to invadopodia (secretion/invasion). Indeed, we see that peripheral circular dorsal ruffle and invadopodia formation is significant-

ly reduced in Rab5-overexpressing Hela cells after 24 hours of treatment with Archazolid B (Figure 3.32).

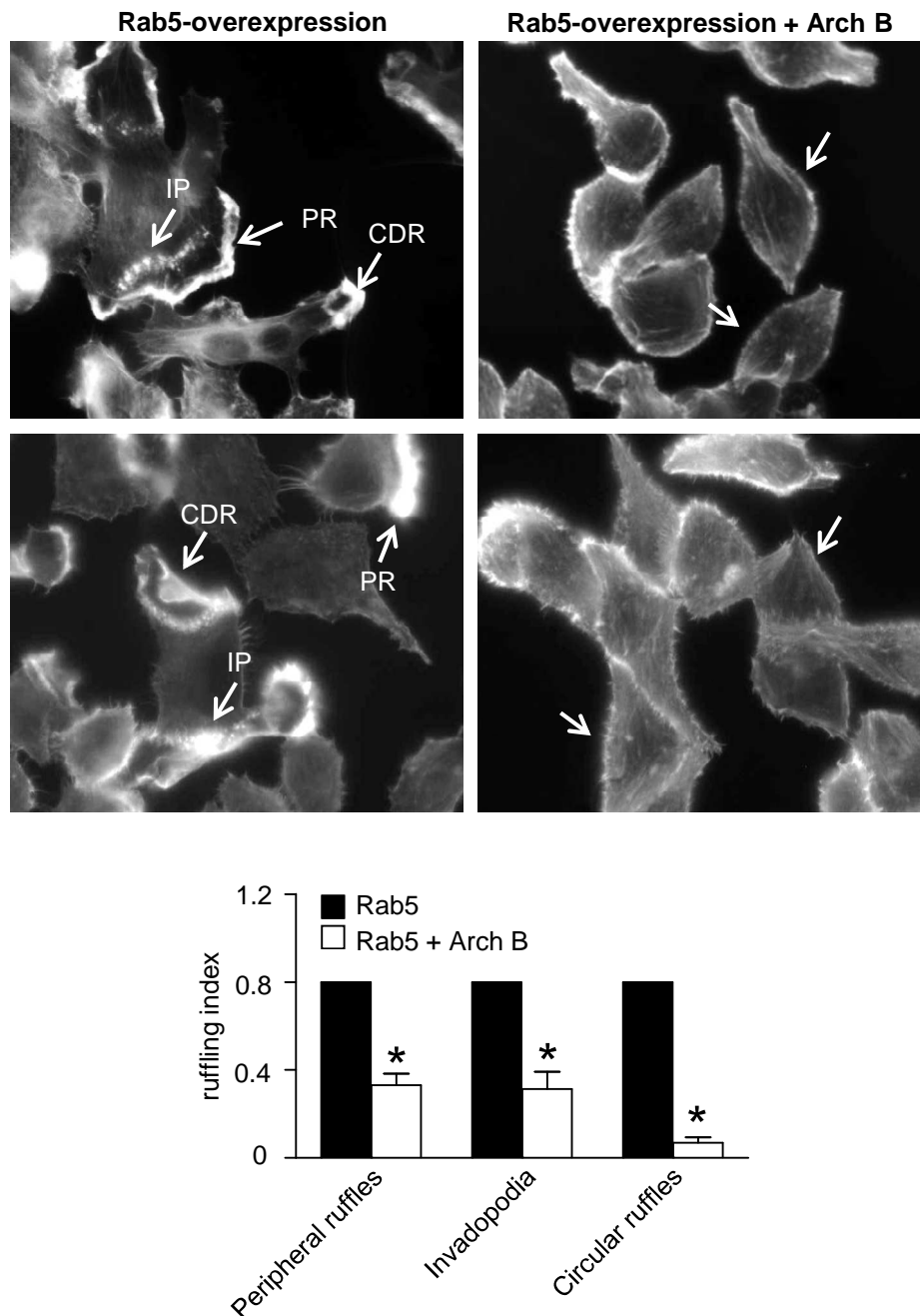


Figure 3.32: Archazolid B represses the formation of peripheral, circular dorsal ruffles and invadopodia in Rab5WT overexpressing Hela cells. Hela cells were transfected with Rab5WT and treated with Archazolid 10 nM for 24 hours. Ruffle formation was induced with 10% FCS and 10 ng/ml HGF for 5 minutes. Samples were stained for fluorescence microscopy with phalloidin-FITC and an antibody raised against Rab5. Number of ruffles in Rab5-overexpressing cells were counted. (PR=Peripheral ruffles; IP=Invadopodia; CDR=Circular dorsal ruffles) Bars represent the mean \pm S.E.M. of three independent experiments performed in triplicates. * $p < 0.05$ (t-test, unpaired).

Furthermore, we could verify that also in T24 cells Rab5WT-overexpression can activate Rac1 (Figure 3.33 A). This Rab5-induced Rac1 activation is inhibited after 24 hours of Archazolid B treatment (Figure 3.33 B). Via confocal microscopy we saw that even if Rab5 is overexpressed, Rac1 is not anymore localized at the plasma membrane of T24 cells after Archazolid B treatment (Figure 33 C)

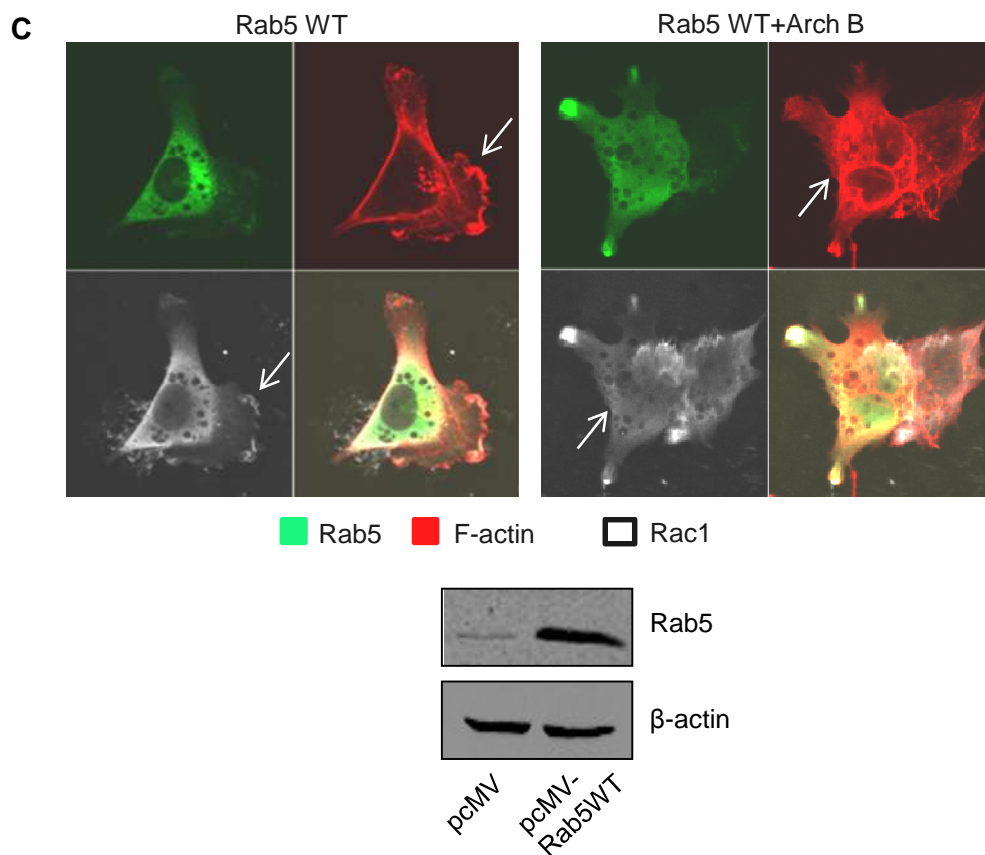
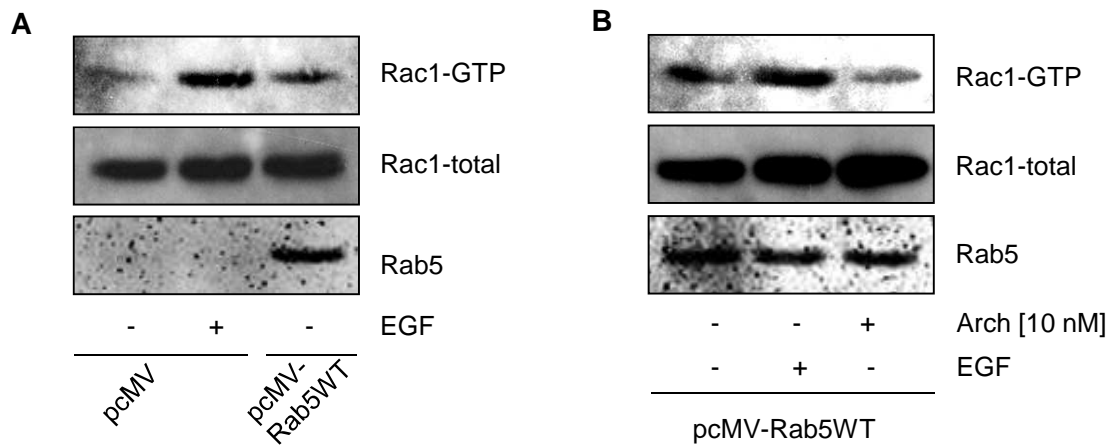
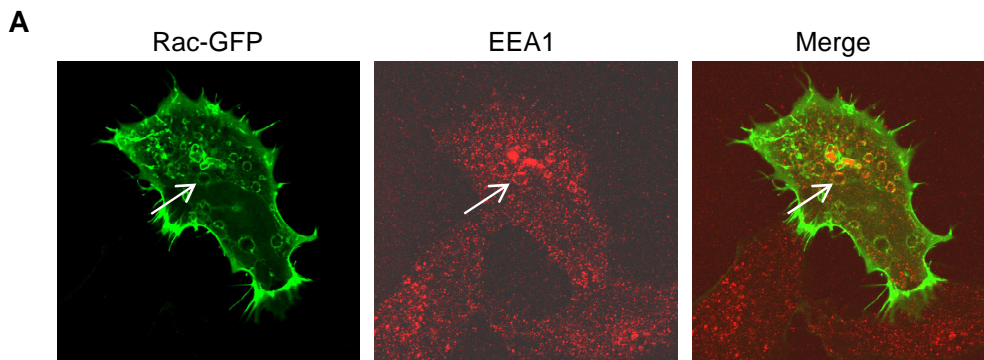


Figure 3.33: Rab5-induced Rac1 activation is inhibited by Archazolid B. (A) T24 cells were transfected with pcMV-Rab5. 24 hours later a Rac1-Pulldown assay (PIERCE) was performed. (B) T24 cells were transfected with pcMV-Rab5. After 16 hours of transfection, T24 cells were treated with Archazolid for another 24 hours. Finally, a Rac1 pulldown assay was performed (PIERCE). (C) T24 cells were transfected with Rab5WT and treated with Archazolid B for 24 hours followed by a staining for confocal microscopy with antibodies raised against Rab5 and Rac1. Representative images out of three independent experiments are shown.

3.3.9. Endosomal localization of the Rho-GTPase Rac1

By Rab5WT overexpression we induced the enlargement of early endosomes. To verify this enlarged endosomes as early endosomes a staining with the early endosome antigen 1 (EEA1) was performed. Beside the Rab5WT overexpression Rac1-GFP was overexpressed. Transfected Rac1-GFP is localized in the enlarged early endosomes of control cells (Figure 3.34 A). Upon treatment with Archazolid B, we determined less precise endosome structures with according Rac1-GFP positive ring structures. This would suggest that upon Archazolid B treatment Rac1 doesn't localize in Rab5 positive early endosomes (Figure 3.34 B).



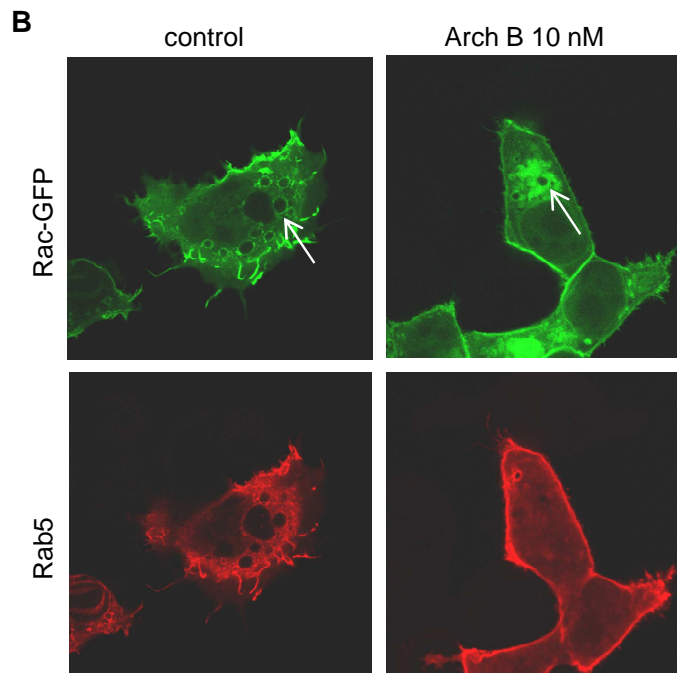


Figure 3.34: Rac1-GFP is less localized in Rab5-induced enlarged endosomes. Rab5WT was overexpressed in HeLa cells followed by a treatment with 10 nM Archazolid B for 24 hours. Cells were fixed with 4 % PFA and a fluorescence staining using antibodies raised against early endosome antigen 1 (EEA1) (A) or Rab5 (B). Samples were analyzed via confocal microscopy. Representative images out of three independent experiments are shown.

To elucidate if the Rac1, which might be still localized in endosomes after Archazolid B treatment, is still active, we transfected HeLa cells in addition to Rab5 and Rac1-GFP with a fluorescently tagged Rac1 interactive binding motive (CRIB-YFP plasmid). This construct acts as a biosensor of Rac1 activation since it can only associate with GTP-loaded Rac1. In control cells the biosensor is recruited to the Rab5 induced enlarged endosomes, indicating active Rac1. In Archazolid B treated cells none of the Rac1 binding motive (CRIB-YFP plasmid) is localized in the enlarged endosomes, therefore no active Rac1 is localized in Archazolid B treated HeLa cells (Figure 3.35).

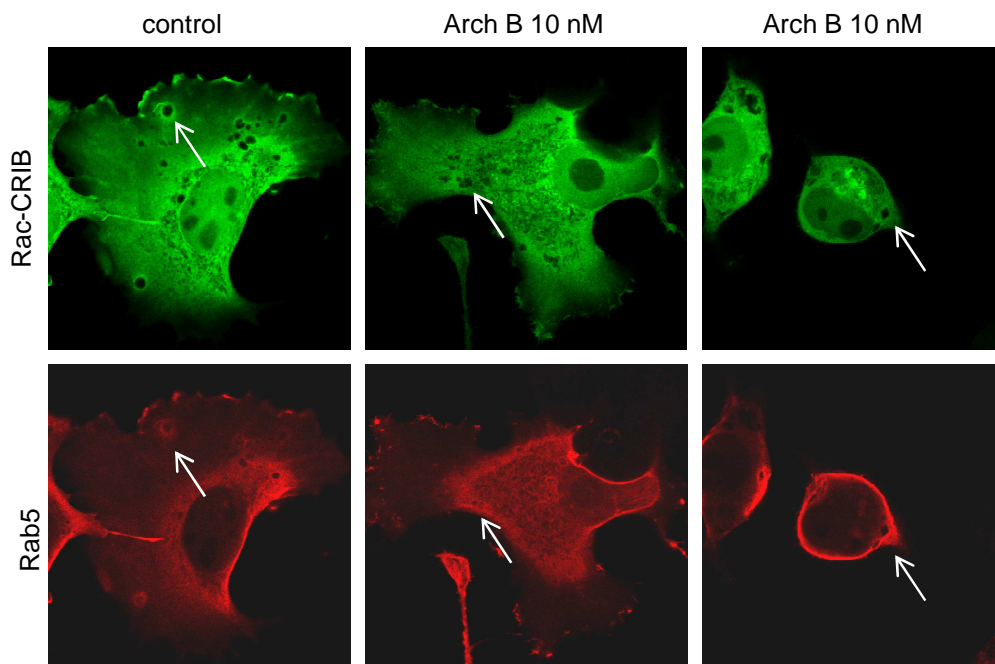


Figure 3.35: No active Rac1 is localized in Rab5-induced enlarged endosomes. Rab5WT, Rac1-HA and CRIB-YFP was overexpressed in HeLa cells followed by a treatment with 10 nM Archazolid B for 24 hours. Cells were fixed with 4 % PFA and a fluorescence staining using an antibody raised Rab5. Samples were analyzed via confocal microscopy. Representative images out of three independent experiments are shown.

DISCUSSION

4.1. Cancer and treatment strategies

The development of metastasis and the occurrence of resistance to nowadays available anti-cancer therapeutics are the main problems in cancer therapy. Current strategies are focused on the selective affecting of deregulated molecular pathways in cancer cells. But there are evidences that also cell processes leading to the abnormal metabolism in cancer cells may be attractive to attack. Because cancer cells show an increased glycolysis, resulting in high lactic acid production and proton accumulation, a new strategy could be to inhibit proton pumps and transporters, which would affect tumor cell survival.^{33,76}

In our study, we show that the V-ATPase inhibitor Archazolid B, which inhibits proton translocation, indicates highly potent characteristics as new potential anticancer agent. Our goal was to characterize Archazolid B concerning its anti-proliferative effects, its potential to induce apoptosis and its mechanism leading to cell migration inhibition. Since bladder cancer⁷⁷ and pancreatic cancer are quite common and often show high invasive and aggressive characteristics, we used for our experiments the highly invasive and resistant urinary bladder cancer cell line T24 and the pancreatic cancer cell line L3.6pl.⁷⁸

4.2. The V-ATPase as potential drug target

The Vacuolar-type ATPase (V-ATPase) is one of the fundamental enzymes in nature. It enables proton transport processes across membranes and regulates the intraorganellar, intra – and extracellular pH.^{26,32} During the last years, it got clear that malfunction of V-ATPase is correlated with a number of diseases such as osteopetrosis, renal acidosis, male infertility or cancer.⁶

We could show that the level of V-ATPase subunit c expression is increased in the highly invasive urinary bladder cancer cells T24 compared to the non-cancerous epithelial breast cells MCF-10A (Figure 3.1 A). Furthermore compared to the low invasive liver cancer cells HepG2, the highly invasive cancer cells T24 and L3.6pl show an increased level of V-ATPase subunit c expression. (Figure 3.1 B). Additionally, the V-ATPase subunit c is localized at the plasma membrane of T24 cells (Figure 3.2) and therefore the V-ATPase is probably responsible for the regulation of the pH not only in acidic organelles, but also in the extracellular space.

Our results are undelined by other studies, where an overexpression of various subunits of the V-ATPase could be shown⁷ and their expression may correlate with the invasive-

ness of these cancer cells⁶⁸. Furthermore it could be shown that the distribution of the V-ATPase in highly invasive cancer cells like MDA-MB-231 differs from the distribution in lowly invasive cancer cells like MCF-7, substantiating the hypothesis of the importance of an acidific microenvironment during cell migration and invasion.^{15,33} Due to its increased expression and different localization in invasive cancer cells, it is assumed that the V-ATPase plays a crucial role in the process of tumor development and metastasis.^{7,15,68}

In most studies regarding the V-ATPase the well known plecomacrolide V-ATPase inhibitors Bafilomycin A₁ and Concanamycin A were used. During this work we wanted to further characterize a new, very potent V-ATPase inhibitor, called Archazolid B. The Archazolids are a novel group of V-ATPase inhibitors. Archazolid, first isolated from the myxobacteria *Archangium gephyra* by Reichenbach and Höfle^{5,79}, seems to specifically and very potently (IC₅₀ values in the nanomolar range) inhibit the V-ATPase when compared with purified Na⁺/K⁺-ATPases and mitochondrial F-ATPase.

In our study, Archazolid B inhibits the lysosomal V-ATPase in the nanomolar range (Figure 3.3). We further discovered that Archazolid B regulates genes involved in the pathways of cell death, proliferation and cancer (Figure 3.4). Since we can observe high expression levels of the V-ATPase in the highly invasive cancer cells T24 and L3.6pl and we see that the new and potent V-ATPase inhibitor Archazolid B affects gene regulation in the field of cancer, we deeply assume that the V-ATPase is an interesting drug target for further investigations.

4.3. The role of V-ATPase in tumor cell growth

4.3.1. Anti-proliferative effect of Archazolid B

Cancer cells are characterized by their abnormal growth regulation, immortality, self-sufficient growth, evasion of apoptosis, sustained angiogenesis, invasion and metastasis.^{80,81} Beside the possible selection of tumor cells, which are able to survive in an unfavourable tumor microenvironment, it has been shown that the acidity also plays a role in resistance to chemotherapy, cell migration and proliferation.⁸²⁻⁸⁵

Archazolid B inhibits the proliferation of the highly invasive cancer cells lines T24 and L3.6pl in picomolar concentrations (Figure 3.5). Archazolid B is even more potent than Archazolid A and the already known plecomacrolide V-ATPase inhibitor Concanamycin A. Furthermore, the inhibition of proliferation is really due to the specific macrolide structure,

since the precursor molecule of the Archazolid B synthesis doesn't show any inhibitory effect. Really prominent is the effect of Archazolid B on the clonogenic survival. With this assay a chemotherapy can be mimicked.⁸⁶ The highly invasive and resistant pancreatic cancer cells L3.6pl were not able to recover from Archazolid B treatment (Figure 3.6). This longtime proliferation effect could be shown for the first time as an effect of a V-ATPase inhibitor.

4.3.2. Inhibition of V-ATPase as attractive method to induce apoptosis

Many cancer therapies, like chemotherapy or radiotherapy, exert their antitumor effect by triggering apoptosis.⁸⁷ Upon Archazolid B treatment apoptotic features like cell shrinkage and DNA condensation were determined (Figure 3.7). Measuring the amount of apoptotic cells, we could show that Archazolid B induces apoptosis in nanomolar concentrations. Interestingly, compared to other chemotherapeutics, Archazolid B induces apoptosis relatively at a late stage. Even though we see morphological changes after 24 hours, apoptosis is measurable from 48 hours on. After 72 hours of Archazolid B treatment, about 60 % of the T24 and L3.6pl cells were apoptotic (Figure 3.9). In WEHI-231 cells (B lymphoma) the Concanamycin A-induced apoptosis was reduced by a pre-incubation with imidazole, a cell-permeable base. The authors suggested herewith that apoptosis is due to intracellular acidification.⁸⁸

In T24 cells we see a slight increase of the S-phase in the cell cycle analysis, which is similar to the determination of a less specific V-ATPase inhibitor Lejimalide.⁸⁹ The authors suggest that the lysosomal signaling, like the release of cystein proteases like Cathepsin B, which is important for the activation of pro-apoptotic molecules like Bid or the inactivation of the anti-apoptotic Bcl-2 family members, might be inhibited leading to a S-phase arrest and induction of apoptosis.⁸⁹⁻⁹²

There exist studies, describing that plecomacrolide V-ATPase inhibitors induce apoptosis via the intrinsic apoptotic pathway. More precisely, in a human submandibular gland ductal cancer cell line HSG, the release of mitochondrial cytochrome c resulting in the caspase-activation upon treatment with Concanamycin A was determined⁹³ as well as in B-cell hybridoma HS-72 caspase-3 activation was measurable.⁹⁴ The involvement of V-ATPase-inhibition in the intrinsic apoptotic pathway is underlined by a study showing that overexpression of Bcl-2 reduces apoptosis in WEHI-231 cells (B lymphoma) induced by

Concanamycin A.⁸⁸ To proof if also Archazolid B treatment affects the intrinsic apoptotic pathway, we first checked the involvement of caspases in the induced cell death. Caspases are the main mediators to induce apoptosis. A failure in their activation is described as a resistance mechanism of cancer cells to apoptosis.^{95,96} A combination of Archazolid B and the Pan caspase-inhibitor QVD-OPh showed no apoptosis induction indicating that the apoptosis induced by Archazolid B is caspase-dependent. Caspases can be activated via the extrinsic receptor pathway or via the mitochondrial intrinsic pathway. Besides caspases the Bcl-2 family members are also involved in the intrinsic apoptotic pathway and their interplay influences the permeability of the outer mitochondrial membrane.⁴⁷ In addition to the downregulation of the anti-apoptotic molecule Bcl-2 upon Archazolid B treatment we see that: the mitochondrial membrane potential is affected, which leads later on to a cytochrome c release (Figure 3.14). Caspases like caspase-9, which forms together with cytochrome c and Apaf-1 the apoptosome, is activated upon Archazolid B treatment. Furthermore, caspase-3 is active, which finally induces cell death (Figure 3.12. C/3.13).

Interestingly, we determined also a quite strong caspase-8 activation (Figure 3.12 A). Possible is that also the extrinsic pathway is involved in the Archazolid B-induced apoptosis. Over the cleavage of Bid, a Bcl-2 family protein with a BH3 –only domain, active caspase-8 activation can also induce the mitochondrial apoptotic pathway. Bid translocates to the mitochondrial membrane causing cytochrome c release. Indeed, in addition to caspase-8 activation, we see a reduction of the pro-Bid, indicating that Archazolid B also induces apoptosis via the extrinsic pathway (Figure 3.12 B).

Similar to the findings of Huss *et al.*⁸, who showed the specific binding of Archazolid B to the V-ATPase, we could see that Archazolid B has no effect on isolated mitochondria. This proves that Archazolid doesn't bind to the mitochondrial F_1F_0 -synthase (data not shown). Since the induction of apoptosis takes quite a while, we suggest that the pH sensitive activation of caspases leading to apoptosis is an indirect effect due to the pH change in intracellular organelles and the cytosol. How the V-ATPase is precisely involved in the induction of apoptosis and why this induction takes quite a while, is the topic of ongoing projects. Especially the involvement of autophagy and metabolism affected by Archazolid B will be further elucidated.

It is suggested that changes in extra - and intracellular pH are significantly involved in mechanisms of multidrug resistance, like a low uptake rate of basic drugs or the sequestration of drug compounds in the lysosomal vesicles.^{84,97,98} Furthermore an increased V-

ATPase activity has been shown to have anti-apoptotic effects.⁹⁹ Combinations of V-ATPase inhibitors in combination with available anti-cancer drugs show increased effects in especially multi-drug resistant cells increasing their sensitivity.^{83,84}

Therefore inhibiting the V-ATPase with Archazolids alone or more reasonable in combination with available therapeutics, would be an attractive new therapeutic approach to increase cancer cell sensitivity.

4.3.3. Effects of Archazolid B on T24 spheroid growth

In commonly used 2D *in vitro* cell systems, essential cellular tissue functions are missing. Therefore the potential to predict the cellular responses of a real organism is limited. The formation of 3D spheroids therefore offers a great opportunity to get a deeper insight into the cellular system before starting animal studies.¹⁰⁰ The T24 spheroids are formed out of anoikis-resistant cells and together with their tissue-like characteristics they can be used as a model of small tumors or micro-metastasis.¹⁰¹

In our study the cell viability of the T24 spheroids was diminished after Archazolid B treatment (Figure 3.15). Since Archazolid B also affects this tissue-like model, it would be really interesting to test the potency of Archazolid B in *in vivo* tumor studies.

4.3.4. The role of the subunit c

Several V-ATPase inhibitors are known, like Bafilomycin, Concanamycin, benzolactine enamides salicylhalamides and lobotamides, which all seem to prominently bind at the c subunit. Also in *Neurospora crassa* it could be shown that mutations in the subunit c of the V-ATPase decreases the sensitivity of bafilomycins 20 - to 60 fold. Kubota *et al.*¹⁰² showed a correlation of the V-ATPase subunit c expression and invasion potential of fibroblasts and human invasive lung cancer cells A549 *in vitro*. In another study, the subunit c (ATP6L) was knocked down using DNA vector-based small interfering RNA (siRNA) in a human hepatocellular carcinoma cell line with highly metastatic potential (HCCLM3). These injected cells showed an effective growth retard and the formation of metastasis was suppressed.⁶⁸

In our experiments we could not see a basal effect on proliferation after 72 hours or apoptosis induction by downregulation of the V₀ subunit c (ATP6L) (Figure 3.16). But in combination with the Archazolid B treatment, the apoptosis-rate increased in the T24 cells. With

the downregulation of the V_0 subunit c by siRNA, we still can detect 30% of mRNA level. Eventually, this amount might be enough to maintain V-ATPase function for a certain time. In combination with Archazolid B the activity is completely inhibited and effects are more prominent. Similar Byun *et al.*¹⁰³ could not determine a lysosomal pH change after 2 days of transfection with siRNA-ATP6L in glial cells, suggesting that ATP6L may function also independently of its role as part of the V-ATPase complex. But they could show that siRNA-ATP6L transfected cells were more sensitive to sodium nitroprusside-induced cell death. Moreover in former studies they showed that cell viability wasn't reduced after siRNA-ATP6L transfection, but in combination with exposure to H_2O_2 significantly decreased cell viability compared to control cells.¹⁰⁴

But indeed, the long-time proliferation/clonogenic survival of siRNA-ATP6L transfected cancer cells is prominently inhibited in our studies (Figure 3.17). This effect could be even increased by additional low dose treatment with Archazolid B (data not shown). Downregulation of the V-ATPase subunit c indeed affects the growth of highly invasive cancer cells. But probably the cells are able to compensate the reduced level of physiological active V-ATPase for a certain time period.

In the multidrug resistant MCF-7/ADR cells the downregulation of ATP6L by siRNA showed increased sensitivity to basic chemotherapeutics like doxorubicin, 5-fluorouracil and vincristine.¹⁰⁵ Tumor acidity obviously plays a crucial role in cancer cell development and seems to be an attractive approach for new treatment options.

But still it is also possible as suggested by Byun *et al.*¹⁰³, that the V-ATPase subunit c might function independently of its role in the V-ATPase complex. This has to be further defined in future studies. Concerning the additional effect of Archazolid B, it is deeply assumed that the increased effects are due to a complete V-ATPase inhibition-but still an additional off-target effect, which might be not as specific, can not be excluded until now.

4.4. Impairment of V-ATPase in tumor cell migration

In a study of Sennoune *et al.* it could be shown that highly invasive MDA-MB231 human breast cancer cells express V-ATPase at the plasma-membrane, whereas no plasma-membrane V-ATPase could be detected in the poorly invasive MCF-7 cell line.¹⁵ They claimed that the V-ATPase has specialized functions in cell growth, differentiation, angio-

genesis and metastasis. With Bafilomycin and Concanamycin a reduction of invasion, especially of the aggressive MDA-MB231 cells, was shown.^{7,15}

Besides the localization of V-ATPase in the lysosomes we could also show that the V_0 subunit c of the V-ATPase is also localized at the plasma membrane of the T24 cells (Figure 3.2 and 3.3), suggesting a profound role in the migration process of these invasive cancer cells. Furthermore, with a pre-treatment of Archazolid B we see inhibitory effects on cell migration on both invasive cell lines we have used. The migration in a 2D wound healing assay as well as the migration through a porous membrane in direction of growth media (Boyden chamber assay) is inhibited (Figure 3.19 and 3.20). As shown in a chemotaxis assay, especially the γ -forward index is significantly reduced upon Archazolid B treatment (Figure 3.21). This would suggest that the proper polarization of the cells including the proper F-actin organization is affected by Archazolid B treatment.

4.4.1. Rac1 signaling

Since we see the strong anti-migratory effects by Archazolid B treatment, we were interested in the underlying molecular mechanism. There are a few studies describing that V-ATPase may play a crucial role during migration and its inhibition results in the reduction of the migration potential of cancer cells⁷; but the precise signaling remains still undefined.

As we suggested after the result of the chemotaxis assay, that Archazolid B might be involved in the process of polarization, we were interested in the main players regulating the cytoskeleton: the Rho-GTPases and PI3K-pathway.

Looking at the process of adhesion, which is a major step during migration, we couldn't see a reduction of adhesion on a fibronectin matrix by Archazolid B treatment. But interestingly, the cell morphology was totally changed, indicating an alteration in the actin-cytoskeleton (Figure 3.22 A). Usually during adhesion and migration, actin condenses at the plasma membrane. All these actin structures are generally described as ruffles. The Rho GTPase Rac1 induces the polymerization of F-actin and is therefore also localized in these ruffles. During the adhesion, the formation of ruffles is almost completely inhibited by Archazolid B treatment and no Rac1 is localized at the plasma membrane (Figure 3.22 A/B). Also during migration, the localization of Rac1 is inhibited as well as its activation is reduced (Figure 3.22 C/D). So far we would suggest, that the proper function of the Rho GTPase Rac1 is affected upon Archazolid B treatment.

Interestingly, using siRNA to downregulate the V_0 subunit c of the V-ATPase, which corresponds to the binding site of Archazolid B, we can determine similar effects. The migration of both highly invasive cancer cells is decreased after siRNA-ATP6L downregulation (Figure 3.23). Furthermore, ruffle formation, Rac1 localization and Rac1 activation is inhibited (Figure 3.24). This indicates that the determined effects of Archazolid B are indeed due to the malfunction of the V-ATPase or more precisely to the V_0 subunit c.

4.4.2. EGF-R and its downstream players

The induction of migration is usually induced upon activation of a growth factor receptor by ligand binding. Herewith the cell gets oriented in direction of nutrients and therefore guides the actin remodeling, leading to the formation of migratory cellular protrusions.¹⁰⁶ After 24 hours of Archazolid B treatment we see that the EGF-R is accumulating at the cell surface, whereas the amount of total EGF-R seems not affected. Also, Bafilomycin A_1 was described to reduce clathrin dependent internalization of the parathyroid hormone related peptide receptor.¹⁰⁷

Moreover we see that the distribution of the EGF-R on the cell surface during migration is changing by Archazolid B treatment. In control cells the EGF-R is clearly localized at the leading edge, whereas this distribution is totally destroyed upon Archazolid B treatment (Figure 3.25). These results would suggest a defect of EGF-R internalization, following in an unorganized localization of EGF-R on the cell surface. Since growth factor receptors are the initial tactic guide to induce the cell polarization, we propose that Archazolid B influences this process leading to undirected cell migration. The influence of V-ATPase inhibition on recycling processes has been reported^{75,107} and is further discussed for Archazolid B below.

Since the accumulated EGF-R seems to be still active after Archazolid B treatment (Figure 3.30 D) it is not surprising that the downstream-target ERK, involved in the MAPK pathway, is increased in its activation (Figure 3.31). The MAPK-pathway is also described as a pro-survival pathway¹⁰⁸, which could be activated upon Archazolid B treatment as a possibility to overcome the cellular stress situation.

Beside its role in cell proliferation it has been described in many studies that PI3K plays a major role in the migration processes.⁵¹ Upon activation of the growth receptor, PI3K becomes activated and induces phosphorylation of PtdIns-2,4- P_2 to PtdIns-2,4,5- P_3 . This is localized at the plasma membrane and usually binds to AKT which therefore gets phos-

phorylated and bound to the plasma membrane. We see that the phosphorylation of AKT as well as its localization at the plasma membrane of migrating cells is inhibited (Figure 3.31). As known, both, Rac1 and AKT, get activated by PI3K and furthermore it is suggested that the activities of Rac1 and AKT are connected and act in a positive feedback loop.¹⁰⁹ Therefore, it would be interesting to test if the activity of PI3K is also diminished upon Archazolid B treatment and if there is a direct connection between AKT and Rac1 activation. Attractive to look at would be for example if a combinatory treatment with Archazolid B and Wortmannin, a PI3K inhibitor, would increase the inhibitory effect of Archazolid B on Rac1 activation and cell migration. To proof a direct Rac1-AKT interaction, it would be interesting if by expression of a constitutive active AKT the reduction of Rac1 activation by Archazolid B could be diminished.

4.4.3. Involvement of V-ATPase in endocytosis

Endocytosis is an important cellular mechanism for the uptake of nutrients, hormones, growth factors and plasma proteins.⁷⁵ Therefore, it is an invaluable process involved in cell survival and migration. Endosomes and lysosomes, where recycling and degradation takes place, are acidified by V-ATPases.²³ The acidic pH is important for the dissociation of ligands from its receptors and degradation processes.⁷⁴ Increase of the pH induced by Bafilomycin has been shown to affect the delivery of endocytosed molecules to late endosomes or lysosomes. But these effects seem to vary between various cell lines.^{110,111}

Similar to Baravalle *et al.*, who showed effects of Bafilomycin A₁ on transferrin recycling and dextran transport⁷⁵, we could see that Archazolid B affects the lysosomal degradation of dextran but not the transferrin receptor recycling after shorttime treatments. But upon a treatment with Archazolid B for 20 hours, we see an inhibition of transferrin uptake and a delay in EGF-internalization (Figure 3.27 and 3.28). Especially the delay in EGF-internalization would underline the determined increase of EGF-R on the cell surface upon Archazolid B treatment. Moreover in the electron-microscopy pictures (Figure 3.8), more multivesicular-bodies (MVBs) appeared after Archazolid B treatment compared with control cells. MVBs are degradative endosomal organelles, mediating trafficking between early and late endosomes¹¹⁰ or are involved in exosome formation and secretion.¹¹² The MVBs were strongly enlarged and contained internal luminal vesicles (ILV) after Archazolid B treatment. This phenomenon appeared also in a study describing the involvement of V-ATPase activity in Notch-Signaling.⁷¹ Since an even more acidic pH is necessary for the lysosomal degradation process, it might be that due to the V-ATPase inhibition by

Archazolid B, the final fusion with lysosomes is not possible anymore, which leads to a stop in the degradative and probably also in the recycling process, resulting in the enlargement of MVBs.

4.4.4. The role of Rab5-recycling

The uptake of human rhinovirus serotype 2 (HRV2) via receptor-mediated endocytosis in HeLa cells is affected by Bafilomycin A₁. Bayer *et al.* showed that Bafilomycin A₁ arrests the transport of the virions in early endosomes, which made them to suggest that the transport of endocytosed macromolecules from early to late endosomes on HeLa cells depends on proper endosome acidification.¹¹³

Palamidessi *et al.* showed for the first time that Rac1 is localized at endosomes and its activation is beside the involvement of GEFs, dependent on the GTPase Rab5.⁵⁶ Rab5 is localized in early endosomes and involved in steps of internalization and separation between degradation of recycling events.¹¹⁴ Since we saw effects on Rac1 localization and activation leading to inhibition of F-actin rearrangement during migration (Figure 3.22) as well as inhibitory effects on the internalization processes (Figure 3.28) we were wondering if Archazolid B inhibits the Rab5-induced Rac1 activation. First of all we could see that in Rab5-overexpressing HeLa cells, the formation of all kind of ruffles, which are described to be regulated by Rac1, is inhibited (Figure 3.32). The peripheral ruffles forming the migratory lamellipodia and the invadopodia, which are involved in the secretion of proteases in the invasion process⁵⁷ are clearly reduced in Rab5-overexpressing cells. Also the circular dorsal ruffles, indicators of internalization events, like endocytosis.^{56,106} are almost completely inhibited. This underlines the inhibitory effect of receptor internalization by Archazolid B treatment described during this study.

Moreover, we see in Rab5 induced enlarged early endosomes less Rac1 localization (Figure 3.34 B). In a pH-sensor study by the group of Sergio Grinstein, it is suggested that by cytosolic pH change, also the energy level of the submembrane is changed. Usually the plasmalemmal inner leaflet is highly negative charged due to the high content of polyphosphoinositides. PI(4,5)P₂ and PI(3,4,5)P₃ activated by PI3K in the migration process are necessary for the recruitment of polycationic proteins, such as Rac1, which contains a cationic motif of intermediate charge (6+), to the plasma membrane.^{115,116} It would be therefore really interesting to test if the V-ATPase inhibition via Archazolid B would change submembranous energy level, which then could explain the reduced localization and binding of the cationic tail of Rac1 at submembranous compartments. Also the re-

duced AKT localization could be explained with this experiment which is planned to be done in the near future.

Looking beside the localization also at the activation of the Rho-GTPase Rac1, we could show that also in our cell system (T24) Rac1 is activated upon Rab5 overexpression, which underlines the results of Palamidessi *et al.* who described this phenomenon in HeLa cells.⁵⁶ But furthermore, the really interesting result is that Archazolid B treatment reduces this Rab5-induced Rac1 activation (Figure 3.33 B). Underlined by confocal microscopy pictures (Figure 3.35), we suggest that due to the inhibition of the V-ATPase by Archazolid B leading to a pH increase in endosomes, the activation of Rac1 via Rab5 is diminished. This would therefore result in reduced localization of active Rac1 in cell protrusions resulting in diminished actin condensation at the cell's front (Figure 3.33 C) and therefore no cell migration is possible anymore.

SUMMARY AND CONCLUSIONS

5.1. Involvement of Archazolid B treatment in tumor cell growth

V-ATPases are known to regulate intra-organell and intracellular pH, which may regulate cell growth and apoptosis. We show that the new V-ATPase inhibitor Archazolid B reduces tumor cell growth and induces caspase-dependent apoptosis foremost over the intrinsic mitochondrial pathway. But still the precise regulation of apoptosis induction by V-ATPase remains to be further elucidated (Figure 5.1). As V-ATPase seems to play an important role in multidrug resistance, V-ATPase inhibitors highlight an attractive new therapeutic target in cancer therapy. Furthermore Archazolid B, as a very specific and potent V-ATPase inhibitor, presents a promising new therapeutic drug for cancer treatment.

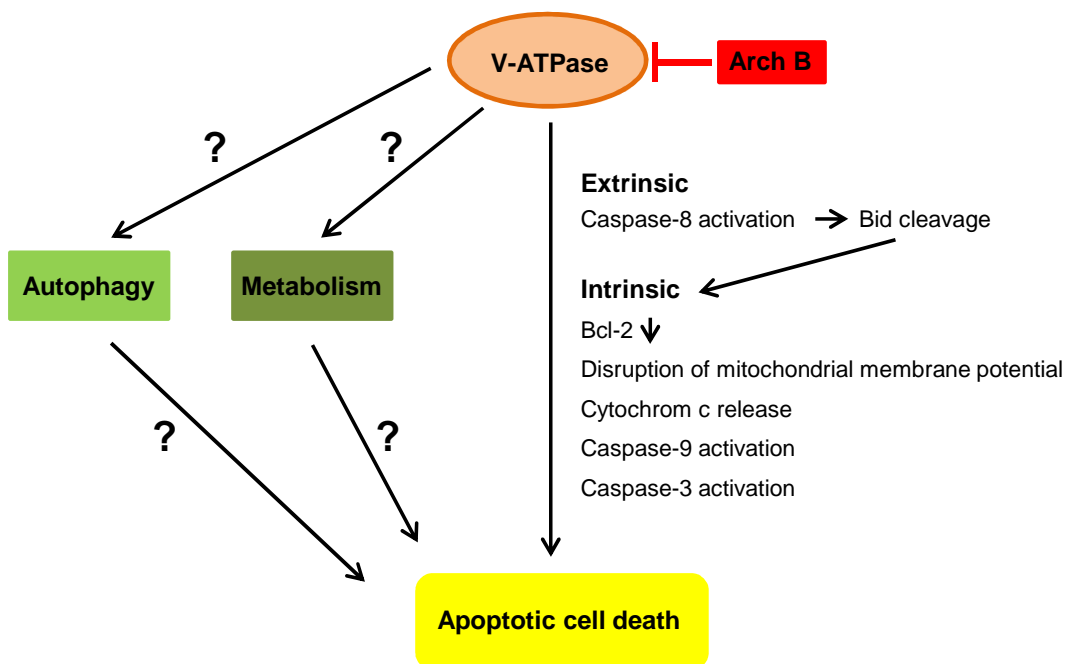


Figure 5.1: Induction of apoptosis by inhibition of the V-ATPase with Archazolid B

5.2. Involvement of V-ATPase inhibition by Archazolid B in cell migration and endocytosis

Archazolid B inhibits tumor cell migration very potently in the nanomolar range. Several indices during these studies suggest a defect in cell polarization. The Rho-GTPase Rac1 is a central regulator of actin remodeling and cell migration. By Archazolid B treatment the activation and localization of Rac1 is inhibited. Furthermore, defects in the internalization and the unorganized distribution of the EGF-R at the cell surface are additional evidences

for a polarization defect. Last, we could see that endocytotic Rac1 activation involving the endosomal GTPase Rab5 is reduced by Archazolid B treatment. It is reported that proper clathrin-dependent internalization of receptor tyrosin kinases like EGF-R is necessary for the activation of the Rho-GTPase Rac in Rab5 positive early endosomes.⁵⁶ Taken together, we conclude, that Archazolid B interferes in the initial steps of endocytosis, leading to a stop of recycling or degradation at early endosome processes. Therefore the re-localization and activation of for example one key player of F-actin re-arrangement, Rac1, is repressed, which finally results in an inhibition of cell migration (Figure 5.2).

For the first time a possible direct mechanism of V-ATPase inhibition leading to cell migration inhibition in highly invasive cancer cells could be herewith described. Archazolid B, as highly potent and specific V-ATPase inhibitor and until now quite uncharacterized, would offer an attractive anti-metastatic compound to inhibit the migration of highly invasive tumor cells.

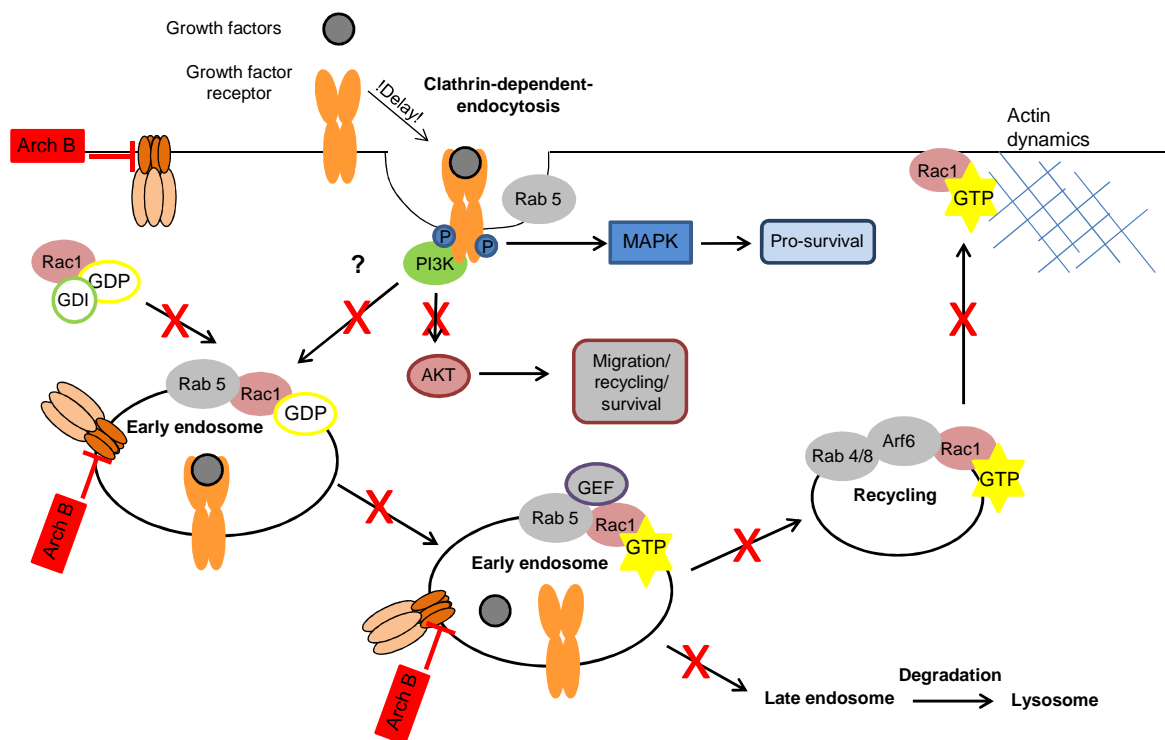


Figure 5.2: Reduction of endosomal Rac1 localization and Rab5-dependent Rac1 activation by Archazolid B leading to repression of actin assembly, which results in cell migration inhibition.

REFERENCES

1. Chaffer CL, Weinberg RA. A perspective on cancer cell metastasis. *Science*. Mar 25 2011;331(6024):1559-1564.
2. Eccles SA, Welch DR. Metastasis: recent discoveries and novel treatment strategies. *Lancet*. May 19 2007;369(9574):1742-1757.
3. Germanov E, Berman JN, Guernsey DL. Current and future approaches for the therapeutic targeting of metastasis (review). *International journal of molecular medicine*. Dec 2006;18(6):1025-1036.
4. Bode HB, Muller R. Analysis of myxobacterial secondary metabolism goes molecular. *Journal of industrial microbiology & biotechnology*. Jul 2006;33(7):577-588.
5. Sasse F, Steinmetz H, Hofle G, Reichenbach H. Archazolids, new cytotoxic macrolactones from *Archangium gephyra* (Myxobacteria). Production, isolation, physico-chemical and biological properties. *The Journal of antibiotics*. Jun 2003;56(6):520-525.
6. Hinton A, Bond S, Forgac M. V-ATPase functions in normal and disease processes. *Pflugers Archiv : European journal of physiology*. Jan 2009;457(3):589-598.
7. Hinton A, Sennoune SR, Bond S, et al. Function of a subunit isoforms of the V-ATPase in pH homeostasis and in vitro invasion of MDA-MB231 human breast cancer cells. *The Journal of biological chemistry*. Jun 12 2009;284(24):16400-16408.
8. Huss M, Sasse F, Kunze B, et al. Archazolid and apicularen: novel specific V-ATPase inhibitors. *BMC biochemistry*. 2005;6:13.
9. Mishra BB, Tiwari VK. Natural products: An evolving role in future drug discovery. *European journal of medicinal chemistry*. Oct 2011;46(10):4769-4807.
10. Reichenbach H, Hofle G. Biologically active secondary metabolites from myxobacteria. *Biotechnology advances*. 1993;11(2):219-277.
11. Wenzel SC, Muller R. Myxobacterial natural product assembly lines: fascinating examples of curious biochemistry. *Natural product reports*. Dec 2007;24(6):1211-1224.
12. Pronzato P. New therapeutic options for chemotherapy-resistant metastatic breast cancer: the epothilones. *Drugs*. 2008;68(2):139-146.
13. Huss M, Vitavska O, Albertmelcher A, et al. Vacuolar H(+)-ATPases: intra- and intermolecular interactions. *European journal of cell biology*. Sep 2011;90(9):688-695.
14. Sennoune SR, Luo D, Martinez-Zaguilan R. Plasmalemmal vacuolar-type H+-ATPase in cancer biology. *Cell biochemistry and biophysics*. 2004;40(2):185-206.
15. Sennoune SR, Bakunts K, Martinez GM, et al. Vacuolar H+-ATPase in human breast cancer cells with distinct metastatic potential: distribution and functional activity. *American journal of physiology. Cell physiology*. Jun 2004;286(6):C1443-1452.
16. Marshansky V, Futai M. The V-type H+-ATPase in vesicular trafficking: targeting, regulation and function. *Current opinion in cell biology*. Aug 2008;20(4):415-426.
17. Farina C, Gagliardi S. Selective inhibition of osteoclast vacuolar H(+)-ATPase. *Current pharmaceutical design*. 2002;8(23):2033-2048.
18. Rojas JD, Sennoune SR, Martinez GM, et al. Plasmalemmal vacuolar H+-ATPase is decreased in microvascular endothelial cells from a diabetic model. *Journal of cellular physiology*. Nov 2004;201(2):190-200.
19. Haass C, Lemere CA, Capell A, et al. The Swedish mutation causes early-onset Alzheimer's disease by beta-secretase cleavage within the secretory pathway. *Nature medicine*. Dec 1995;1(12):1291-1296.

20. Nishiguchi M, Tokugawa K, Yamamoto K, et al. Increase in secretion of glial cell line-derived neurotrophic factor from glial cell lines by inhibitors of vacuolar ATPase. *Neurochemistry international*. May 2003;42(6):493-498.
21. Otani H, Yamamura T, Nakao Y, et al. Insulin-like growth factor-I improves recovery of cardiac performance during reperfusion in isolated rat heart by a wortmannin-sensitive mechanism. *Journal of cardiovascular pharmacology*. Feb 2000;35(2):275-281.
22. Izumi H, Torigoe T, Ishiguchi H, et al. Cellular pH regulators: potentially promising molecular targets for cancer chemotherapy. *Cancer treatment reviews*. Dec 2003;29(6):541-549.
23. Nishi T, Forgac M. The vacuolar (H⁺)-ATPases--nature's most versatile proton pumps. *Nature reviews. Molecular cell biology*. Feb 2002;3(2):94-103.
24. Hirata T, Nakamura N, Omote H, Wada Y, Futai M. Regulation and reversibility of vacuolar H⁽⁺⁾-ATPase. *The Journal of biological chemistry*. Jan 7 2000;275(1):386-389.
25. Saroussi S, Nelson N. The little we know on the structure and machinery of V-ATPase. *The Journal of experimental biology*. Jun 2009;212(Pt 11):1604-1610.
26. Forgac M. Vacuolar ATPases: rotary proton pumps in physiology and pathophysiology. *Nature reviews. Molecular cell biology*. Nov 2007;8(11):917-929.
27. Feniouk BA, Kozlova MA, Knorre DA, Cherepanov DA, Mulikidjanian AY, Junge W. The proton-driven rotor of ATP synthase: ohmic conductance (10 fS), and absence of voltage gating. *Biophysical journal*. Jun 2004;86(6):4094-4109.
28. Junge W, Lill H, Engelbrecht S. ATP synthase: an electrochemical transducer with rotatory mechanics. *Trends in biochemical sciences*. Nov 1997;22(11):420-423.
29. Junge W, Panke O, Cherepanov DA, Gumbiowski K, Muller M, Engelbrecht S. Inter-subunit rotation and elastic power transmission in F₀F₁-ATPase. *FEBS letters*. Aug 31 2001;504(3):152-160.
30. Grabe M, Wang H, Oster G. The mechanochemistry of V-ATPase proton pumps. *Biophysical journal*. Jun 2000;78(6):2798-2813.
31. Murata T, Yamato I, Kakinuma Y, Leslie AG, Walker JE. Structure of the rotor of the V-Type Na⁺-ATPase from *Enterococcus hirae*. *Science*. Apr 29 2005;308(5722):654-659.
32. Beyenbach KW, Wieczorek H. The V-type H⁺ ATPase: molecular structure and function, physiological roles and regulation. *The Journal of experimental biology*. Feb 2006;209(Pt 4):577-589.
33. Fais S, De Milito A, You H, Qin W. Targeting vacuolar H⁺-ATPases as a new strategy against cancer. *Cancer research*. Nov 15 2007;67(22):10627-10630.
34. Bowman EJ, Siebers A, Altendorf K. Bafilomycins: a class of inhibitors of membrane ATPases from microorganisms, animal cells, and plant cells. *Proceedings of the National Academy of Sciences of the United States of America*. Nov 1988;85(21):7972-7976.
35. Drose S, Bindseil KU, Bowman EJ, Siebers A, Zeeck A, Altendorf K. Inhibitory effect of modified bafilomycins and concanamycins on P- and V-type adenosinetriphosphatases. *Biochemistry*. Apr 20 1993;32(15):3902-3906.
36. Kinashi H, Someno K, Sakaguchi K. Isolation and characterization of concanamycins A, B and C. *The Journal of antibiotics*. Nov 1984;37(11):1333-1343.
37. Werner G, Hagenmaier H, Drautz H, Baumgartner A, Zahner H. Metabolic products of microorganisms. 224. Bafilomycins, a new group of macrolide antibiotics. Production, isolation, chemical structure and biological activity. *The Journal of antibiotics*. Feb 1984;37(2):110-117.

38. Huss M, Ingenhorst G, Konig S, et al. Concanamycin A, the specific inhibitor of V-ATPases, binds to the V(o) subunit c. *The Journal of biological chemistry*. Oct 25 2002;277(43):40544-40548.
39. Bowman BJ, Bowman EJ. Mutations in subunit C of the vacuolar ATPase confer resistance to bafilomycin and identify a conserved antibiotic binding site. *The Journal of biological chemistry*. Feb 8 2002;277(6):3965-3972.
40. Wang Y, Inoue T, Forgac M. Subunit a of the yeast V-ATPase participates in binding of bafilomycin. *The Journal of biological chemistry*. Dec 9 2005;280(49):40481-40488.
41. Xie XS, Padron D, Liao X, Wang J, Roth MG, De Brabander JK. Salicylhalamide A inhibits the V0 sector of the V-ATPase through a mechanism distinct from bafilomycin A1. *The Journal of biological chemistry*. May 7 2004;279(19):19755-19763.
42. Bockelmann S, Menche D, Rudolph S, et al. Archazolid A binds to the equatorial region of the c-ring of the vacuolar H⁺-ATPase. *The Journal of biological chemistry*. Dec 3 2010;285(49):38304-38314.
43. Huss M, Wieczorek H. Inhibitors of V-ATPases: old and new players. *The Journal of experimental biology*. Feb 2009;212(Pt 3):341-346.
44. Yamaguchi H, Wyckoff J, Condeelis J. Cell migration in tumors. *Current opinion in cell biology*. Oct 2005;17(5):559-564.
45. Cotter TG, Lennon SV, Glynn JG, Martin SJ. Cell death via apoptosis and its relationship to growth, development and differentiation of both tumour and normal cells. *Anticancer research*. Sep-Oct 1990;10(5A):1153-1159.
46. Kerr JF, Wyllie AH, Currie AR. Apoptosis: a basic biological phenomenon with wide-ranging implications in tissue kinetics. *British journal of cancer*. Aug 1972;26(4):239-257.
47. Fulda S, Debatin KM. Extrinsic versus intrinsic apoptosis pathways in anticancer chemotherapy. *Oncogene*. Aug 7 2006;25(34):4798-4811.
48. Danial NN, Korsmeyer SJ. Cell death: critical control points. *Cell*. Jan 23 2004;116(2):205-219.
49. Weinberg RA. *The biology of cancer* 2007.
50. Fresno Vara JA, Casado E, de Castro J, Cejas P, Belda-Iniesta C, Gonzalez-Baron M. PI3K/Akt signalling pathway and cancer. *Cancer treatment reviews*. Apr 2004;30(2):193-204.
51. Jiang P, Enomoto A, Takahashi M. Cell biology of the movement of breast cancer cells: intracellular signalling and the actin cytoskeleton. *Cancer letters*. Nov 1 2009;284(2):122-130.
52. Vivanco I, Sawyers CL. The phosphatidylinositol 3-Kinase AKT pathway in human cancer. *Nature reviews. Cancer*. Jul 2002;2(7):489-501.
53. Markman B, Dienstmann R, Tabernero J. Targeting the PI3K/Akt/mTOR pathway--beyond rapalogs. *Oncotarget*. Nov 2010;1(7):530-543.
54. Hall A. Rho GTPases and the actin cytoskeleton. *Science*. Jan 23 1998;279(5350):509-514.
55. Sahai E, Marshall CJ. RHO-GTPases and cancer. *Nature reviews. Cancer*. Feb 2002;2(2):133-142.
56. Palamidessi A, Frittoli E, Garre M, et al. Endocytic trafficking of Rac is required for the spatial restriction of signaling in cell migration. *Cell*. Jul 11 2008;134(1):135-147.
57. Ridley AJ. Life at the leading edge. *Cell*. Jun 24 2011;145(7):1012-1022.
58. Lanzetti L, Di Fiore PP. Endocytosis and cancer: an 'insider' network with dangerous liaisons. *Traffic*. Dec 2008;9(12):2011-2021.
59. Scita G, Di Fiore PP. The endocytic matrix. *Nature*. Jan 28 2010;463(7280):464-473.

60. Roethle PA, Chen IT, Trauner D. Total synthesis of (-)-archazolid B. *Journal of the American Chemical Society*. Jul 25 2007;129(29):8960-8961.
61. Nicoletti I, Migliorati G, Pagliacci MC, Grignani F, Riccardi C. A rapid and simple method for measuring thymocyte apoptosis by propidium iodide staining and flow cytometry. *Journal of immunological methods*. Jun 3 1991;139(2):271-279.
62. Waterhouse NJ, Trapani JA. A new quantitative assay for cytochrome c release in apoptotic cells. *Cell death and differentiation*. Jul 2003;10(7):853-855.
63. Bradford MM. A rapid and sensitive method for the quantitation of microgram quantities of protein utilizing the principle of protein-dye binding. *Analytical biochemistry*. May 7 1976;72:248-254.
64. Pfaffl MW. A new mathematical model for relative quantification in real-time RT-PCR. *Nucleic acids research*. May 1 2001;29(9):e45.
65. Eberwine J, Spencer C, Miyashiro K, Mackler S, Finnell R. Complementary DNA synthesis in situ: methods and applications. *Methods in enzymology*. 1992;216:80-100.
66. Eberwine J, Yeh H, Miyashiro K, et al. Analysis of gene expression in single live neurons. *Proceedings of the National Academy of Sciences of the United States of America*. Apr 1 1992;89(7):3010-3014.
67. Laemmli UK. Cleavage of structural proteins during the assembly of the head of bacteriophage T4. *Nature*. Aug 15 1970;227(5259):680-685.
68. Lu X, Qin W, Li J, et al. The growth and metastasis of human hepatocellular carcinoma xenografts are inhibited by small interfering RNA targeting to the subunit ATP6L of proton pump. *Cancer research*. Aug 1 2005;65(15):6843-6849.
69. Aerts JL, Gonzales MI, Topalian SL. Selection of appropriate control genes to assess expression of tumor antigens using real-time RT-PCR. *BioTechniques*. Jan 2004;36(1):84-86, 88, 90-81.
70. Wyllie AH, Kerr JF, Currie AR. Cell death: the significance of apoptosis. *International review of cytology*. 1980;68:251-306.
71. Vaccari T, Duchi S, Cortese K, Tacchetti C, Bilder D. The vacuolar ATPase is required for physiological as well as pathological activation of the Notch receptor. *Development*. Jun 2010;137(11):1825-1832.
72. Chen Z, Gibson TB, Robinson F, et al. MAP kinases. *Chemical reviews*. Aug 2001;101(8):2449-2476.
73. Tokunaga E, Oki E, Egashira A, et al. Dereglulation of the Akt pathway in human cancer. *Current cancer drug targets*. Feb 2008;8(1):27-36.
74. Presley JF, Mayor S, McGraw TE, Dunn KW, Maxfield FR. Bafilomycin A1 treatment retards transferrin receptor recycling more than bulk membrane recycling. *The Journal of biological chemistry*. May 23 1997;272(21):13929-13936.
75. Baravalle G, Schober D, Huber M, Bayer N, Murphy RF, Fuchs R. Transferrin recycling and dextran transport to lysosomes is differentially affected by bafilomycin, nocodazole, and low temperature. *Cell and tissue research*. Apr 2005;320(1):99-113.
76. Huber V, De Milito A, Harguindey S, et al. Proton dynamics in cancer. *Journal of translational medicine*. 2010;8:57.
77. Otto W, Burger M, Fritsche HM et al. The enlightenment of bladder cancer treatment: origin and progress of photodynamic diagnosis. *Future Oncol*: Sep 2011 7(9):1057-66.
78. Bruns CJ, Harbison MT, Kuniyasu H, Eue I, Fidler IJ. In vivo selection and characterization of metastatic variants from human pancreatic adenocarcinoma by using orthotopic implantation in nude mice. *Neoplasia*. Apr 1999;1(1):50-62.
79. Reichenbach H, Höfle, G. *Myxobacteria as producers of secondary metabolites*. In: Grabley S., Thiericke, R. (eds) *Drug discovery from nature*: Springer, Berlin Heidelberg New York; 1999.

80. Hanahan D, Weinberg RA. The hallmarks of cancer. *Cell*. Jan 7 2000;100(1):57-70.
81. Hanahan D, Weinberg RA. Hallmarks of cancer: the next generation. *Cell*. Mar 4 2011;144(5):646-674.
82. Morita T, Nagaki T, Fukuda I, Okumura K. Clastogenicity of low pH to various cultured mammalian cells. *Mutation research*. Aug 1992;268(2):297-305.
83. Raghunand N, Martinez-Zaguilan R, Wright SH, Gillies RJ. pH and drug resistance. II. Turnover of acidic vesicles and resistance to weakly basic chemotherapeutic drugs. *Biochemical pharmacology*. May 1 1999;57(9):1047-1058.
84. Martinez-Zaguilan R, Raghunand N, Lynch RM, et al. pH and drug resistance. I. Functional expression of plasmalemmal V-type H⁺-ATPase in drug-resistant human breast carcinoma cell lines. *Biochemical pharmacology*. May 1 1999;57(9):1037-1046.
85. Martinez-Zaguilan R, Seftor EA, Seftor RE, Chu YW, Gillies RJ, Hendrix MJ. Acidic pH enhances the invasive behavior of human melanoma cells. *Clinical & experimental metastasis*. Mar 1996;14(2):176-186.
86. Franken NA, Rodermond HM, Stap J, Haveman J, van Bree C. Clonogenic assay of cells in vitro. *Nature protocols*. 2006;1(5):2315-2319.
87. Fulda S, Debatin KM. Targeting apoptosis pathways in cancer therapy. *Current cancer drug targets*. Nov 2004;4(7):569-576.
88. Akifusa S, Ohguchi M, Koseki T, et al. Increase in Bcl-2 level promoted by CD40 ligation correlates with inhibition of B cell apoptosis induced by vacuolar type H(+)-ATPase inhibitor. *Experimental cell research*. Jan 10 1998;238(1):82-89.
89. McHenry P, Wang WL, Devitt E, et al. Iejimalides A and B inhibit lysosomal vacuolar H⁺-ATPase (V-ATPase) activity and induce S-phase arrest and apoptosis in MCF-7 cells. *Journal of cellular biochemistry*. Mar 1 2010;109(4):634-642.
90. Blomgran R, Zheng L, Stendahl O. Cathepsin-cleaved Bid promotes apoptosis in human neutrophils via oxidative stress-induced lysosomal membrane permeabilization. *Journal of leukocyte biology*. May 2007;81(5):1213-1223.
91. Stoka V, Turk B, Schendel SL, et al. Lysosomal protease pathways to apoptosis. Cleavage of bid, not pro-caspases, is the most likely route. *The Journal of biological chemistry*. Feb 2 2001;276(5):3149-3157.
92. Stoka V, Turk V, Turk B. Lysosomal cysteine cathepsins: signaling pathways in apoptosis. *Biological chemistry*. Jun 2007;388(6):555-560.
93. Aiko K, Tsujisawa T, Koseki T, et al. Involvement of cytochrome c and caspases in apoptotic cell death of human submandibular gland ductal cells induced by concanamycin A. *Cellular signalling*. Aug 2002;14(8):717-722.
94. Ishisaki A, Hashimoto S, Amagasa T, Nishihara T. Caspase-3 activation during the process of apoptosis induced by a vacuolar type H(+)-ATPase inhibitor. *Biology of the cell / under the auspices of the European Cell Biology Organization*. Sep 1999;91(7):507-513.
95. Fulda S, Debatin KM. Modulation of apoptosis signaling for cancer therapy. *Archivum immunologiae et therapeuticae experimentalis*. May-Jun 2006;54(3):173-175.
96. Mashima T, Tsuruo T. Defects of the apoptotic pathway as therapeutic target against cancer. *Drug resistance updates : reviews and commentaries in antimicrobial and anticancer chemotherapy*. Dec 2005;8(6):339-343.
97. Mahoney BP, Raghunand N, Baggett B, Gillies RJ. Tumor acidity, ion trapping and chemotherapeutics. I. Acid pH affects the distribution of chemotherapeutic agents in vitro. *Biochemical pharmacology*. Oct 1 2003;66(7):1207-1218.
98. Raghunand N, Mahoney BP, Gillies RJ. Tumor acidity, ion trapping and chemotherapeutics. II. pH-dependent partition coefficients predict importance of

- ion trapping on pharmacokinetics of weakly basic chemotherapeutic agents. *Biochemical pharmacology*. Oct 1 2003;66(7):1219-1229.
99. Torigoe T, Izumi H, Ishiguchi H, et al. Enhanced expression of the human vacuolar H⁺-ATPase c subunit gene (ATP6L) in response to anticancer agents. *The Journal of biological chemistry*. Sep 27 2002;277(39):36534-36543.
 100. Pampaloni F, Reynaud EG, Stelzer EH. The third dimension bridges the gap between cell culture and live tissue. *Nature reviews. Molecular cell biology*. Oct 2007;8(10):839-845.
 101. Grimshaw MJ, Cooper L, Papazisis K, et al. Mammosphere culture of metastatic breast cancer cells enriches for tumorigenic breast cancer cells. *Breast cancer research : BCR*. 2008;10(3):R52.
 102. Kubota S, Seyama Y. Overexpression of vacuolar ATPase 16-kDa subunit in 10T1/2 fibroblasts enhances invasion with concomitant induction of matrix metalloproteinase-2. *Biochemical and biophysical research communications*. Nov 19 2000;278(2):390-394.
 103. Byun YJ, Lee SB, Lee HO, et al. Vacuolar H⁺ -ATPase c protects glial cell death induced by sodium nitroprusside under glutathione-depleted condition. *Journal of cellular biochemistry*. Aug 2011;112(8):1985-1996.
 104. Byun YJ, Lee SB, Kim DJ, et al. Protective effects of vacuolar H⁺ -ATPase c on hydrogen peroxide-induced cell death in C6 glioma cells. *Neuroscience letters*. Oct 2 2007;425(3):183-187.
 105. You H, Jin J, Shu H, et al. Small interfering RNA targeting the subunit ATP6L of proton pump V-ATPase overcomes chemoresistance of breast cancer cells. *Cancer letters*. Jul 18 2009;280(1):110-119.
 106. Buccione R, Orth JD, McNiven MA. Foot and mouth: podosomes, invadopodia and circular dorsal ruffles. *Nature reviews. Molecular cell biology*. Aug 2004;5(8):647-657.
 107. Tawfeek HA, Abou-Samra AB. Important role for the V-type H(+)-ATPase and the Golgi apparatus in the recycling of PTH/PTHrP receptor. *American journal of physiology. Endocrinology and metabolism*. May 2004;286(5):E704-710.
 108. Kohno M, Pouyssegur J. Targeting the ERK signaling pathway in cancer therapy. *Annals of medicine*. 2006;38(3):200-211.
 109. Barber MA, Welch HC. PI3K and RAC signalling in leukocyte and cancer cell migration. *Bulletin du cancer*. May 2006;93(5):E44-52.
 110. Clague MJ, Urbe S, Aniento F, Gruenberg J. Vacuolar ATPase activity is required for endosomal carrier vesicle formation. *The Journal of biological chemistry*. Jan 7 1994;269(1):21-24.
 111. van Weert AW, Dunn KW, Gueze HJ, Maxfield FR, Stoorvogel W. Transport from late endosomes to lysosomes, but not sorting of integral membrane proteins in endosomes, depends on the vacuolar proton pump. *The Journal of cell biology*. Aug 1995;130(4):821-834.
 112. Trajkovic K, Hsu C, Chiantia S, et al. Ceramide triggers budding of exosome vesicles into multivesicular endosomes. *Science*. Feb 29 2008;319(5867):1244-1247.
 113. Bayer N, Schober D, Prchla E, Murphy RF, Blaas D, Fuchs R. Effect of bafilomycin A1 and nocodazole on endocytic transport in HeLa cells: implications for viral uncoating and infection. *Journal of virology*. Dec 1998;72(12):9645-9655.
 114. Woodman PG. Biogenesis of the sorting endosome: the role of Rab5. *Traffic*. Sep 2000;1(9):695-701.
 115. Yeung T, Gilbert GE, Shi J, Silvius J, Kapus A, Grinstein S. Membrane phosphatidylserine regulates surface charge and protein localization. *Science*. Jan 11 2008;319(5860):210-213.

116. Koivusalo M, Welch C, Hayashi H, et al. Amiloride inhibits macropinocytosis by lowering submembranous pH and preventing Rac1 and Cdc42 signaling. *The Journal of cell biology*. Feb 22 2010;188(4):547-563.

APPENDIX

7.1. Abbreviations

ANOVA	Analysis of variance between groups
Arch	Archazolid
Arf6	ADP-ribosylation factor 6
μM	micro molar (10^{-6})
APS	Ammonium persulfat
ATP	Adenosin-5`-triphosphat
Bcl-2	B-cell lymphoma
BSA	Bovine serum albumin
cDNA	Complementary Desoxyribonucleic acid
Co	Control
Conc A	Concanamycin A
DMEM	Dulbecco`s Modified Essential Medium
DMSO	Dimethylsulfoxid
DNA	Desoxyribonucleic acid
DTT	Dithiothreitol
ECL	Enhanced chemoluminescence
EDTA	Ethylendiamin-N`, N`, N`, N`-tetraessigsäure
ER	Endoplasmatic reticulum
EtBr	Ethidiumbromid
EtOH	Ethanol
FACS	Fluorescence-activated cell sorter
FCS	Fetal calf serum
Fig	Figure
FL	Fluorescence
FSC	Forward scatter
GTP/GDP	Guanosine-5'-triphosphate/-diphosphate
h	Hour(s)
HEPES	N-(2-hydroxyethyl)piperazine-N'-(2-ethanesulfonic acid)
HFS	Hypotonic fluorochrome solution
HRP	Horeseradish peroxidase
kDa	Kilo Dalton
l	Liter

MAPK	Mitogen-activated protein kinase
MMP	Mitochondrial membrane potential
MeOH	Methanol
mM	milli molar (10^{-3})
mRNA	messenger RNA
NaAc	Natriumacetat
NaF	Sodium fluorid
NaOH	Natriumhydroxid
NEAA	Non-essential amino acids
nM	Nano molar (10^{-9})
nt	Non-targeting
PAA	Polyacrylamid
PAGE	Polyacrylamid-Gelelectrophorese
PARP	Poly-ADP-ribose polymerase
PBS	Phosphate buffered saline
PVDF	Polyvinylidenfluorid
Q-VD-OPh	N-(2-Quinoly)valyl-aspartyl-(2,6-difluorophenoxy
RNA	Ribonucleic acid
RNasen	Ribonuclease
rpm	rotations per minute
RT	Room temperature
SD	Standard derivation
SDS	Sodium dodecyl sulfat
sec	Second
Ser	Serine
SSC	Sideward scatter
Tax	Paclitaxel
TBE	Tris, Borat, EDTA-Puffer
TBS-T	Tris-gepufferte Kochsalzlösung mit Tween
T/E	Trypsin/EDTA
TEMED	N, N, N, N'-Tetramethylethylendiamin
TRAIL	TNF-related apoptosis inducing ligand
Tris	Trishydroxymethylaminomethane

7.2. Publications

7.2.1. Original publications

Amina Zoubeidi, Anousheh Zardan, Romina M. Wiedmann, Eliana Beraldi and Martin Gleave **Hsp27 promotes prostate cancer cell survival in IGF-1 signaling by a p90RSK-dependent phosphorylation and inactivation of BAD** Cancer Res. 2010 Mar 15;70(6):2307-17. Epub 2010 Mar 2

Andrea S. Rothmeier*, Uta M. Schneiders*, Romina M. Wiedmann, Ivan Ischenko, Christiane J. Bruns, Anita Rudy, Stefan Zahler, Angelika M. Vollmar **The marine compound Spongistatin 1 targets pancreatic tumour progression and metastasis** Int J Cancer. 2010 Sep 1;127(5):1096-105.

* Authors contribute equally to this work

Romina M. Wiedmann, Amina Zoubeidi, Marc Gemain, Anousheh Zardan, Eliana Beraldi and Martin Gleave **Up-regulation of Hsp27 in prostate cancer induces resistance to proteasome inhibitor through Bax interaction**

Under preparation

Romina M. Wiedmann, Karin v. Schwarzenberg, Ingrid Chen, Dirk Trauner, Johanna Liebl, Andrea Palamidessi, Giorgio Scita, Stefan Zahler and Angelika M. Vollmar **The V-ATPase inhibitor Archazolid B inhibits cell migration via inhibition of the Rho-GTPase Rac1**

Under preparation

Karin v. Schwarzenberg, Romina M. Wiedmann, Michael Günther, Thomas Efferth, Gerhard Wanner, Dirk Trauner and Angelika M. Vollmar **The potent V-ATPase inhibitor Archazolid B induces a stress response and alters the metabolism of tumor cells.**

Under preparation

J. Herrmann, R. M. Wiedmann, Y.A. Elnakady, A. Ullrich, M. Rohde, U. Kazmaier, A.M. Vollmar, R. Müller **Pretubulysin: From a hypothetical biosynthetic intermediate to potential lead in tumor therapy.**

Under preparation

7.2.2. Poster presentations/abstracts

Romina Wiedmann, Amina Zoubeydi, Marc Gemain, Anousheh Zardan, Eliana Beraldi and Martin Gleave **Up-regulation of Hsp27 in prostate cancer induces resistance to proteasome inhibitor through Bax interaction.** AACR-Conference, San Diego, USA, 2008

Romina Wiedmann, Ingrid Chen, Dirk Trauner, Angelika M. Vollmar and Anita Rudy **Archazolid B, a new potent compound to treat metastatic pancreatic cancer.** SyntheseFest 2009, LMU Munich, Germany

Romina Wiedmann, Ingrid Chen, Dirk Trauner, Angelika M. Vollmar and Anita Rudy **Archazolid B, a new potent compound to treat metastatic pancreatic cancer.** interact 2009", Munich, Germany

Romina Wiedmann, Ingrid Chen, Stefan Zahler, Rolf Müller, Uli Kazmaier, Dirk Trauner and Angelika M. Vollmar **Natural compounds inhibiting cell migration as a source for new potential anti-metastatic drugs.** 11th Young Scientist Meeting of the German Society for Cell Biology: "Imaging Cell Migration", Munich, Germany

Romina Wiedmann, Ingrid Chen, Dirk Trauner, Anita Rudy, Stefan Zahler and Angelika M. Vollmar **Archazolid B, a new V-ATPase-inhibitor of myxobacterial origin, exhibits anti-metastatic potential.** 5th International Conference On Tumor Microenvironment, (ICTM, AACR & INC), Versailles, France

Romina Wiedmann, Ingrid Chen, Dirk Trauner, Stefan Zahler, Karin v. Schwarzenberg and Angelika M. Vollmar **The potent V-ATPase-inhibitor Archazolid B inhibits tumor cell growth and the metastatic process.** 51st Annual meeting of the DGPT, Mainz, Germany

Romina M. Wiedmann, Ingrid Chen, Dirk Trauner, Karin v. Schwarzenberg, Johanna Liebl, Stefan Zahler and Angelika M. Vollmar **The potent V-ATPase-inhibitor Archazolid B inhibits tumor cell migration via inhibition of the Rho-GTPase Rac.** 77th Annual meeting of the DGPT, Frankfurt, Germany

Karin von Schwarzenberg, Romina M. Wiedmann, Trauner Dirk, Angelika M. Vollmar **The novel V-ATPase inhibitor archazolid B induces apoptosis in highly resistant tumor**

cells involving the mitochondria and autophagy. 77th Annual meeting of the DGPT, Frankfurt, Germany

7.3. Grants

July 2006

DAAD Travel grant

Travel support for an internship at the Prostate Centre at Vancouver General Hospital, Vancouver, Canada

March 2010

DGPT Travel Grant

Convention Travel to the 51st Annual meeting of the “Deutschen Gesellschaft für Experimentelle und Klinische Pharmakologie und Toxikologie“ (DGPT), Mainz, Germany

March 2011

DGPT Travel Grant

Convention Travel to the 77th Annual meeting of the “Deutschen Gesellschaft für Experimentelle und Klinische Pharmakologie und Toxikologie“ (DGPT), Frankfurt, Germany

July 2011

Travel grant of the “Life Science Munich” Graduate School

Travel support for a 4-week research stay at the group of Prof. Dr. Giorgio Scita, IFOM Foundation, Institute FIRC of Molecular Oncology, University of Milan, Italy.

7.4. Curriculum vitae

Personal data

Name	Romina Madeleine Wiedmann
Date of Birth	May 7 th , 1983
Place of Birth	Mutlangen, Germany
Nationality	German

7.5. Acknowledgement

I want to deeply thank Prof. Dr. Angelika M. Vollmar for giving me the opportunity to do my PhD-thesis in her laboratories. I always appreciated the great enthusiastic scientific support and guidance, whenever needed. Also supporting the participation at the “Life-science-Munich” graduate school with all its advantages and time consumption as well as providing the possibility to collaborate with the group of Prof. Dr. Giorgio Scita, IFOM Foundation, Institute FIRC of Molecular Oncology, Milan, Italy was always deeply honored by me.

Many thanks to Prof. Dr. Zahler for being the second examiner. The inspiring scientific discussions and effective suggestions and tips helped me a lot performing this project.

Thanks to Prof. Dr. Biel, Prof. Dr. Trauner, Prof. Dr. Wahl-Schott and Prof. Dr. Paintner for the interest in this work and being part of the examiner committee. Furthermore many thanks to Prof. Dr. Trauner and his group for the synthesis of Archazolid B.

“Mille grazie” to Prof. Dr. Scita and Dr. Andrea Palamidessi for their enthusiastic and profound efforts to finalize this great project. Thank you to all lab members for all their help.

Thanks to all PostDocs, Anita Rudy, Karin von Schwarzenberg and Johanna Liebl, who were involved in this project and supervised me. All of you helped me at various stages of this work. Especially, thank you to Karin for the support to finalize this project; and Hanna for having always an open door for answering and discussing many scientific questions.

I thank all people in the Vollmar lab for creating such a great lab environment. Thanks Bettina for the great emotional support during the final run. Especially I want to thank Sabine and Elisabeth. Thank you Sabine for our great time together. I really enjoyed our last writing months together and I always deeply appreciated your advice and help. Elisabeth, thank you for being there whenever I needed an open ear. You listened and discussed with me science and private life and gave me good advices whenever needed.

Also, I want to thank Ingrid-not only for her efforts to synthesize the Archazolid B-even more for being such a great friend.

Thanks to the “Life Science Munich” Graduate school - especially Beate Hafner and Cornelia Kellermann for the great organization of inspiring and informative lectures, workshops and retreats. And of course, thanks the LSM student crew-for effective group work and fun times beside our science life.

Thank you to Laura and Nici for the great distraction outside the lab! Thank you for listening to all my science problems and always making me to laugh, again.

Also, thank you to Sebastian. You appeared to be at my side just in the very right moment. Thanks for all the encouragement and patience during the final run.

Last but not least, I want to thank my whole family for their undescrivable support. Especially: Mama and Papa: you made me to what I am! Without your love, trust and help I couldn't have done the way I went. Thanks for your endless support and motivation. Also the love and encouragement by my beloved grandmother Toni will be always in my heart.